Programa de Doctorado Biomedicina y Oncología Molecular

Cell intrinsic and extrinsic mechanisms in the modulation of ageing and age-related diseases

Doctoral Thesis

Sandra Freitas Rodríguez

February 2021

RESUMEN DEL CONTENIDO DE TESIS DOCTORAL

1.- Título de la Tesis	
Español/Otro Idioma: Mecanismos intrínsecos y extrínsecos a la célula en la regulación del envejecimiento y de las enfermedades asociadas	Inglés: Cell-intrinsic and -extrinsic mechanisms in the modulation of ageing and age-related diseases

2.- Autor	
Nombre: Sandra Freitas Rodríguez	DNI/Pasaporte/NIE:
Programa de Doctorado: Biomedicina y Oncología Molecular	
Órgano responsable: Universidad de Oviedo	

RESUMEN (en español)

El envejecimiento es un proceso aparentemente inexorable que implica un deterioro funcional progresivo que tiene un claro impacto sobre la calidad de vida. Durante los últimos años se han llevado a cabo multitud de aproximaciones experimentales para tratar de dilucidar los aspectos funcionales y mecanísticos relacionados con la modulación molecular del envejecimiento y de sus enfermedades asociadas. Sin embargo, debido a la compleja naturaleza de este proceso, aún se desconoce el trasfondo molecular existente entre las vías intercelulares y sistémicas subyacentes al mismo. En este contexto, la presente Tesis Doctoral ha tenido como objetivo evaluar la implicación relativa de los mecanismos intrínsecos y extrínsecos a la célula en el progreso del envejecimiento y de sus enfermedades asociadas. En primer lugar, hemos secuenciado y anotado manualmente el genoma de dos tortugas gigantes caracterizadas por una gran longevidad. Así, utilizando una aproximación dirigida por hipótesis, hemos identificado diversas variantes específicas de linaje que afectan algunas de las características clave implicadas en el progreso del envejecimiento, como son la reparación del ADN, la protección frente al cáncer o la inmunovigilancia. Además, también hemos tratado de dilucidar la participación de mecanismos extrínsecos a la célula en el progreso del fenotipo progeroide. Concretamente hemos explorado la implicación de GDF11 en el deterioro asociado a la edad en un modelo murino de envejecimiento acelerado, así como la repercusión de la citoquina RANKL producida por los osteocitos en el progreso del fenotipo patológico característico del mismo. Por último, hemos caracterizado la función del hierro y de la matriptasa-2 (*Tmprss6*), un regulador negativo de la hormona circulante conocida como hepcidina, en el establecimiento de un desorden metabólico asociado a la edad como es la obesidad, para lo cual hemos utilizado un modelo murino deficiente en *Tmprss6* alimentado con una dieta rica en grasa. En conjunto, la presente Tesis Doctoral ha tratado de esclarecer la contribución relativa de los mecanismos intrínsecos y extrínsecos a la célula en la regulación del envejecimiento y de enfermedades relacionadas, contribuyendo a arrojar algo de luz sobre las futuras bases moleculares para el desarrollo de nuevas estrategias terapéuticas dirigidas a mejorar la calidad de vida en el contexto del envejecimiento.

RESUMEN (en inglés)

The functional deterioration that involves ageing clearly impacts on the quality of life of elderly population, increasing their vulnerability to illness and death. During the last decades, many experimental approaches have been employed to address functional and mechanistic questions concerning the molecular modulation of ageing and age-related diseases. However, many aspects regarding the complex interconnection between the intercellular pathways and the systemic mechanisms that regulate these processes remain to be fully elucidated. Based on the presented background, this Doctoral Thesis has aimed to evaluate the relevance of intrinsic *vs.* extrinsic factors implicated in ageing and age-related diseases. Hence, we have identified, using a hypothesis-driven approach, lineage-specific variants presented in the genome of two long-lived giant tortoises that may underlie its extraordinary lifespan. These changes, which may be categorized as cell-intrinsic alterations, mainly affect processes involved in several hallmarks of ageing and cancer, such as DNA repair or immunosurveillance. Moreover, we have explored the impact of cell-extrinsic mechanisms on progeroid features and longevity, concretely

evaluating the function of GDF11 in age-dependent decline, as well as the pivotal contribution of osteocyte-derived RANKL to the pathological alterations observed in a murine model of accelerated ageing. Finally, we have characterized the role of iron and matriptase-2 (*Tmprss6*), a negative regulator of the circulating factor hepcidin, in the establishment of an age-related metabolic disorder as obesity by using a *Tmprss6*-deficient mouse model challenged with high-fat diet. Together, this experimental work has provided biological insights aimed to clarify the regulatory cell-intrinsic and -extrinsic mechanisms that integrate the organismal communication during ageing and disease, and hopefully, may have shed some light on the development of novel therapeutic strategies designed to improve the quality of life in a gradually aged world.

SR. PRESIDENTE DE LA COMISIÓN ACADÉMICA DEL PROGRAMA DE DOCTORADO EN BIOMEDICINA Y ONCOLOGÍA MOLECULAR

Abbreviations

B.W.	body weight
BAT	brown adipose tissue
BMD	bone mineral density
bp	base pair
BSA	bovine serum albumin
BV/TV	bone volume/tissue volume
CAPS	3-[cyclohexylamino]-1-propanesulfonic acid
cDNA	complementary deoxyribonucleic acid
Ct.Th	cortical thickness
DNA	deoxyribonucleic acid
ECM	extracellular matrix
EDTA	ethylenediaminetetraacetic acid
ELISA	enzyme-linked immunosorbent assay
H&E	haematoxylin and eosin
HBSS	hank's balanced salt solution
HFD	high-fat diet
HGPS	Hutchinson-Gilford progeria syndrome
HPR	horseradish peroxidase
IRIDA	iron-refractory iron deficiency anaemia
KO	knockout
MRI	magnetic resonance imaging
mRNA	messenger ribonucleic acid
MYA	million years ago
NHEJ	non-homologous end joining
OCT	optimal cutting temperature compound
PBS	phosphate-buffered saline

PCR	polymerase chain reaction
PFA	paraformaldehyde
PVDF	polyvinylidene difluoride
qRT-PCR	quantitative reverse transcriptase-PCR
RNA	ribonucleic acid
RT-PCR	reverse transcriptase-PCR
SDS	sodium dodecyl sulfate
SDS-PAGE	sodium dodecyl sulfate polyacrylamide gel electrophoresis
SEM	standard error of the mean
SVF	stromal-vascular fraction
Tb.N	trabecular number
Tb.Sp	trabecular separation
Tb.Th	trabecular thickness
TBS-T	tris-buffered saline with tween 20
Tris	tris(hydroxymethyl)aminomethane
VCO_2	volume of CO_2
VO_2	volume of O_2
WAT	white adipose tissue
WT	wildtype
μCT	micro-computed tomography

Contents

Introduction

The idea of overcoming ageing and achieving immortality has historically been pursued by authors, philosophers, and scientists for centuries. Ageing has long been conceived as an extremely complex process that inexorably leads to death, generating considerable drawbacks in health during its progression. Despite its presumed stochastic appearance, the ageing course is very similar among individuals and even among species, suggesting that the mechanisms underlying ageing are widely conserved across evolution (Singh *et al.* 2019). However, this apparently universal phenomenon is still poorly understood and thereby is particularly difficult to define. The first evidences regarding the external manipulation of lifespan of different model organisms raised multiple questions about which signalling pathways and genetic programmes were critical in the control of ageing (Kenyon *et al.* 1993; Bitto *et al.* 2015). Since then, many studies have employed diverse *in vitro* and *in vivo* approaches to address functional and mechanistic questions concerning the molecular modulation of ageing and age-related diseases. These answers have recently contributed to establish nine categories that summarize the molecular and cellular changes resulting from the physiological decline throughout life, which are known as the hallmarks of ageing (López-Otín *et al.* 2013).

The hallmarks of ageing: from cell-intrinsic to cell-extrinsic mechanisms

The above-mentioned signatures of ageing are subdivided into three groups: causative or primary hallmarks, comprising genomic damage, telomere shortening, epigenetic alterations and loss of proteostasis; antagonistic hallmarks, characterized by nutrient sensing dysregulation, mitochondrial dysfunction, and cellular senescence induction; and integrative hallmarks that manifest as aged phenotype progresses, which include the exhaustion of the stem-cell pool and changes in intercellular communication (López-Otín *et al.* 2013). This classification has contributed to conceptualize the molecular alterations involved in ageing from individual cells to the organismal level. However, this global attempt to define ageing has also evidenced the current limits of our knowledge in this field and has raised some critical questions. The molecular and cellular alterations considered as age-related cell-intrinsic defects have been proposed as the main drivers of ageing for years (Rossi *et al.* 2005; Choudhury *et*

al. 2007). However, it has recently been established that cell-non-autonomous mechanisms, including those derived from the exhaustion of the stem cell pool, the accumulation of senescent cells, deregulated nutrient sensing, and chronic low-grade inflammation can act similarly over organismal ageing progression by affecting mechanical and functional properties of tissues and organs (López-Otín *et al.* 2013; Freitas-Rodríguez *et al.* 2017) (**Figure 1**). Consequently, ageing is no longer studied as a mere deterioration process that is intrinsic to the cell. Instead, current research takes into account the associated changes occurring at an intercellular level and, subsequently, at the tissue and organismal levels. Thus, understanding the mechanisms that drive ageing is not possible without unveiling the relative contribution of cell-intrinsic *versus* extracellular factors, as well as the interactions between them, during the process of ageing.
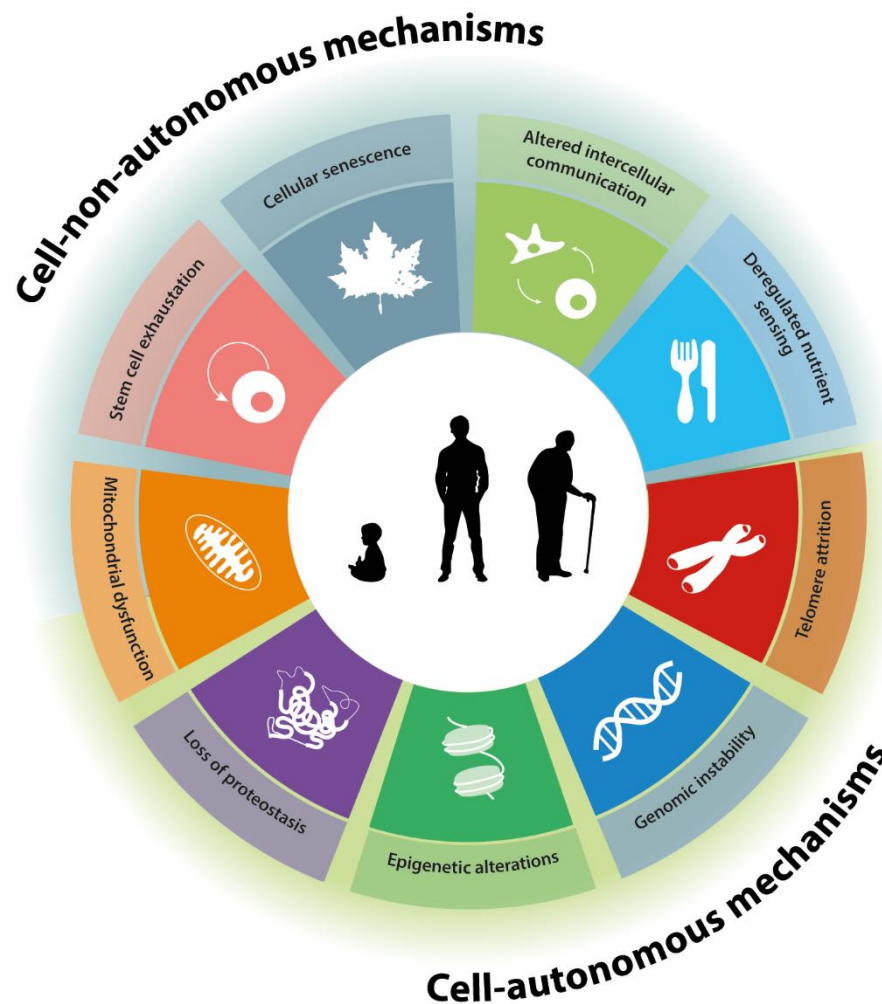

Figure 1. The hallmarks of ageing categorized as cell-autonomous and cell-non-autonomous mechanisms. Adapted from López-Otín *et al.* 2013.

Regarding cell-intrinsic alterations, a large number of genetic variants have been identified as key modulators of longevity. The first ageing regulators were discovered by using conventional approaches that were characterized by the small number of genes examined (gene-by-gene approach) and the use of living model organisms, which usually involved long-term experiments and high maintenance costs (Klass 1983; Mitchell *et al.* 2015). Nowadays, the availability of high-throughput technologies has provided the scientific community with useful *-omics* data to gain an understanding of the intrinsic alterations that may modulate ageing from a genome-wide perspective (de Magalhaes *et al.* 2010). The accomplishment of the Human Genome Project contributed to identify the gene alterations causative of many age-related diseases, but it also led to a greater understanding of the genetic bases of ageing (Tacutu *et al.* 2018). Likewise, the analysis of the genome of long-lived species has allowed the identification of adaptations that contribute to longevity and disease resistance, pointing towards certain molecular factors and pathway as central nodes of lifespan regulation across the evolution (Ma and Gladyshev 2017). For instance, our laboratory has contributed to define the signatures of these evolutionary adaptations by analysing the genome of the bowhead whale, an extreme case of long-living mammal resistant to cancer and other age-associated diseases (Keane *et al.* 2015). Nevertheless, a large part of the evolutionarily conserved determinants of longevity remains to be elucidated, probably due to the complex interaction among critical control nodes shared by multiple biological routes and their modulation at the organism level.

On the other hand, an increasing number of studies have tried to elucidate the regulatory mechanisms that systemically integrate those cell-intrinsic alterations that take place during physiological and pathological ageing. In this regard, systemic factors have recently emerged as key players in ageing modulation, acting in a paracrine and endocrine manner over cells and tissues and coordinating their decline (López-Otín *et al.* 2013). Although few rejuvenating or pro-ageing factors have been identified to date, many current studies have focused on these secreted molecules, or in the cells that produce them, in order to find new anti-ageing therapies. For example, many studies have pointed to senescent cells as one of the main effectors of tissue functional decline over time, not only due to their non-proliferative nature, which restricts the regenerative potential of the tissue, but also because of the factors secreted by these cells (van Deursen 2014; Pignolo *et al.* 2020). The secretory phenotype associated with senescent

cells or "senescence-associated secretory phenotype" (SASP) is characterized by the production and release of pro-inflammatory cytokines and proteases to the cellular microenvironment. These factors act locally on neighbouring cells or systematically, generating a phenotype of chronic inflammation that progressively alters tissue architecture and homeostasis, also by inducing the conversion to secondary senescent cells (Borghesan *et al.* 2020). In fact, SASP is part of the pro-inflammatory status that many cells and tissues develop over time, a condition often named inflammageing, which is considered as a risk factor for many age-associated chronic diseases (Ferrucci and Fabbri 2018).

Recent studies have compared senescence and ageing processes, suggesting that aged cells may also secrete pro-ageing factors that induce "gero-conversion" of their nearby cells, thereby contributing to the progression of ageing-associated alterations (Schmeer *et al.* 2019). In this context, there are evidences supporting the idea that the changes produced in an aged tissue can lead to the physiological and functional decay of other healthy tissues, which could explain the coordination between the different organs and systems during the organismal ageing (López-Otín *et al.* 2013). The first observations regarding ageing modulation by cell-extrinsic factors derived from the development of parabiosis models during the 20th century (Finerty 1952). Since animals in parabiosis only share their circulation, the establishment of this type of model allows researchers to determine whether exclusively systemic factors can alter the tissue function. Thus, this experimental approach has demonstrated that the stem cells of skeletal muscle from aged animals can recover their proliferative and regenerative potential after being exposed to the factors present in the serum of young animals (Conboy *et al.* 2005); or that age-associated cardiac hypertrophy can be reverted by the exposure to a young circulatory microenvironment (Loffredo *et al.* 2013). In contrast, exposure of young animals to an aged systemic milieu is capable of inhibiting myogenesis (Brack *et al.* 2007) and neurogenesis (Villeda *et al.* 2011), demonstrating that tissue decline can be extrinsically modulated by the existence of secreted factors that may be systemically transported.

Another critical component of the cell-extrinsic space is the extracellular matrix (ECM), a dynamic structure composed of a set of proteins that exert a variety of functions during development and tissue homeostasis through their unique biochemical and biomechanical properties. Hence, it is not surprising that dysregulation of the ECM

structure may contribute to the ageing process (Freitas-Rodríguez *et al.* 2017). Proteases constitute an extensive group of enzymes that catalyse the breakdown of proteins by hydrolysis of their peptide bonds and that are involved in multiple biological processes. For this reason, protease activity needs to be tightly regulated, since impaired or dysregulated proteolytic function has been associated with ageing and many pathological conditions (Puente *et al.* 2003; Quirós *et al.* 2015; Pérez-Silva *et al.* 2016). Thus, the resulting modifications that take place by proteolytic dysregulation in the ECM during ageing ultimately impact on its structure and composition, thereby altering ECM biological functions (Kular *et al.* 2014; Birch 2018). Consequently, an aged ECM negatively affects its environment, which includes critical cellular compartments, such as the stem cell pool or senescent cells, underpinning the onset of ageing and age-related diseases (Ermolaeva *et al.* 2018).

Together, the numerous pathways involved in ageing modulation by cell-intrinsic and -extrinsic mechanisms underscore the complexity of the time-dependent functional decline of living organisms, but they also provide the molecular basis to develop new therapeutic approaches based on targeting some of these integrative mechanisms.

Human premature ageing syndromes

Our improved understanding of the molecular bases of ageing also derives from studies on premature ageing syndromes. Accelerated ageing syndromes, also known as progeroid syndromes or progeria, are a group of extremely rare genetic disorders characterized by displaying many of the clinical features associated with physiological ageing (Kubben and Misteli 2017). However, contrary to normal ageing, the symptoms appear in the first years of life of the patient (Gordon *et al.* 2014b; Melzer *et al.* 2020). Although progeroid syndromes share many of their phenotypic outcomes, they are caused by a variety of mutations, thereby involving different underlying mechanisms. Consequently, they constitute a great opportunity to explore the variety of biological pathways implicated in their phenotypic manifestations, which might also impinge on the development of physiological ageing features (Carrero *et al.* 2016).

Hutchinson-Gilford progeria syndrome (HGPS) is one of the most widely studied premature ageing syndromes. Commonly, this disorder is caused by a *de novo*

point mutation (p.G608G) in the *LMNA* gene, which encodes lamin A and lamin C isoforms. This specific mutation activates a cryptic splicing donor site whose use results in the loss of an aminoacidic sequence located at the C-terminus of prelamin A, which is essential for its post-translational cleavage by the metalloprotease ZMPSTE24 (De Sandre-Giovannoli *et al.* 2003; Eriksson *et al.* 2003). Thus, this mutation leads to the accumulation of a toxic protein called progerin that causes assembly defects in the nuclear envelope, eventually leading to the activation of DNA damage pathways (Gordon *et al.* 2014b). These alterations compromise tissue homeostasis and give rise to multiple clinical manifestations, such as growth impairment, lipodystrophy, bone abnormalities and, most importantly, several cardiovascular alterations that are responsible for the death of patients from myocardial infarction or stroke at an average age of 14.6 years (Gordon *et al.* 2014a; Rivera-Torres *et al.* 2016; Hamczyk *et al.* 2018b). Similar to HGPS, mandibuloacral dysplasia (MAD) is another genetic condition originated by mutations in key elements essential for the proper assembly of the nuclear envelope, whose clinical manifestations include lipodystrophy and skeletal and metabolic abnormalities among others. Attending to its causal mutations, MAD is categorized as MAD with type A lipodystrophy (MADA), which is caused by the homozygous p.R527H *LMNA* mutation (Novelli *et al.* 2002); or MAD with type B lipodystrophy (MADB), which is caused by compound heterozygous mutations in *ZMPSTE24* gene (Agarwal *et al.* 2003). Both types of MAD lead to the accumulation of unprocessed prelamin A and the subsequent disruption of the nuclear architecture.

Considering the low prevalence of premature ageing disorders, the use of murine models of these diseases has been critical to gain insights into their molecular basis, as well as to evaluate the potential therapeutic effect of different anti-ageing interventions. Over the last years, a variety of progeroid mouse models have been generated, allowing the elucidation of the regulatory pathways involved in the pathogenesis of these syndromes (Folgueras *et al.* 2018). In this context, our laboratory has generated two mouse models of accelerating ageing, *Lmna*$^{G609G/G609G}$ knock-in mice and *Zmpste24*-deficient mice, which mimic the genetic defects found in the above-mentioned syndromes. Thus, the first one harbours the c.1827C>T (p.G609G) mutation in the gene *Lmna*, which is equivalent to the c.1824C>T (p.G608G) mutation present in patients with HGPS. The second one is a knockout (KO) mouse model that lacks the metalloprotease Zmpste24, which is responsible for the last step of lamin A

maturation. Both mouse models accumulate either prelamin A or an aberrant isoform of this unprocessed protein (progerin) at the nuclear envelope (**Figure 2**), and recapitulate many of the phenotypes observed in HGPS patients, including shortened lifespan, growth retardation, alopecia, osteoporosis, kyphosis, lipodystrophy, and several cardiovascular pathologies (Pendás *et al.* 2002; Yang *et al.* 2006; Osorio *et al.* 2011; Villa-Bellosta *et al.* 2013; Rivera-Torres *et al.* 2016). The use of both models has contributed to unravel the molecular bases of these disorders (Varela *et al.* 2005; Osorio *et al.* 2012; Hamczyk *et al.* 2018b), as well as to evaluate different anti-ageing interventions, such as diet modulation, microbiota transplants or *in vivo* CRISPR/Cas9-based therapies (Bárcena *et al.* 2018; Bárcena *et al.* 2019; Santiago-Fernández *et al.* 2019). Remarkably, the accumulation of progerin is also observed during normal ageing (Scaffidi and Misteli 2006), for example, in the vascular smooth muscle cells (VSMCs) of aged patients with atherosclerotic lesions (Olive *et al.* 2010; Ragnauth *et al.* 2010; Liu *et al.* 2013b). Together, these findings highlight the usefulness of these mouse models not only in progeria research, but also to delve deeper in our understanding of normal ageing and its related diseases.

Cell-intrinsic and -extrinsic alterations in progeroid mouse models

As it occurs in physiological ageing, the progeroid phenotype observed in many of the premature ageing mouse models is triggered by a tight interplay between cell-intrinsic and -extrinsic mechanisms. Since most of these mouse models have been generated by mimicking the genetic causal mutations observed in their human counterparts, the contribution of cell-intrinsic alterations to the onset of the progeroid phenotype is more intuitive. For example, progeroid mouse models harbouring mutations in components of the DNA repair machinery exhibit irreparable genomic damage that finally leads to genomic instability and transcriptional alterations (Lans *et al.* 2019). Similarly, the accumulation of progerin triggers the development of nuclear abnormalities that lead to most of the molecular mechanisms that impair genome maintenance (Vermeij *et al.* 2016). In addition, epigenetic modulation is another intrinsic mechanism with a prominent role in the control of lifespan whose imbalance contributes to the progression of the progeroid features exhibited by these mouse models. For instance, *Zmpste24*-deficient mice display aberrant epigenetic

modifications of histones, such as the hypoacetylation of H4 or H2B, which jeopardize DNA repair machinery recruitment and alter the expression of genes involved in the control of cell proliferation and metabolism (Krishnan *et al.* 2011; Osorio *et al.* 2010); or the enhanced trimethylation of H3K9, which promotes chromatin compaction (Liu *et al.* 2013a).
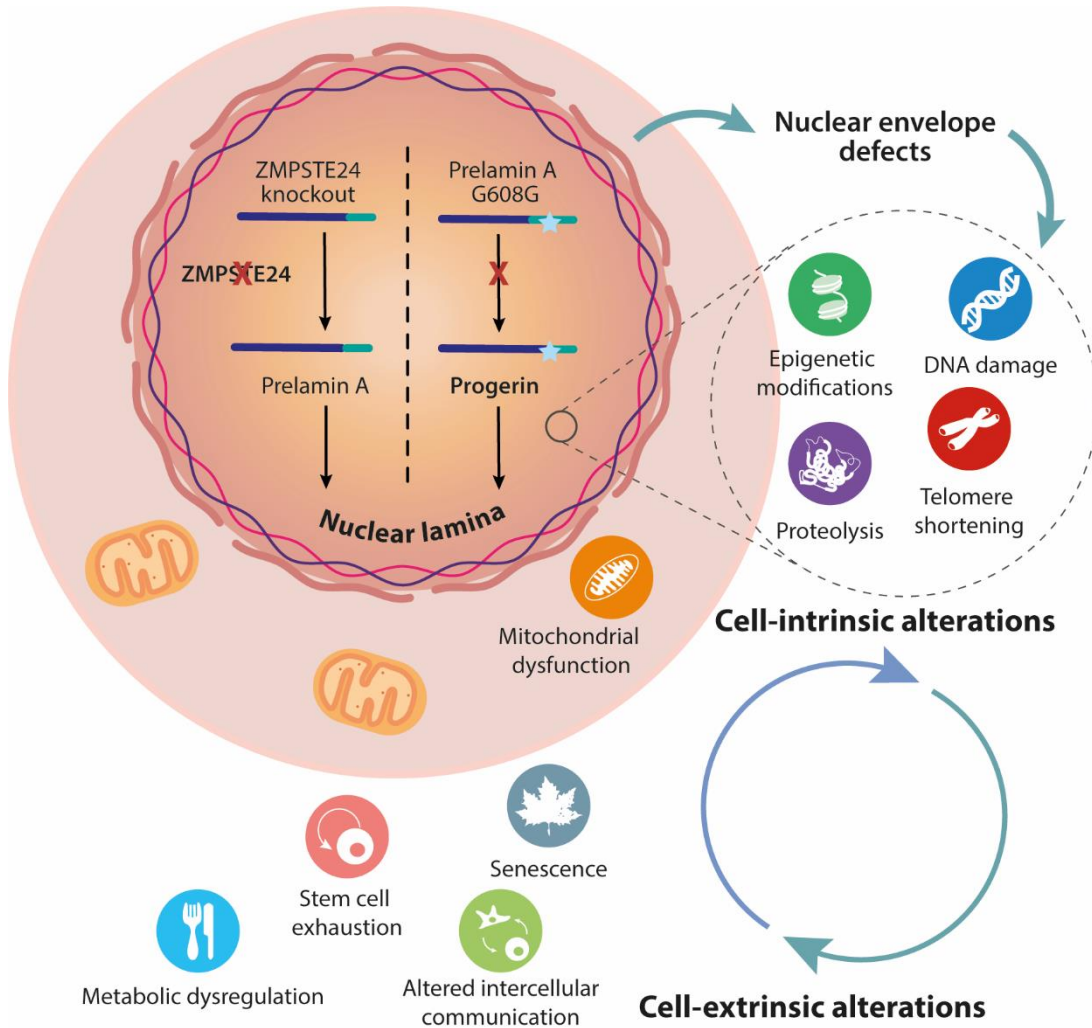

Figure 2. Cellular defects that underlie premature ageing disorders split into cell-intrinsic and -extrinsic alterations. Normal processing of prelamin A requires multiple post-translational modifications to generate its mature form lamin A, favoring the normal assembly of the nuclear envelope. In HGPS cells, the presence of the genomic mutation G608G activates a cryptic splicing site that hampers its processing by the protease ZMPSTE24, leading to the accumulation of a toxic isoform of prelamin A named progerin. The incorrect processing of prelamin A, either by the presence of HGPS mutation or by the absence of ZMPSTE24, leads to the disruption of the nuclear envelope and induces cell-intrinsic defects, such as DNA damage or epigenetic modifications. These cell-intrinsic alterations promote the onset of other hallmarks of ageing, such as senescence or intercellular communication dysfunction that can exert cell-extrinsic effects that promote the ageing process. Hence, this tight interplay between

cell-intrinsic and -extrinsic hallmarks in an ageing context finally triggers the classical phenotypes observed in progeroid syndromes. Adapted from Kubben and Misteli, 2017.

Together, these alterations directly impact on transcriptional processes that modulate gene expression across diverse tissues and organs. Therefore, in addition to the relevance of these cell-intrinsic changes as drivers of the premature ageing phenotype, these intrinsic perturbations can also promote the development of cell-extrinsic alterations that systemically coordinate the progression of progeroid features, which ultimately determine the health and lifespan of these organisms (**Figure 2**). In this regard, the relevance of cell-extrinsic factors in the progression of the progeroid phenotype has been evidenced by the generation of the Zmpste24-mosaic mouse model by our laboratory. These mice harbour 50% *Zmpste24*-deficient cells coexisting with another 50% wild-type cells. The presence of only a half of normal cells is enough to completely rescue the striking phenotype of accelerated ageing of *Zmpste24$^{-/-}$* mice (de la Rosa *et al.* 2013), suggesting that structural or secreted factors can modulate the onset of progeria in a systemic manner.

One of the cell-extrinsic mechanisms that directly contribute to the organismal decline of progeroid mice is the exhaustion of the stem cell pool compartment, which can be triggered by genomic alterations that impair their proliferation capacity (Espada *et al.* 2008; Song *et al.* 2013; Cho *et al.* 2013; Yang *et al.* 2017). Likewise, stem cell defects can be caused by altered epigenetic regulation of different signalling pathways (Molofsky *et al.* 2005; Oguro *et al.* 2006; Wang *et al.* 2016; Hu *et al.* 2019), as well as by secreted factors that exert a detrimental effect on their niche thereby affecting stem cell behaviour.

Notably, recent works have also highlighted the relevance of cellular senescence in a context of accelerated ageing. Thus, the generation of transgenic mouse strains carrying senescent cell-specific reporters and suicide cassettes has allowed the tracking of their *in vivo* dynamics over time, as well as the impact of their specific elimination. In this context, selective removal of senescent cells has shown a positive effect on the progeroid features and lifespan of *BubR1*$^{H/H}$ mice, which harbour a mutation that impairs chromosomal segregation (Baker *et al.* 2011). Also, similar results over healthspan were observed using senolytic drugs that selectively removed senescent cells in *Ercc1$^{-/\Delta}$* progeroid mice (Zhu *et al.* 2015) carrying a mutation in a

component of the nucleotide excision repair (NER) machinery, reinforcing the notion on the interplay between cell-intrinsic and -extrinsic mechanisms as part of the ageing process.

Likewise, systemic mechanisms responsible for the development of progeria also include alterations in cell-cell communication. Thus, *Zmpste24*$^{-/-}$ mice exhibit hyperactivation of inflammatory signalling pathways, a situation that is exacerbated by the secretion of senescence-associated proinflammatory cytokines (Osorio *et al.* 2012). Altered intercommunication also manifests through the dysregulation of multiple nutrient sensing routes that eventually jeopardize metabolic homeostasis in progeroid mice by affecting central nodes of metabolic control, such as autophagy, somatotropic axis or lipid metabolism (Mariño *et al.* 2008; Mariño *et al.* 2010; Peinado *et al.* 2011).

In summary, premature ageing features result from a complex crosstalk between cellular and extracellular mechanisms, resembling the molecular bases of physiological ageing. Thus, it is feasible to use progeroid mouse models to gain a better understanding of the interactions between both mechanisms and, hopefully, discover more effective interventions to manage progeria and even normal ageing.

Bone resorption and vascular calcification: two closely related processes from an ageing perspective

Among the clinical manifestations that are frequently found in many progeroid syndromes and physiological ageing, atherosclerosis and osteoporosis stand out, *a priori* being two unrelated chronic conditions that have traditionally been attributed to independent processes associated with age. Osteoporosis is the most prevalent bone disorder worldwide, and is characterized by a progressive loss of bone mass that usually involves an increase in the risk of fracture (Yang *et al.* 2020). Although the molecular bases of this disease are not fully understood, it is well established that the dysregulation of bone metabolism has a critical role in its pathogenesis (Compston *et al.* 2019). To accomplish its functions and preserve its integrity, bone tissue needs to be constantly replaced in a process called bone remodelling. Thus, bone homeostasis is maintained by the coordinated actions of two opposite processes: i) bone formation, which is maintained by the action of the osteoblasts; and ii) bone resorption, which is

carried out by osteoclast cells. This osteoblast–osteoclast coupling is based on the reciprocity between both cell types that mutually regulate their differentiation and activity. In this context, osteoblasts secrete a variety of primary cytokines, such as *macrophage colony-stimulating factor* (M-CSF), *receptor activator of nuclear factor kappa-B ligand* (RANKL), and osteoprotegerin (OPG) that regulate the activation of the molecular programs responsible for osteoclast differentiation. Conversely, osteoclast precursors produce bone morphogenetic proteins (BMPs) and other growth factors that induce the expression of transcription factors, such as *runt-related transcription factor 2* (RUNX2) and osterix (OSX), which promote osteogenesis thereby ensuring the balance between formation and resorption during bone remodeling (Lerner *et al.* 2019). In addition, osteocytes, the terminally differentiated form of osteoblasts, also control this process by secreting factors that modulate the function of bone-forming osteoblasts and bone-resorbing osteoclasts (Sims and Walsh 2012; Chen *et al.* 2018).

In a physiological context, bone has classically been considered as a passive organ system whose functions were restricted to provide a consistent scaffold to support the whole body, allowing an appropriate mobility. However, multiple studies have emphasised a wide variety of roles for bone tissue besides its structural functions, such as the control of calcium metabolism, the niche for hematopoietic stem cells or the regulation of several metabolic pathways through the secretion of growth factors, cytokines or peptide hormones (Han *et al.* 2018). Therefore, it is not surprising that those genetic alterations that affect the production of secreted factors involved in the function of bone cells lead to dysregulation of bone homeostasis and cause bone disorders (Baron and Kneissel 2013; Wu *et al.* 2016). In addition, given the potential systemic role of bone tissue, it is conceivable that the loss of bone homeostasis might also contribute to the onset of other pathologies, such as atherosclerosis or chronic kidney disease (Naves *et al.* 2008).

As mentioned above, osteoporosis and atherosclerosis have been considered for many years as independent processes whose sole connection was their increasing prevalence with age. However, recent data provided by epidemiologic and clinical studies suggest a direct relationship between impaired bone metabolism and vascular calcification, emphasising that a dysregulation of bone turnover can promote the calcification of soft tissues (Raggi *et al.* 2007; Chen *et al.* 2020). Thus, excessive bone

resorption can promote the accumulation of mineral components like phosphorus or calcium within soft tissues, inducing the expression of osteogenic factors, such as RUNX2 or BMP2, which trigger the acquisition of an osteoblast-like phenotype by vascular smooth muscle cells (VSMCs) (Shanahan *et al.* 2011; Durham *et al.* 2018). These events lead to the thickening of intimal and medial vascular layers, contributing to the loss of elasticity of the vasculature (**Figure 3**), which is one of the main features of vascular ageing usually observed in the elderly population.
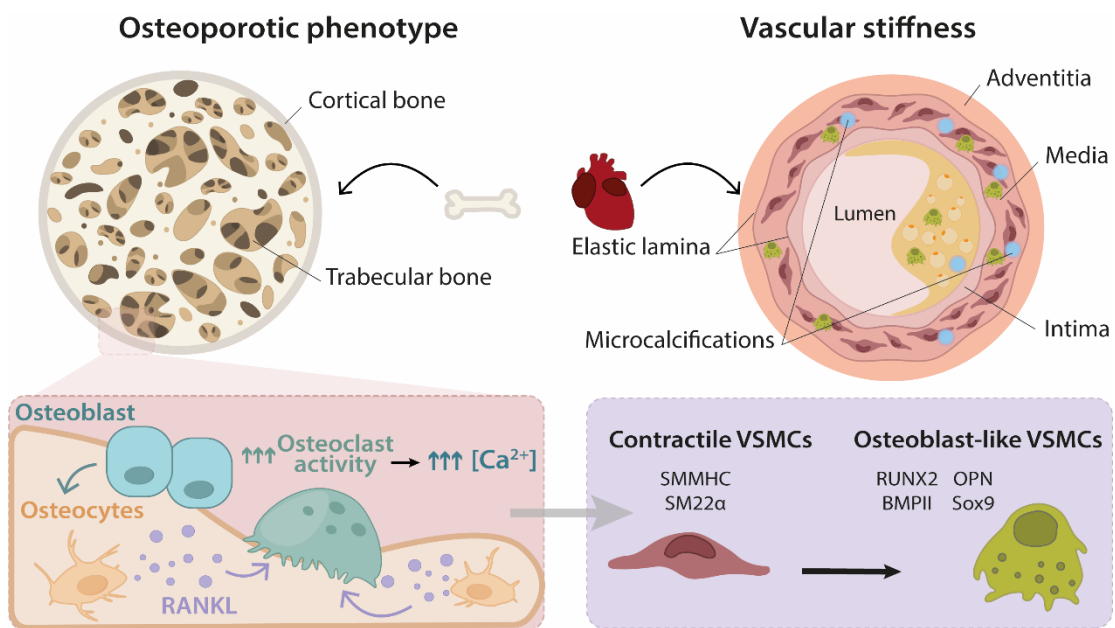

Figure 3. Relationship between RANKL-mediated bone resorption and the molecular mechanisms involved in the onset of vascular calcification.

Although several studies have demonstrated the benefits of inhibiting bone resorption to slow down the progression of vascular stiffness and atherosclerosis in different pathological contexts (Caffarelli *et al.* 2017), a better understanding of the molecular connections between both processes is still required. Furthermore, considering that atherosclerosis, vascular calcification, and loss of bone mass are among the main clinical features observed in premature ageing syndromes, we can take advantage of the use of progeroid mouse models to explore their biological relationship. In this regard, a previous study of our laboratory demonstrated that combined treatment with statins and aminobisphosphonates extends the longevity and ameliorates age-related phenotypes of *Zmpste24*-deficient mice (Varela *et al.* 2008).

However, it is still unclear whether these effects are exclusively derived from the inhibition of the farnesylation and geranylgeranylation of prelamin A, which ultimately blocks the accumulation of progerin and its subsequent detrimental consequences over the cell or whether the anti-osteoporotic properties of aminobisphosphonates also contribute to improve the overall health status of *Zmpste24*^{-/-} mice by maintaining bone homeostasis and preventing vascular calcification. Consequently, we wondered about the functional relevance of exclusively inhibiting bone resorption and its possible effect on the establishment of vascular stiffness, and the amelioration of the progeroid phenotype.

Metabolic dysregulation in ageing and age-associated diseases

A common crossroad in the pathogenesis of ageing and metabolic disorders is the critical involvement of altered intercellular communication (López-Otín *et al.* 2016). Numerous studies have demonstrated the effectiveness of metabolism-based interventions, such as inhibition of trophic signalling, exercise or caloric restriction, in ameliorating the features of ageing and progeria, as well as increasing the lifespan of various animal models (López-Otín *et al.* 2016; Neufer *et al.* 2015; Bitto *et al.* 2016; Mattison *et al.* 2017). In fact, the first evidence demonstrating the possibility of extending lifespan through genetic manipulation comes from the generation of specific mutants of *Caenorhabditis elegans* affecting *daf-2*, an ortholog of the mammalian insulin and insulin-like growth factor-1 (IGF1) receptors (Kimura *et al.* 1997). This observation was further confirmed later in mice, demonstrating that these pathways are well conserved through evolution as central nodes of lifespan regulation (Vitale *et al.* 2019). Nevertheless, the modulation of endocrine pathways by specific gene mutations has a peculiarity; despite the fact that these are considered as cell-intrinsic alterations, they also exert cell-non-autonomous effects on the ageing process (Russell and Kahn 2007; López-Otín *et al.* 2016). For instance, the generation of a mouse strain lacking the insulin receptor specifically in the adipose tissue (FIRKO mice) yielded mice with increased lifespan, presumably as a consequence of the systemic effect caused by modulating insulin signalling (Bluher *et al.* 2003). In addition, besides insulin and IGF1 signalling, there are other endocrine regulators that modulate ageing. Several studies

have demonstrated that the overexpression of KLOTHO, a protein located at the cell membrane that also exists as a circulating factor (Shiraki-Iida *et al.* 1998; Imura *et al.* 2004), extended lifespan in mice, at least in part by inhibiting the insulin/IGF-1 axis (Kurosu *et al.* 2005; Kuro 2019). Moreover, tissue-specific overexpression of KLOTHO is sufficient to rescue some of the premature ageing features of *Klotho*-deficient mice, supporting its role in the modulation of ageing as a circulating factor (Kuro *et al.* 1997; Kurosu *et al.* 2005).

Many of the alterations found in pathways involved in the control of energy metabolism during ageing are triggered by the adipose tissue dysfunction associated to age decline (Bustos and Partridge 2017; Spinelli *et al.* 2020). Thus, increased number of senescent cells promotes systemic inflammation and, thereby, adipose tissue impairment (Liu *et al.* 2020). In this regard, several markers of inflammation are associated with the accumulation of immune cells in visceral adipose tissue, including proinflammatory cytokines such as IL-6, TNF-α or TFG-β1 (Kratz *et al.* 2014). In particular, the loss of lipid homeostasis is at least partly driven by the low-grade inflammation concomitantly associated with ageing and obesity, which is eventually triggered by adipose tissue dysfunction (Unamuno *et al.* 2018; Tam *et al.* 2020). Moreover, both systemic dysregulation of adipose tissue function and loss of lipid homeostasis are two conditions involved in the pathogenesis of metabolic disorders, such as type 2 diabetes mellitus (T2DM) and obesity, or associated pathologies such as cardiovascular disease (CVD) (Hajer *et al.* 2008; Huby *et al.* 2015).

Together, as mentioned above, the possibility of designing specific interventions targeting metabolic pathways may allow to ameliorate the symptoms of ageing and age-related diseases, especially taking advantage of their ability to exert a systemic effect through the control of energy metabolism. Moreover, the benefits obtained using the aforementioned approaches highlight the relevance of understanding the relationship between metabolic diseases and ageing, and the necessity of looking for key molecular connectors between both pathologies to find new interventions aimed at achieving a healthy ageing state.

Contribution of iron imbalance to the pathogenesis of metabolic disorders

Iron is an indispensable element required for a broad range of critical processes essential for cell survival, including oxygen transport, DNA synthesis or oxidation-reduction reactions involved in energy production. Consequently, cells require the coordination between all pathways and mechanisms involved in iron regulation to preserve its intracellular and systemic levels. On one hand, cellular iron homeostasis is maintained by a coordinated post-transcriptional regulation of several genes involved in the uptake, storage, and export of iron (Muckenthaler *et al.* 2017). On the other hand, systemic iron levels are mainly controlled by two regulators, ferroportin and hepcidin. The first one, ferroportin, is the only known iron exporter from cells to plasma that exerts its main function in enterocytes, macrophages, and hepatocytes, whereas hepcidin is a circulating peptide hormone with antimicrobial functions whose expression is up-regulated by iron overload, promoting its binding to ferroportin and stimulating its degradation. This phenomenon leads to the cellular retention of iron and, therefore, to the reduction of its serum levels (**Figure 4**) (Bogdan *et al.* 2016). Since both cellular and systemic iron levels need to be tightly regulated, the perturbation of the mechanisms that control iron metabolism causes the development of pathological conditions characterized by either the accumulation of iron or its deficiency (Dev and Babitt 2017). In this context, previous studies in our laboratory demonstrated that type II transmembrane serine protease matriptase-2 (encoded by *Tmprss6*) (Folgueras *et al.* 2008) also plays a relevant role in iron metabolism, since its deficiency in mice causes a striking phenotype of iron deficiency anemia resulting from the marked up-regulation of hepcidin in the liver (Folgueras *et al.* 2008). Moreover, *Tmprss6*-deficient mice mimic the symptoms observed in human patients with iron-refractory iron deficiency anemia (IRIDA), a disease triggered by autosomal mutations in *TMPRSS6* and characterized by the lack of hematological improvement following oral iron administration (Ramsay *et al.* 2009).
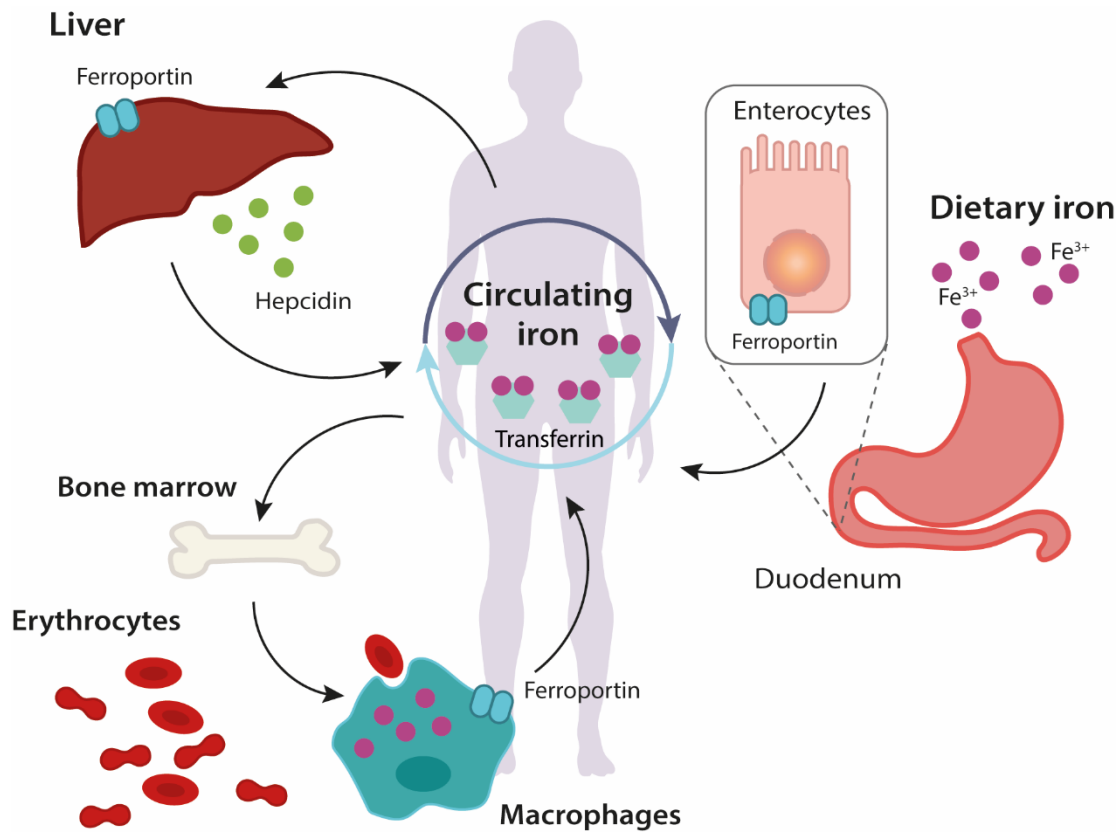
Figure 4. Regulatory mechanisms implicated in the maintenance of cellular and systemic iron homeostasis. The absorption of iron takes place in the duodenum, concretely by the enterocytes, in which iron is either stored associated to cellular ferritin or released directly into the circulation by the basolateral exporter ferroportin. The efflux of iron into the systemic circulation is inhibited by hepcidin, a peptide hormone produced by hepatocytes that binds to ferroportin an induces its degradation. In addition, systemic levels of iron are controlled by macrophages, which break down senescent red blood cells and release iron again into the circulation by the exporter ferroportin. Extracellular iron circulates in the plasma bound to transferrin, and is internalized and stored into cells, such as hepatocytes, by several transferrin-dependent mechanisms.

Several studies have suggested the existence of a relationship between ageing and inappropriate contents of iron in different tissue compartments. In this regard, anaemia is a common feature of the elderly (Stauder *et al.* 2018), which has negative effects over multiple conditions such as muscle strength, cognition, or longevity (Roy 2011; Ashraf *et al.* 2018). Furthermore, the dysregulation of iron homeostasis has also detrimental consequences in age-associated pathologies such as cancer, cardiovascular diseases, or neurodegenerative diseases (Brown *et al.* 2020; Cornelissen *et al.* 2019; Lei *et al.* 2012; Toyokuni 2011). In addition to the above-mentioned disorders, iron

homeostasis is intimately related to the inflammatory response. This relationship is well established, emphasizing that iron levels must be tightly regulated to avoid oxidative stress (Galaris *et al.* 2019). Hence, elevated iron levels increase disease susceptibility, specially by promoting the pathogenesis of inflammatory conditions such as autoimmune disorders, or predisposition to infection (Cronin *et al.* 2019; Weiss *et al.* 2019). In fact, iron dysregulation can eventually trigger metabolic disorders related to inflammation, such as obesity, insulin resistance or non-alcoholic fatty liver disease (NAFLD) (Hubler *et al.* 2015; Simcox and McClain 2013; Dongiovanni *et al.* 2011). Thus, considering the evidences supporting the close association between an inappropriate iron balance and ageing, and their possibly shared link with metabolic dysregulation (Bekri *et al.* 2006; Pihan-Le Bars *et al.* 2016), it would be interesting to explore the relative contribution of matriptase-2, a negative regulator of the circulating factor hepcidin, in the establishment of an age-related metabolic condition such as obesity.

Objectives

The extraordinary improvement in life expectancy over the past century emphasizes the benefits of understanding the molecular mechanisms that regulate ageing and other associated disorders. Far from being only triggered by intracellular stress signalling pathways, ageing progression also requires the systemic coordination of different organs and systems, presumably through cell-extrinsic mechanisms. This complexity highlights the relevance of unveiling the relative contribution of cell- and non-cell-autonomous mechanisms to the ageing process. Nonetheless, the interrelation between these mechanisms may also be conceived as a new therapeutic opportunity in which the amelioration of one or more hallmarks of ageing might have a broader effect on the process of ageing as a consequence of their systemic action.

To gain further insight into the biology of ageing, in this Doctoral Thesis we have studied the functional relevance of cell-intrinsic and -extrinsic mechanisms in the regulation of ageing and other age-related diseases by using different technical approaches. First, we manually annotated and compared the genome of two long-lived giant tortoises in order to unveil intrinsic variants underlying their extraordinary lifespan. Further, we analysed the effect of cell-extrinsic mechanisms on progeroid features and longevity using a murine model of accelerated ageing. Finally, we studied the influence of iron and matriptase-2 (*Tmprss6*), a negative regulator of the circulating factor hepcidin, in the establishment of an age-related metabolic disorder as obesity by using a *Tmprss6*-deficient mouse model challenged with a high-fat diet.

The specific objectives of the present Doctoral Thesis were:

I.- Identification of cell-intrinsic determinants of longevity in the genome of two long-lived giant tortoises by means of a manual annotation approach.

II.- Assessment of the functional relevance of cell-extrinsic mechanisms to the development of the progeroid phenotype in murine models of premature ageing.

III.- Characterization of the role of iron and matriptase-2, a negative regulator of the circulating factor hepcidin, in the development of HFD-induced obesity using a mouse model deficient in matriptase-2.

Experimental procedures

Molecular Biology and Biochemistry methods

General methods

Basic Molecular Biology techniques employed in this work, including genomic DNA isolation, agarose gel electrophoresis or PCR analysis, which are not detailed below, were performed following standard protocols.

Gene variant validation by Sanger sequencing

DNA samples from different tortoises from the Galapagos Islands, including the islands of Santa Cruz (*Chelonoidis porteri*), Española (*Chelonoidis hoodensis*), Isabela (*Chelonoidis becki* and *Chelonoidis vicina*), Pinzón (*Chelonoidis duncanensis*) and Pinta (*Chelonoidis abingdonii*), as well as from the Aldabra atoll (*Aldabrachelys gigantea*), were used. Also, two sets of DNA samples were used as continental outgroups: the first one includes the species *Chelonoidis chilensis*, *Chelonoidis carbonaria* and *Chelonoidis denticulata* for Galapagos Islands tortoises, and the second one includes *Stigmochelys pardalis* for Aldabra tortoise.

Locus-specific primer pairs were used to validate the existence of specific SNPs by carrying out PCR experiments and subsequent Sanger sequencing. For the study of specific variants, primers were designed to target the region where the identified variants were located. To study copy-number variations, different primer pairs were designed for each copy in order that copies could be amplified separately. When this method was not feasible, a region harbouring different nucleotide variants in each copy was selected to be amplified by PCR. Accordingly, detailed analysis of the resulting sequencing electropherograms allowed the distinction of different copies. In all cases, PCR reactions were carried out with 10 ng of DNA under the same general conditions. Only the melting temperature (Tm) was changed depending on the specific primer pairs that were used. PCR reactions were performed as follows: 95 °C, 3 minutes of denaturalization; 95 °C, 60 s; Tm, 30 s of annealing; 72 °C, 30 s of extension; 35 cycles; 72 °C, 7 minutes; 20 °C, 5 minutes. Resulting PCR products were analysed by electrophoresis in a 2% agarose gel to confirm the success of the reaction. Subsequently, PCR products were sequenced using the Sanger method. Sequencing reactions were performed with 1 µL of one of the primers used for PCR amplification

at 10 µM and 50 ng of the amplified DNA in a total volume of 10 µL. When feasible, results from manual annotation were also confirmed by RNA-Seq data obtained from *C. abingdonii* whole blood and from an *A. gigantea* granuloma. Primer sequences used for variant validations and other additional information about PCR reactions are summarized in **Supplementary Information, Table S3**.

DNA genotyping

DNA was extracted by alkaline lysis from mouse tail biopsies. *Tmprss6*$^{-/-}$ mice genotyping was performed by Southern-blot analysis, as previously described (Folgueras *et al.* 2008). *Zmpste24*$^{-/-}$ mice were genotyped using with the following oligonucleotides: 5′-GCTGGCCTTGTTGCTGGAAT-3′, 5′-GCTTCCTCCCTGAGC CAACC-3′ and 5′-CTTCCGGAGCGGATCTCAAA-3′. PCR was performed as follows: 95 °C, 1 minute of denaturalization; 95 °C, 15 s/ 60 °C, 30 s of annealing/ 72 °C, 45 s of extension, 35 cycles. Size for mutant band was 303 base pairs (bp) and 520 bp for wildtype (WT) band. *RANKL*$^{fl/fl}$ mice genotyping was performed with the following primer sequences: 5′-GGCACATGGTCACTTGGTAG-3′ and 5′-AGCTTT TAGAATGCCAATAATTAAA-3′. PCR was performed as follows: 95 °C, 1 minute of denaturalization; 95 °C, 15 s/ 57 °C, 30 s of annealing/ 72 °C, 30 s of extension, 35 cycles. Product size was 290 bp for floxed allele and 150 bp for WT band. *Dmp1-Cre* mice were genotyped using the following oligonucleotides: 5′-TTGCCTTTCTCTCCA CAGGT-3′, 5′-CATGTCCATCAGGTTCTTGC-3′, 5′-CTAGGCCACAGAATTGAA AGATCT-3′ and 5′-GTAGGTGGAAATTCTAGCATCATCC-3′. PCR was performed as follows: 95 °C, 1 minute of denaturalization; 95 °C, 30 s/ 60 °C, 15 s of annealing/ 72 °C, 45 s of extension, 35 cycles. Product size was 167 bp for transgene allele and 324 bp for sample positive control band.

RNA isolation

About 30-50 mg of frozen tissue were homogenized with a T 10 basic ULTRA-TURRAX homogenizer in TRIzol reagent (Life Technologies). Total RNA was isolated by using the RNeasy mini kit (Qiagen). RNA spin columns were eluted in 20 µL of nuclease-free water (Life Technologies). RNA concentration and purity (260/280

nm ratio) were determined with a NanoDrop ND-100 spectrophotometer (NanoDrop Technologies).

Real-time quantitative PCR (qPCR)

1-4 µg of total RNA were used to synthesize cDNA with the ThermoScript RT-PCR system (Invitrogen) following manufacturer's instructions. qPCR was carried out in triplicate for each sample with 100 ng of cDNA using Taqman PCR Master Mix (Applied Biosystems) or Power SYBR® Green PCR Master Mix (Life Technologies) and an Applied Biosystems 7300HT Real-Time PCR System. *Hamp* mRNA levels were quantified using Taqman assays (Applied Biosystems). *Actb* and *Rn18s* were used as endogenous controls to normalize gene expression in liver or adipose tissue samples, respectively. Relative expression is represented as relative quantification, using the RQ value (RQ=$2^{-\Delta\Delta Ct}$). Primer sequences are listed in **Supplementary Information, Table S5**.

Protein isolation and Western-blot analysis

Collected tissues were snap frozen in dry ice. About 50 mg of frozen tissue samples were homogenized with a T 10 basic ULTRA-TURRAX homogenizer in 200 µL of RIPA buffer (100 mM Tris-HCl (pH 7.4), 150 mM NaCl, 1% Triton X-100, 2% SDS, 50 mM EDTA) supplemented with cOmplete protease inhibitors (Roche) and PhosSTOP phosphatase inhibitors (Sigma). Protein concentration was determined by using the bicinchoninic acid assay (Pierce BCA protein assay kit). 20 µg of white adipose tissue (WAT) samples or 50 µg of liver samples were separated in 10% SDS-PAGE gels and transferred in CAPS buffer (10 mM 3-[cyclohexylamino]-1-propanesulfonic acid, pH 10.5, and 20% methanol) onto polyvinylidene difluoride (PVDF) membranes (Millipore). To analyse circulating protein levels, 3 µL of plasma samples were separated in 14% SDS-PAGE gels and transferred using the aforementioned conditions. Blots were blocked with 3-5% non-fat dry milk in TBS-T buffer (20 mM Tris-HCl (pH 7.4) 150 mM NaCl, and 0.05% Tween 20) for 1 hour at room temperature and incubated overnight at 4 °C with 3-5% bovine serum albumin (BSA) in TBS-T buffer with rabbit polyclonal antibodies against phospho-HSL-Ser660

(Cell Signaling, #4126, 1:4000), HSL (Cell Signaling, #4107, 1:4000), and ATGL (Cell Signaling, #2138, 1:4000); rabbit monoclonal anti-GDF11/8 antibody (Abcam, #ab124721); and mouse monoclonal antibodies against HPRT (Santa Cruz, #sc-376938, 1:1000) and TfR1 (Thermo Fisher, #13-6800, 1:1000). Finally, blots were incubated for 2 h at room temperature in 1.5% non-fat dry milk in TBS-T buffer with horseradish peroxidase-coupled (HPR) secondary antibodies, washed and developed with Immobilon Western Chemiluminescent HRP substrate (Millipore). Chemiluminescent images were acquired with a Fujifilm LAS3000 mini apparatus.

ELISA assays

Blood samples collected using EDTA or heparin anticoagulants were centrifuged at 1000g at 4 ºC, and the supernatant was stored at -80 ºC until analysis. For metabolic determinations, plasma insulin, leptin and ferritin levels were quantified by using enzyme-linked immunosorbent assay (ELISA) kits (Millipore ELISA Kit, #EZRMI-13K; R&D ELISA Kit, #MOB00; Abcam ELISA Kit, #ab157713), following manufacturer's instructions.

Determination of liver triglycerides

Liver triglycerides were determined by using the EnzyChrom Triglyceride Assay Kit from BioAssay Systems (ETGA-200), according to the manufacturer's protocol. For sample preparation, 50 mg of tissue were homogenized in 500 µL of 5% Triton X-100. Once homogenized, samples were introduced in a water bath at 80 °C and left inside for 5 minutes allowing them to reach 100 °C in the water bath. We repeated this procedure twice, allowing the samples to settle at room temperature between cycles. After that, samples were centrifuged for 5 minutes at 13000 rpm. The supernatant was recovered and diluted 8-fold in MilliQ water. 10 µL of this dilution was used for the assay. Samples obtained from anti-HJV-treated *Tmprss6$^{-/-}$* and wild-type mice required a further dilution prior the assay.

Adipocyte and stromal-vascular fraction isolation

Adipocytes and stromal-vascular fractions (SVF) were isolated from epididymal WAT samples. 100 mg of this tissue were minced with surgical scissors and incubated at 37 °C for 45 minutes with constant agitation in Hank's Balanced Salt Solution (HBSS) containing 2 mg/mL of collagenase I and II (Sigma) and 2% BSA. After digestion, samples were centrifuged for 10 minutes at 300g in conical tubes at 4 °C. The upper fat layer containing floating adipocytes was collected into a separated tube and washed with HBSS buffer. The pellet containing the stromal vascular fraction was resuspended in HBSS buffer and filter through 100 µm nylon mesh. Both fractions were centrifuged once more for 10 minutes at 400g at 4 °C. Isolated adipocytes and SVF fractions were snap-frozen and kept at -80 °C until analysis.

Iron quantification

Determination of total iron content in liver, spleen and isolated adipocytes and SVF obtained from the adipose tissue was carried out by using the Iron Assay Kit from Sigma (MAK025). For sample preparation, 50 mg of liver, 10 mg of spleen or the isolated fractions from the adipose tissue were gently homogenized in 250 µL of Iron Assay Buffer. The homogenates were centrifuged at 13000 rpm for 10 minutes at 4 °C to remove insoluble material. 120 µL of the recovered tissue supernatants were incubated with 5 µL of 1 M SDS for 5 minutes on ice. After that, samples were centrifuged again for 5 minutes at 13000 rpm at 4 °C and 100 µL of the recovered supernatant was used for the iron assay following manufacturer's instructions. Samples obtained from iron-treated mice required a further dilution prior the assay. Iron content was normalized to total protein content in the sample, which was quantified by the BCA assay.

Animal model procedures

Animal care

All animal procedures were approved and performed in accordance with the guidelines of the Committee for Animal Experimentation at the Universidad de Oviedo. Animals were housed in a pathogen-free facility under a photoperiod of 12 h light/12 h dark, 22 ± 2 ºC of temperature, $50 \pm 10\%$ of relative humidity and *ad libitum* access to water and food. For tissue collection, mice were euthanized by cervical dislocation. If male displayed fight wounds in the course of the experiments, they were removed from the experimental cohort according to pre-established exclusion criteria.

Mutant mice strains

Tmprss6$^{-/-}$ and *Zmpste24*$^{-/-}$ mice generation have been previously described (Folgueras *et al.* 2008; Pendás *et al.* 2002). *Tmprss6*$^{-/-}$ and *Zmpste24*$^{-/-}$ were backcrossed 10 and 9 generations, respectively, to C57BL/6N background. *RANKL*$^{fl/fl}$ and *Dmp1-Cre* mice were obtained from Jackson Laboratories and interbred to generate *RANKL*$^{fl/+}$/*Dmp1-Cre* mice strain. After that, *RANKL*$^{fl/+}$/*Dmp1-Cre* mice were crossed with *Zmpste24*-heterozygus mice, and the resulting *RANKL*$^{fl/+}$/*Zmpste24*$^{+/-}$/*Dmp1-Cre* progeny was interbred to obtain *RANKL*$^{fl/fl}$/*Zmpste24*$^{-/-}$/*Dmp1-Cre* mice.

Administration of bioactive compounds

For recombinant GDF11 (rGDF11) administration, 6-week-old *Zmpste24*$^{-/-}$ mice were given a daily intraperitoneal injection of either rGDF11 (PeproTech) at 0.1 mg/kg or vehicle.

For iron treatment experiments, iron-treated *Tmprss6*$^{-/-}$ mice were injected intraperitoneally with 120 µg per g body weight (B.W.) of iron-dextran (Sigma) for 12 weeks every other week, starting on postnatal day 15, whereas iron-treated *Tmprss6*$^{+/+}$ mice were injected intraperitoneally with 40 µg per g B.W. of iron-dextran for 20 weeks every other week, starting on postnatal day 15.

For the experiments based on antibody administration, 6-week-old male *Tmprss6*$^{-/-}$ mice under a high-fat diet (HFD) diet were injected intravenously once per

week with 20 mg/kg of anti-hemojuvelin (HJV; h5F9-AM8) or anti-IgG antibodies for 18 weeks. Antibodies were dissolved in a buffer containing 30 mM histidine (pH 6.0) 8% w/v sucrose and 0.02% Tween 80. The injection volume administered to the mice was always below 100 µL.

Diet-induced obesity by high-fat diet administration

For diet-induced obesity, 4-week-old *Tmprss6*^{-/-}, iron-treated *Tmprss6*^{-/-} and wild-type male mice were fed a high-fat diet containing 60% fat (Harlan D12492) for 20 weeks after weaning.

Blood and plasma analysis

To evaluate the levels of circulating GDF11 over time, blood was extracted under anaesthesia from the facial vein of *Zmpste24*^{-/-} mice before and 2 h after rGDF11 administration, and collected into EDTA-coated tubes. Blood was centrifuged at 1000g at 4 ℃, and the supernatant was stored at -80 ℃ until analysis.

For hematological determinations on HFD-fed mice, complete blood counts were analyzed using Abacus junior vet equipment (Diatron labs). To monitor the efficacy of anti-HJV or anti-IgG treatment on HFD-fed *Tmprss6*^{-/-} mice, 100 µL of blood were extracted directly from the facial vein after anesthetizing the mice with isoflurane every other week since first injection. For blood glucose determination, blood samples were obtained from the tail vein and measured with Accu-Chek glucometer (Roche Diagnostics). For all other measurements, blood was extracted directly from the heart after anaesthetizing the mice and collected into heparinized or EDTA-coated tubes. Blood was centrifuged at 1000g at 4 ℃, and the supernatant was stored at -80 ℃ until analysis. Levels of iron, cholesterol and triglycerides were determined in IDEXX Laboratorios (Barcelona, Spain). All the above-mentioned biochemical parameters were determined in plasma samples obtained from HFD-fed mice upon overnight fasting.

Glucose and insulin tolerance test

Prior to studies, *Tmprss6$^{-/-}$*, iron-treated *Tmprss6$^{-/-}$* and wild-type male mice were fasted overnight. For glucose tolerance test, mice received an intraperitoneal injection of glucose of 1 g per kg of body weight. For insulin tolerance test, mice received an intraperitoneal injection of 0.75 IU of insulin per kg of body weight. Blood glucose levels were determined with a glucometer as described above. Areas under the curve were calculated using GraphPad Prism 6.0 software.

Metabolic and locomotor activity measurements

All measurements were performed using the Comprehensive Laboratory Animal Monitoring System (Oxymax CLAMS system by Columbus Instruments) and analyzed following manufacturer's instructions. *Tmprss6$^{-/-}$*, iron-treated *Tmprss6$^{-/-}$* and wild-type male mice were housed individually and kept on HFD chow on a 12:12-hour light–dark cycle. Mice were monitored for 48 h and the first 24 h were discarded in the analysis, considering them as acclimation period. Total ambulatory activity and food consumption were measured. Food intake was normalized to body weight. Rates of oxygen consumption (VO$_2$), CO$_2$ production (VCO$_2$) and energy expenditure (EE) were determined and normalized to lean mass. Areas under the curve were calculated using GraphPad Prism 6.0 software.

Treadmill exhaustion test

RANKL$^{fl/fl}$/Zmpste24$^{-/-}$/Dmp1-Cre, *RANKL$^{fl/fl}$/Zmpste24$^{-/-}$* and wild-type mice endurance capacity was determined by using an incremental test in the treadmill (Panlab 8700, Barcelona, Spain) with an inclination of 10 grades. The three-minute-steps started in 0.1 m/s with increments of 0.025 m/s until the mouse reached its maximum capacity. This method was adapted from other protocols previously described (Lira *et al.* 2013; Codina-Martínez *et al.* 2020). Since mice underwent a previous adaptation period, not aversive stimuli were observed, and our results were reproducible in repeated tests.

Morphometric and histological techniques

Micro-CT analysis of tibias

Tibias of 6-6.5-month-old *RANKL^{fl/fl}/Zmpste24^{-/-}/Dmp1-Cre*, *RANKL^{fl/fl}/Zmpste24^{-/-}* and wild-type mice were stored at 4 °C in 90% ethanol prior the analysis. The region of proximal metaphysis to mid-diaphysis of all samples was scanned by high-resolution micro-computed tomography (µCT) (SkyScan 1174, SkyScan, Bruker, Kontich, Belgium). The small sample-holder device for micro-CT (µCT) was used to fit the specimen with the long axis perpendicular to the base of the specimen holder and the X-ray source. Images were obtained by using 50 kV X-ray tube voltage and 800 µA. All specimens were scanned at 9.6-pixel size resolution using 0.5 mm aluminum filter. For each specimen, a series of 970 projection images were obtained with a rotation step of 0.3° and a frame averaging of 2 for a total rotation of 180°. The scanning time for each sample was approximately 2 h using an exposure time of 5500 ms. Flat field correction was performed at the beginning of each scan. The images obtained during scanning were reconstructed using the software NRecon (SkyScan). Correction values for attenuation coefficient, beam hardening, smoothing and ring-artifact reduction were the same in all samples.

Morphometric analysis in 2D and 3D was done using the software provided by the manufacturer (CTAn). Region of interest (ROI) was manually delimited in each sample. For the analysis of the diaphyseal cortical region, 100 slices were chosen. Global grayscale threshold levels for this area were between 95 and 255 for the tibia and 102-255 for the femur. For the trabecular region, a total of 150 slices were selected and adaptive grayscale threshold levels between 63 and 255 were used. The morphometric parameters examined were mineral bone density (BMD), ratio of bone volume/tissue volume (BV/TV), trabecular thickness (Tb.Th), trabecular number (Tb.N), and trabecular separation (Tb.Sp) for the trabecular area. For the cortical region, tissue mineral density (TMD), cortical thickness (Ct.Th) and cortical bone porosity (Ct.B.Po) were examined. Parameters were named according to the ASBMR (America Society for Bone and Mineral Research) histomorphometry nomenclature (Dempster *et al.* 2013).

Determination of body composition by magnetic resonance imaging

Body composition of *Tmprss6$^{-/-}$*, iron-treated *Tmprss6$^{-/-}$* and wild-type male mice feed with HFD was analyzed by magnetic resonance imaging (MRI) using a 3T MR-scanner (MR Solutions Ltd., Guilford, Surrey, UK). All scans were performed in the coronal plane after anesthetizing the mice with 3% isoflurane. Visceral and subcutaneous fat were quantified using a FIJI (Schindelin *et al.* 2012) plugin provided by A. Nistal (SCTs Universidad de Oviedo).

Histological analysis of adipose tissue and liver fat content

Tissues from *Tmprss6$^{-/-}$*, iron-treated *Tmprss6$^{-/-}$* and wild-type male mice were fixed in 4% buffered paraformaldehyde solution (PFA) and embedded in paraffin by standard procedures. Paraffin sections were stained with hematoxylin and eosin (H&E) for adipose tissue evaluation. The number of adipocytes and their mean diameter were determined in 5 µm tissue sections of epididymal fat pads by computer-assisted image analysis. For each sample, 4 different fields were analyzed, and 100 adipocytes were measured. For brown adipose tissue (BAT) droplet quantification, pictures from BAT sections stained with H&E were analyzed with Image J software. For lipid detection, liver samples were embedded in Tissue-Tek OCT compound (Sakura Finetechnical) and stored at -80 ℃. Samples were sectioned at 10 µm thickness and stained with Oil Red O. All tissues were examined by a pathologist (Dr. M.T. Fernández-García) in a blinded fashion.

Bioinformatics and Statistical methods

Manual annotation of CheloAbing 1.0

For manual annotation of selected genes, genomic sequences were obtained from the human protein database in Ensembl and used as reference to manually predict the corresponding homologues in the genome of *C. abingdonii*, which had been previously sequenced and assembled using the BATI algorithm (Blast, Annotate, Tune, Iterate) (Quesada *et al.* 2010). This algorithm allows the annotation of the position and intron/exon boundaries of genes in novel genomes from tblastn results. Afterwards, tblastn results are integrated to search for novel homologues in the explored genome. Those cases with a low identity level between human and *C. abingdonii* were treated separately using sequences from closer relatives, such as the chicken (*Gallus gallus*), the green anole lizard (*Anolis carolinensis*) and other turtles like *Pelodiscus sinensis*, the western painted turtle (*Chrysemys picta bellii*) or the green turtle (*Chelonia mydas*) as reference. Sequencing data have been deposited at the Sequence Read Archive (https://www.ncbi.nlm.nih.gov/sra).

To identify relevant truncations, point mutations or copy-number variations in the gene sequences of *C. abingdonii*, several comparations were performed using alignments of protein sequences from human (*Homo sapiens*), mouse (*Mus musculus*), Sauria (*A. carolinensis*), chicken (*G. gallus*), and the other turtles (*P. sinensis*, *C. picta bellii* and *C. mydas*). Interesting changes in genomic reads from *A. gigantea* were also listed. Protein residues in all alignments have been numbered using the human transcript as reference. Venn diagrams showing redundancy between the different categories established were performed using the nVenn algorithm (Pérez-Silva *et al.* 2018).

Statistical analysis

Results are expressed as mean ± SEM (standard error of the mean). Data were analyzed for normal distribution using Shapiro–Wilk test. Differences between two groups were compared by parametric two-tailed Student's t-test or non-parametric Mann–Whitney test. Student t-test was Welch-corrected for variables with different variances. Log-rank/Mantel-Cox test was used for survival analysis and one-tailed

Fisher's exact test was used to compare the number of mice between groups at the age corresponding to 200 days of lifespan in the survival distribution. All comparisons between groups of mice were performed in animals of similar age. A value of P less than 0.05 was considered statistically significant. Statistically significant differences are shown with asterisks (*P<0.05, **P<0.01, ***P<0.001). ROUT method (Q=0.5%) was used to detect and clear outliers in data sets. Statistical tests were performed using SPSS, Microsoft Excel and GraphPad Prism.

Results

I.- Manual characterization and comparative analysis of the genome of two long-lived giant tortoises

Comparative analyses that search for genetic differences between closely related long- and short-lived species have emerged as a useful approach to unveil novel candidate genes and pathways that might play a role in regulating ageing-related deterioration. Thus, in order to uncover intrinsic genetic adaptations which could impact systemically in the modulation of life expectancy, and following previous studies carried out in our laboratory (Keane *et al.* 2015; Warren *et al.* 2017), we decided to analyse the genome of two long-lived species of giant tortoises: the last representative member of the subspecies *C. abingdonii*, also known as Lonesome George, and the Aldabra giant tortoise (*A. gigantea*). Thus, giant tortoises constitute one of the few groups of vertebrates with an exceptional longevity, in excess of 150 years, according to some estimates (de Magalhaes and Costa 2009). As shown in **Figure 5**, the split between the two clades leading to the Galapagos and the Aldabra giant tortoises occurred about 40 million years ago (MYA), whereas the split between the ancestors of these tortoises and the ancestors of humans is placed approximately 312 MYA. Divergence times between taxa were obtained using the TimeTree database (Kumar *et al.* 2017).

In order to clarify the usage of the different taxonomic terms throughout the **Results** and **Discussion** sections, it is important to mention that the term "tortoises" generally refers to land turtles. This implicates that all tortoises are turtles, but not all the turtles can be categorized as tortoises. Hence, in the present Doctoral Thesis, the term "giant tortoises" refers to *C. abingdonii*, other tortoises from the Galapagos Islands (described in the **Experimental Procedures** section) and *A. gigantea*, whereas the term "tortoises" also includes *Gopherus agassizii*. Additionally, the terms Testudines, Chelonii or "turtles" are used as synonyms to refer to all turtles.
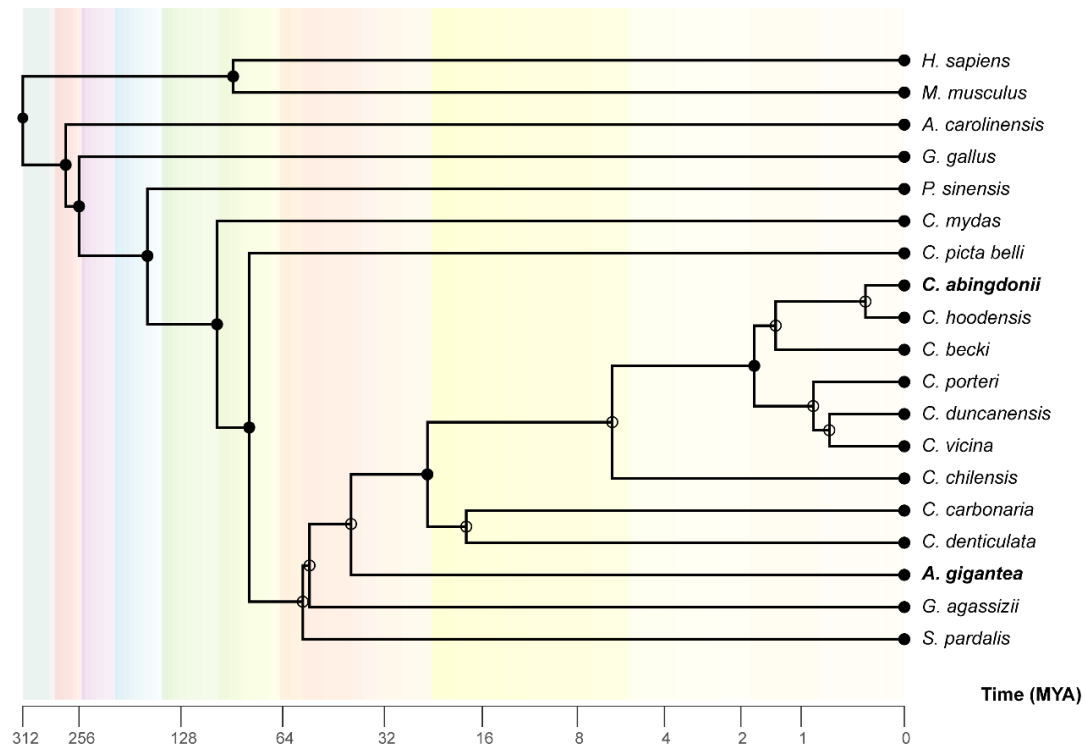
Figure 5. Time-tree showing evolutionary divergence between some of the studied species. The divergence between *C. abingdonii* and humans occurred 312 MYA, whereas the divergence between *C. abingdonii* and *A. gigantea* occurred approximately 40 MYA. Data were obtained from the TimeTree public database on the tree of life and its evolutionary timescale.

Hypothesis-driven comparative analysis reveals lineage-specific changes in *C. abingdonii* and *A. gigantea* genomes

We manually annotated about 3,000 genes potentially involved in determining the developmental features of this taxonomic group and their longevity. In relation with longevity, we payed special attention to those genes involved in processes such as DNA repair and the maintenance of the genomic stability, intercellular communication, immunosurveillance or cancer resistance. We established hypothesis-driven gene sets based on our experience in the selected fields and an exhaustive revision of available literature on each subject. Redundancy among established categories is shown in **Figure 6**. For manual annotation, we used the first version of the sequenced and assembled genome of *C. abingdonii* (CheloAbig 1.0.) and genomic sequences from *A. gigantea*. Then, by comparing to the human orthologue, we focused on identifying the

putatively most relevant truncations, amino acid changes and copy-number variations that might be of functional relevance in these species. The most relevant results are summarized in **Supplementary Information, Table S1**. When feasible, we confirmed the presence of these variants with the RNA-Seq data obtained from *C. abingdonii* blood and *A. gigantea* granuloma. Next, in order to establish lineage-specific conclusions, we validated the most interesting changes by PCR amplification, followed by Sanger sequencing, using a panel of genomic DNA samples from giant tortoises endemic to several islands of the Galapagos Archipelago. Therefore, we carried out PCR experiments with locus-specific primer pairs targeting the region where the identified variants were located. To study copy-number variations, we performed PCR reactions with primer pairs that allowed the amplification of each copy separately. When this approach was not feasible, we amplified and sequenced a target region harbouring a different nucleotide variant in each copy to allow the distinction of both copies when examining the resulting electropherogram (**Supplementary Information, Table S2**). In total, we validated more than 100 variants belonging to the different categories previously established, which were found in the genome of several tortoises, some of them exclusively affecting giant tortoises.

Figure 6. Venn diagram showing the redundancy among all genes manually annotated grouped in each category. The diagram represents all genes related to each category that have been manually annotated, according to the classification established before annotation. The number of genes belonging to each group are indicated.

As mentioned above, manual annotation allowed us to find numerous variants in the genome of giant tortoises that might impinge on their developmental features, immunity, metabolism, stress response, cancer susceptibility and ageing. However, in this Doctoral Thesis, we only focused on the description, analysis and discussion of those changes affecting putative modulators of cancer resistance, immune competence, and ageing-associated decline, among other possible mechanisms involved in longevity extension (López-Otín *et al.* 2013). Thus, within the previously established categories of cancer, ageing, and immunity, we annotated 400, 467 and 857 genes, respectively (**Figure 6, 7A**). Although sometimes it is difficult to assign genes to a unique category given the widespread impact of certain pathways, the selection of gene sets used in this work was done in order to minimize the redundancy among the three categories (**Figure 7A**). The most relevant genomic variants, including single-nucleotide variations (SNVs), copy-number alterations or truncations, found in each category and the overlap among groups are represented in the Venn diagram shown in **Figure 7B**. These results will be further discussed below.
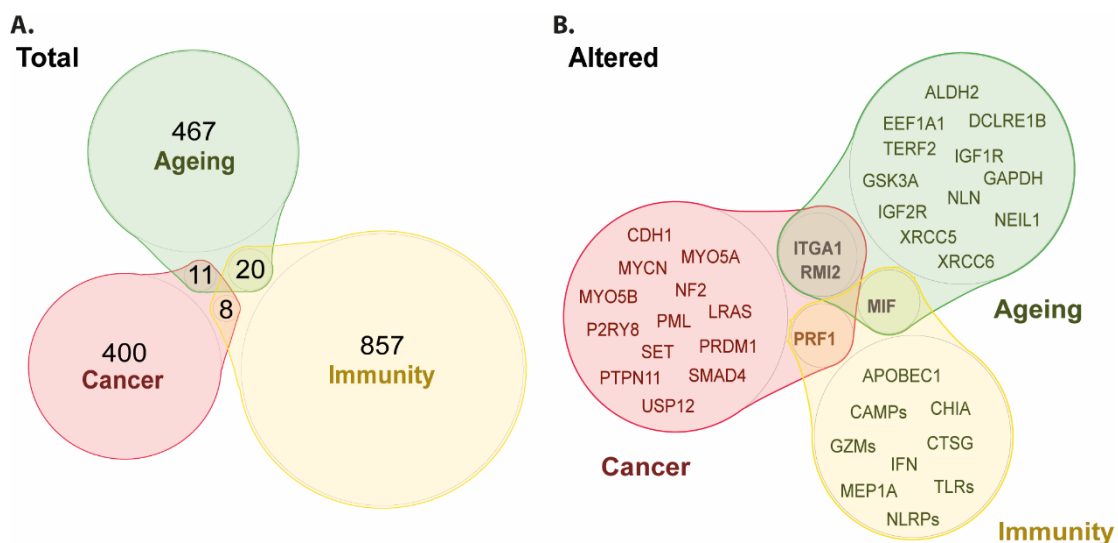

Figure 7. Venn diagrams showing the relationships among cancer-, ageing- and immunity-related genes. **A.** Total number of genes related to each category that have been manually annotated. **B.** Those genes showing potentially interesting genetic alterations after annotation.

Giant tortoises carry specific lineage variants which impinge on multiple hallmarks of ageing

In order to delve deeper into the putative determinants of the exceptional longevity of giant tortoises, we selected a set of 467 genes potentially involved in ageing modulation for manual supervised annotation. In this context, we found that both giant tortoise genomes showed several alterations in genes that have been categorized into six of the hallmarks of ageing —genomic instability, telomere attrition, loss of proteostasis, deregulated nutrient sensing, mitochondrial dysfunction and altered intercellular communication— (López-Otín *et al.* 2013), and that also impinge on other relevant processes such as cancer progression (Gorbunova *et al.* 2014) (**Figures 8-10**).

Maintaining the integrity of the genome is an essential requirement to preserve cellular functions and prevent irreversible genomic mutations that contribute to age-related decline. Therefore, genomic instability is considered as a primary hallmark of ageing (López-Otín *et al.* 2013). In this regard, we found and validated a duplication affecting two key genes involved in DNA repair mechanisms, *NEIL1* and *RMI2* (**Figures 8, 9**). NEIL1 is a key protein of the base-excision repair process whose expression has been linked to extended lifespan in several species (MacRae *et al.* 2015). Likewise, *RMI2*, as *NEIL1*, is exclusively duplicated in tortoises, suggesting an enhanced ability to resolve homologous recombination intermediates, which limits DNA crossover formation in cells (Daley *et al.* 2014). Moreover, we identified and validated a variant in XRCC6, a helicase involved in non-homologous DNA end-joining (NHEJ) of double-strand DNA breaks, which may affect a known sumoylation site (p.K556R) (**Figures 8, 9**). Besides giant tortoises, this lysine is also changed in the naked mole rat (p.K556N) (Kim *et al.* 2011), the longest-lived rodent, which suggests a putative process of convergent evolution. Interestingly, sumoylation is induced following DNA damage and has been shown to play a key role in the DNA repair response (Cremona *et al.* 2012), suggesting a putative functional relevance of this variant in the regulation of the repair of double-strand DNA breaks in these animals (**Figure 9**).
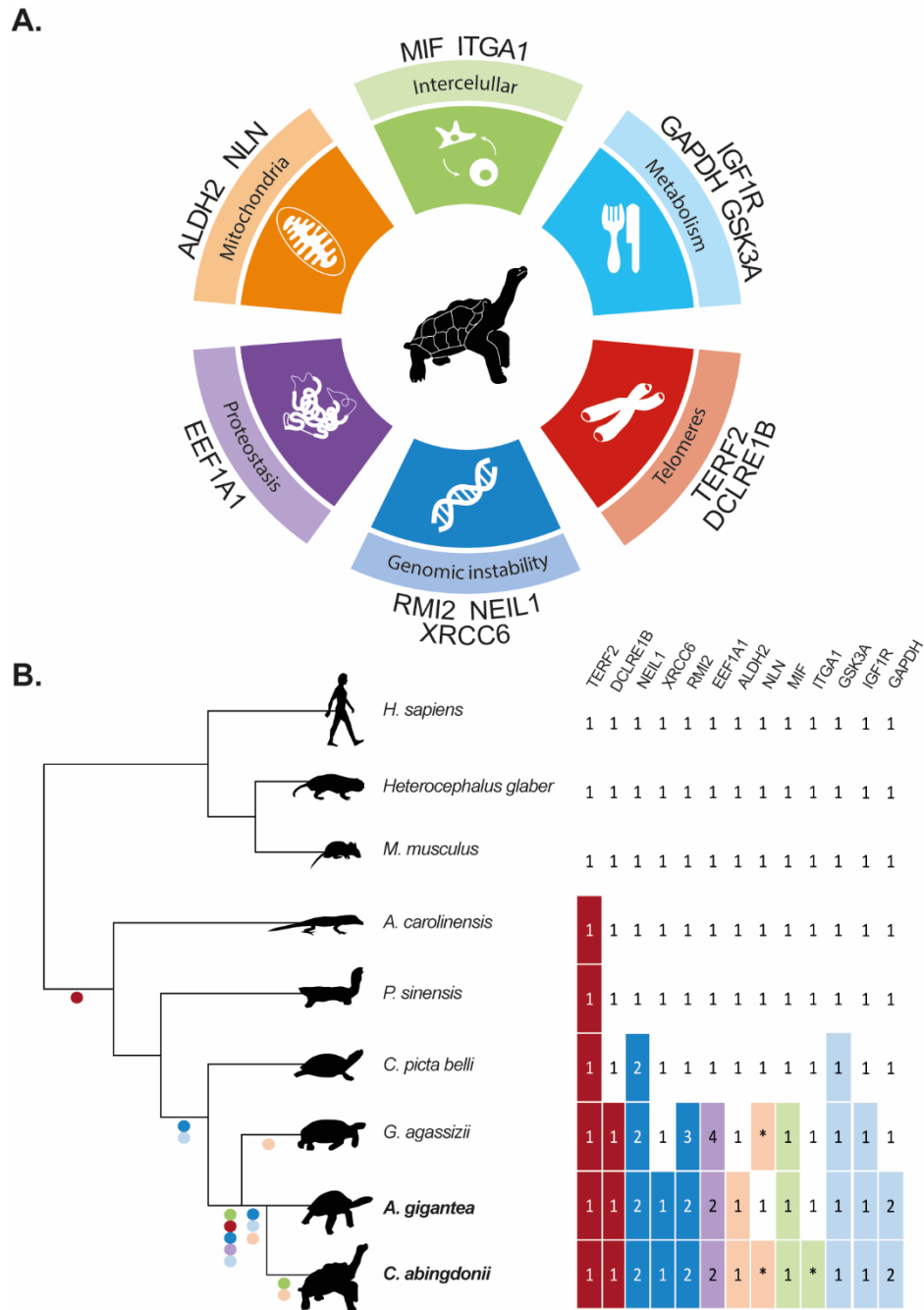
Figure 8. Genomic basis of longevity in giant tortoises. **A.** Genes potentially implicated in *C. abingdonii* and *A. gigantea* longevity extension, classified according to their putative role in the different hallmarks of ageing. **B.** Tables indicate copy-number variations and relevant variants of age-related genes found in *C. abingdonii*, *A. gigantea* and other species. Within these tables, numbers indicate gene copy numbers, and asterisks represent pseudogenization events. Dots in colours represent the presence of the variant related to each hallmark.

Regarding telomere attrition, another primary hallmark of ageing defined by the constant loss of genomic material in each cell division that triggers cell cycle arrest and cellular senescence (López-Otín *et al.* 2013), giant tortoises harbour one variant in DCLRE1B (p.R498C). DCLRE1B is an exonuclease that participates in the protection of telomeres against NHEJ-mediated repair and plays a key role in telomeric loop (T-loop) formation after being recruited by telomeric repeat binding factor 2 (TERF2). Thus, the p.R498C variant may potentially affect its binding interface with TERF2. This change, together with other variants found in DNA repair genes with a possible impact on telomere dynamics (Tong *et al.* 2015; Ribes-Zamora *et al.* 2013), highlights the relevance of telomere maintenance as a regulatory mechanism of longevity in tortoises.
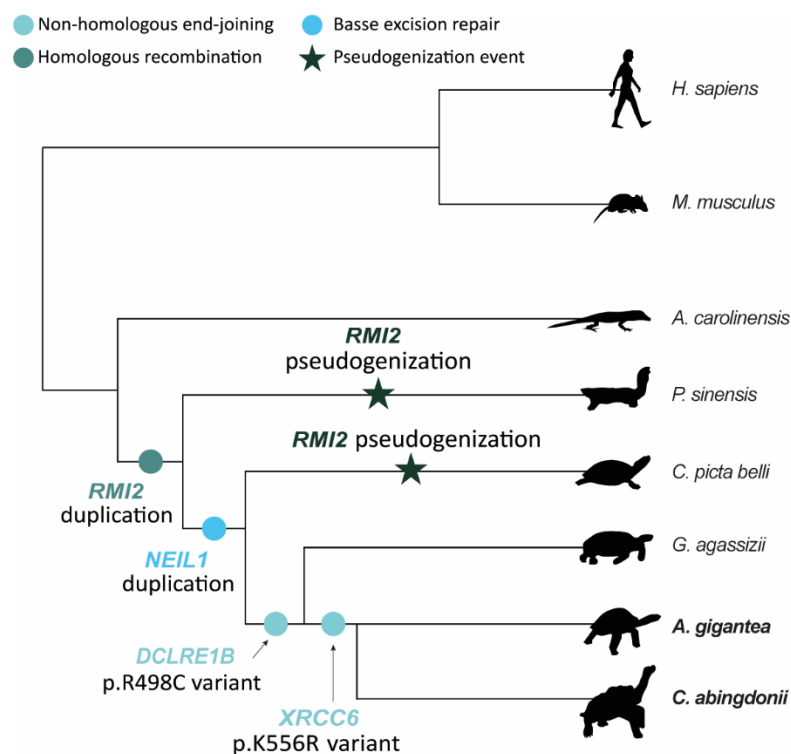
Figure 9. DNA repair response in giant tortoises. Copy-number variations and putative function-altering point variants found in *C. abingdonii*, *A. gigantea* and closely related species.

Likewise, we found changes potentially affecting proteostasis, a process that ensures the fitness of the cellular proteome. We independently found specific expansions of the elongation factor gene EEF1A1 in *C. abingdonii*, *A. gigantea* and *G. agassizii*, as described with the automatic annotation. This gene encodes an isoform of the alpha subunit of the elongation factor-1 complex, which is responsible for the

delivery of tRNAs to the ribosome. Notably, this expansion may have a critical effect on lifespan since overexpression of EEF1A1 orthologues in *Drosophila melanogaster* has been linked to an increased lifespan in this species (Shikama *et al.* 1994) (**Figure 8**).

In addition to the impact on physiological processes such as the regulation of the body size (White *et al.* 2019), metabolic modulation is also essential to the control of longevity, being deregulated nutrient sensing an antagonist hallmark of ageing (López-Otín *et al.* 2013; López-Otín *et al.* 2016; Kroemer *et al.* 2018). For this reason, we hypothesized that the analysis of genes that play a pivotal role in metabolic pathways might also provide new insights into the genetic mechanisms underlying the extreme lifespan of giant tortoises. Whereas our results on genes related to growth hormone and stanniocalcins suggested that these systems were well conserved, we annotated a variant in the insulin-like growth factor (IGF) receptor IGF1R (p.N724D), which is likely to affect its interaction with IGF1/2 ligands (Whittaker *et al.* 2001) (**Figures 8**). Given that decreased IGF signalling correlates with extended longevity in multiple organisms (Vitale *et al.* 2019), this aspartic residue, which is specific for tortoises (including *G. agassizii*), may provide an attractive target to study the cellular mechanisms underlying the exceptional lifespan of these animals. Likewise, we identified an interesting variant (p.R272Q) affecting the activation loop of GSK3A, a negative regulator in the hormonal control of glucose homeostasis, in *C. abingdonii* and all tested tortoises from the Galapagos Islands and Aldabra Atoll, as well as their continental outgroups, *G. agassizii* and *C. picta bellii*. Interestingly, the inhibition of GSK3 can extend lifespan in *D. melanogaster* (Castillo-Quan *et al.* 2016), which points to a critical role of this enzyme in the regulation of longevity across the evolution. In addition, we identified an expansion of *GAPDH* in giant tortoises, as well as the pseudogenization of the protease gene *NLN* in tortoises, both genes being involved in energy metabolism and mitochondrial function. Furthermore, we identified two variants (p.Q366M and p.M487T) likely affecting the function of ALDH2. ALDH2 is a mitochondrial aldehyde dehydrogenase involved in alcohol metabolism and lipid peroxidation, among other detoxification processes (Ohta *et al.* 2004). Notably, the p.Q366M variant, which may alter the NAD-binding site of ALDH2, was exclusively found in Galapagos giant tortoises, but not in their continental close relative *C. chilensis*, nor in the more distantly related Aldabra or Agassiz's tortoises. These

variants, along with those above-mentioned in GAPDH and NLN, might contribute to modulate another antagonistic hallmark of ageing such as mitochondrial dysfunction (**Figure 8**) (López-Otín *et al.* 2013), and help to preserve the metabolic fitness of these organisms throughout their life.

A suitable communication between cells is essential to guarantee an appropriate response to external stimuli, allowing species to adapt to the changing environmental conditions and ensuring their subsistence over time. For this reason, we analysed multiple key genes involved in the regulation of intercellular communication pathways and stress response, which could impinge on longevity as an integrative hallmark of ageing (López-Otín *et al.* 2013). We detected a premature stop codon affecting ITGA1 (p.R990*), an essential integrin involved in cell–matrix and cell–cell interactions, exclusively in *C. abingdonii*. Also, we identified in tortoises a variant affecting MIF (p.N111C), a trimeric protein with extensive interactions between subunits. In addition to its role as a proinflammatory cytokine, MIF also possesses a catalytic site of unknown function between the subunits that conform the homotrimer. The aforementioned variant is expected to cause the formation of inactivating interchain disulphide bonds between the subunits of the trimer, which inhibits the intracellular signalling cascades mediated by MIF receptor CD74 (Fan *et al.* 2013).

Regarding environmental stress adaptations, we found that, despite living terrestrially, giant tortoises conserve hypoxia-related changes in their genome, such as the presence of globin GbX and a specific variant in the transcription factor TP53 (p.S106E) (**Figure 10**). Globins play an essential role in oxygen binding and transport, but they are also involved in nitric oxide metabolism and detoxification of reactive oxidative species (Hoffmann *et al.* 2018). Particularly, it has been reported that the role of GbX in oxygen binding and transport is similar to that of haemoglobin (Hgb), and that deoxygenated GbX is involved in nitrite reduction to nitric oxide, suggesting that the presence of GbX may participate in the response mechanisms to anoxia/hypoxia underlying the exceptional tolerance to hypoxic conditions of these vertebrates (Corti *et al.* 2016; Jacobsen *et al.* 2012; Lutz *et al.* 2003). Furthermore, the aforementioned variant in TP53, which is present in Testudines, has been linked to hypoxia resistance in some mammals and fishes (Zhao *et al.* 2013), highlighting the important role of hypoxia adaptation in the evolutionary history of these species.

Therefore, these results point out the relevance of intercellular signalling modulation in an aged context, suggesting that the changes found in these animals could be important to respond effectively to the environmental stress that usually underlie the ageing process.
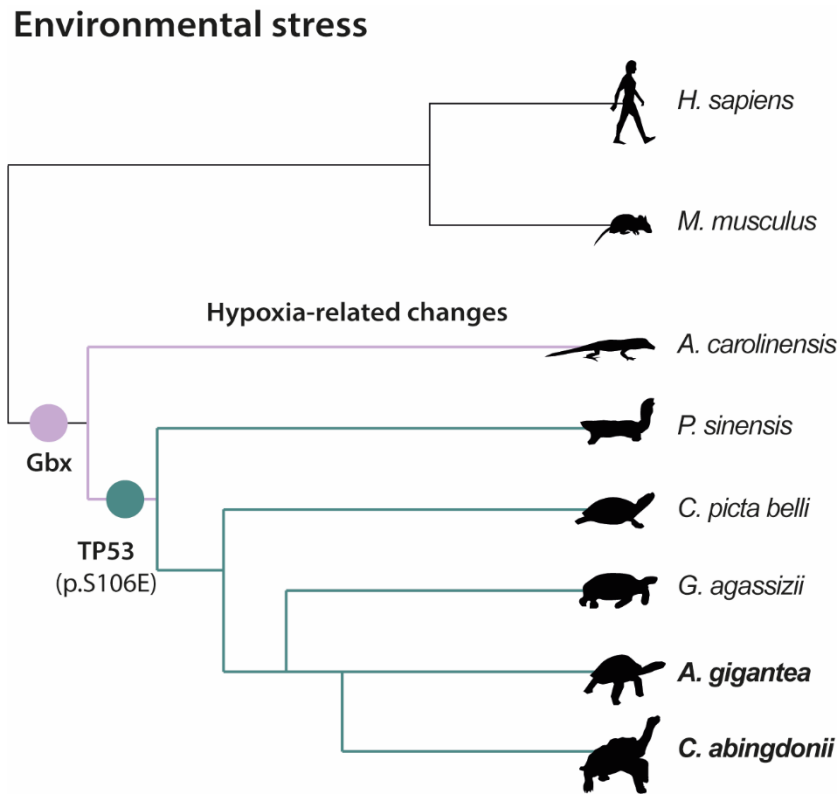
Figure 10. Genomic adaptations to environmental stress and hypoxia response. Presence of GbX and TP53 variant (p.S106E) in *C. abingdonii*, *A. gigantea* and closely related species. Dots in colours represent the presence of the variant.

Lineage-specific changes in the genome of giant tortoises involved in cancer resistance and immunosurveillance

Cancer and ageing are two interrelated processes, since extended lifespan entails cells have more time to accumulate mutations, increasing the probability of carcinogenesis (Caulin and Maley 2011). In an attempt to explore this question, we selected 400 genes involved in cancer whose alterations had been associated with tumorigenesis (Futreal *et al.* 2004), either as oncogenes or as tumour suppressors. Although most genes presented a highly conserved amino acid sequence when compared with the sequences of other organisms, we identified alterations in several tumorigenesis-related genes (**Figure 11**). We found that several putative tumour

suppressors were expanded in turtles compared with other vertebrates, including duplications in *SMAD4*, *NF2*, *PML*, *PTPN11* and *P2RY8*.
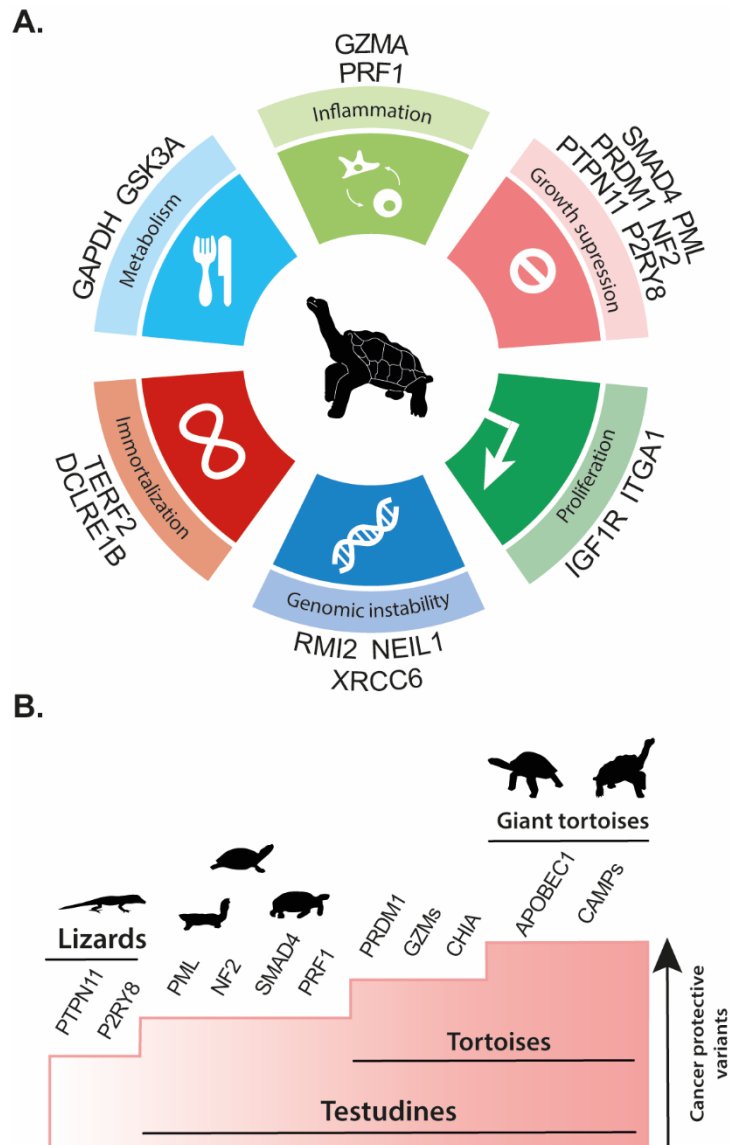
Figure 11. Genomic basis of cancer resistance in giant tortoises. **A.** Genes potentially implicated in *C. abingdonii* and *A. gigantea* cancer resistance classified according to their putative role in the different hallmarks of cancer (Hanahan and Weinberg 2011). **B.** The graph indicates the copy-number variations accumulated throughout the turtle lineage, emphasizing the specific amplification of *PRDM1*, *GZMs*, *CHIA*, *APOBEC1* and *CAMPs* specifically in tortoises and giant tortoises.

Likewise, we found giant-tortoise specific duplications affecting two putative proto-oncogenes, *MYCN* and *SET* (**Supplementary Information, Table S2**). However, some of the novel copies identified show evidence of loss of function or

dominant negative functions, which might actually point to a lower tumorigenic potential. Taken together, these results suggest that multiple gene copy-number alterations may have influenced the mechanisms of spontaneous tumour growth in these animals.

Finally, we decided to analyse around 800 genes involved in immune function, since the immune system is under strong selective pressure and has important implications in physiological and pathological processes in most species (Barreiro and Quintana-Murci 2010). In this context, we found a genomic expansion of *PRF1* in giant tortoises and other turtles, compared with chickens (one copy), *A. carolinensis* (two copies) and most mammals (one copy). *PRF1* encodes perforin, a protein component of the cytotoxic T lymphocyte (CTL) and NK cell secretory granules (Voskoboinik *et al.* 2015). Both *C. abingdonii* and *A. gigantea* possess 12 copies of this gene (validated by Sanger sequencing), although three of them have been pseudogenized in *C. abingdonii* (**Supplementary Information, Tables S1 and S2**). Likewise, we found a tortoise-specific duplication of *PRDM1*, a transcriptional repressor that drives the maturation of B-lymphocytes into Ig-secreting isotypes (Lin *et al.* 1997) (**Figure 11**). In addition, we detected and validated by Sanger sequencing an expansion of the chymase locus, containing granzymes (GZMs), in giant tortoises (**Supplementary Information, Table S2**). Both expansions are expected to affect cytotoxic T lymphocyte and natural killer functions, which play important roles in the defence against both pathogens and cancer (Voskoboinik *et al.* 2015; Dotiwala *et al.* 2016). Other concurrent expansions involve *APOBEC1*, *CAMP* and *CHIA* genes (**Figure 11**, **Supplementary Information, Tables S1 and S2**), which participate in viral, microbial, fungal and parasite defence, respectively. These results suggest that the innate immune system in turtles, and especially in tortoises, may play a more relevant role than in mammals, in comparison to the adaptive immunity (Zimmerman *et al.* 2010). Altogether, the expansions of tumour suppressor genes observed in Testudines, as well as their powerful immune system could contribute to explain their apparent natural resistance to cancer (Garner *et al.* 2004).

II.- Functional analysis of the contribution of cell-extrinsic mechanisms to the development of a premature ageing phenotype

Previous studies in our laboratory using a mosaic mouse model, in which *Zmpste24*-deficient cells coexist with *Zmpste24*-proficient cells in similar proportions, showed a complete absence of progeroid phenotype, supporting the relevance of cell-extrinsic mechanisms in the establishment of this pathology (de la Rosa *et al.* 2013). On this basis, we decided to study the role of factors that could have an organismal effect on the ageing process. To this end, we studied the effect of GDF11 (growth differentiation factor 11) and RANKL (receptor activator of nuclear factor kappa-B ligand) on premature ageing and longevity using *Zmpste24*$^{-/-}$ mouse model, since this mouse model phenocopies many of the features of natural ageing and shows reduced lifespan.

GDF11, originally identified as a regulator of skeletal muscle growth (Gamer *et al.* 2001), gained a great attention in the last few years when found in the blood of young mice and was proposed as a powerful anti-ageing factor due to numerous reports regarding its capacity to rejuvenate several aged tissues, such as heart, skeletal muscle, and brain (Loffredo *et al.* 2013; Sinha *et al.* 2014; Katsimpardi *et al.* 2014). Nevertheless, as further discussed, other studies have reached conflicting conclusions regarding the rejuvenating properties of GDF11. On the other hand, RANKL, stands as a pivotal cytokine in the regulation of bone resorption in physiologic and pathological conditions such as osteoporosis (Xiong *et al.* 2011; Xiong *et al.* 2018), a common age-related feature with a putative impact on cardiovascular disease and, ultimately, lifespan. Thus, we wondered whether the role of both factors in ageing and age-related disorders would have an overall effect on the progeroid phenotype of *Zmpste24*-deficient mice and, particularly, on their longevity.

GDF11 administration does not increase longevity of *Zmpste24*-deficient mice

Based on the proposed anti-ageing functions of GDF11, we analysed the *in vivo* effect of GDF11 administration on the lifespan of *Zmpste24*-deficient mice. To

evaluate whether all attributed anti-ageing properties of GDF11 may have an overall effect on longevity, we first determined whether GDF11 levels decline with age in our mouse model in the same manner as it had been reported in physiological ageing (Loffredo *et al.* 2013; Olson *et al.* 2015). To this end, we performed western-blot analyses with plasma samples obtained from the same wild-type and *Zmpste24*^{-/-} mice at the age of 1.5 months and 3 months, to monitor a possible decline over time. We established these two-time points considering that the average lifespan of these mutant mice is 4 months and that accelerated ageing symptoms start to manifest around the second month. For this purpose, we used the same commercial antibody as the one previously reported in the original study by Loffredo *et al.*, in which GDF11 was first identified as an anti-ageing factor (Loffredo *et al.* 2013). Of note, other work demonstrated that this antibody also recognizes GDF8 (myostatin), a closely related member of the TGF-β superfamily that shares 89% identity in amino acid sequence in the mature active form, questioning those previous published data that showed a GDF11 decline with age (Egerman *et al.* 2015). However, at the time of performing these experiments, no alternative reliable assay capable of detecting endogenous GDF11 in mouse serum had been described (Egerman *et al.* 2015; Smith *et al.* 2015). Taking into account these premises, we observed a patent decrease in GDF11/8 plasma levels in *Zmpste24*^{-/-} mice compared with wild-type littermates at the age of 3 months. Interestingly, no significant differences were found when analysing plasma samples that had been obtained from the same individuals 1.5 months earlier, prior to the development of any ageing phenotype (**Figure 12A, B**). Ponceau S staining from the corresponding western-blot showed equivalent loading in all lanes. Altogether, these results indicate that the reduction in GDF11/8 blood levels observed in *Zmpste24*^{-/-} versus wild-type mice occurs upon the manifestation of the progeroid phenotype.

We next tested whether GDF11 could be one of the circulating factors capable of slowing down the ageing symptoms and extending the lifespan of *Zmpste24* [-/-] mice, considering its overall effect on a number of aged tissues and the above-mentioned observations (**Figure 12B**). To test this hypothesis, we did use the same commercial recombinant GDF11 protein (PreproTech) and at the same dosage (0.1 mg/kg, daily) that had been reported to have an anti-ageing effect (Loffredo *et al.* 2013; Sinha *et al.* 2014; Katsimpardi *et al.* 2014). By using this approach, we were able to detect by western-blot an increase in circulating GDF11/8 plasma levels in progeroid *Zmpste24*^{-}

$^{/-}$ mice 1 to 2 h after rGDF11 injection (**Figure 13**), similar to what had previously been described (see Loffredo *et al*. 2013, Figure S5). Even though the used antibody was able to recognize both GDF11 and GDF8, it was reasonable to speculate that the protein increase we observed in the blood of the same individual within a 1-2 h temporal window corresponded to rGDF11. Moreover, alternative detection methods have also demonstrated that daily intraperitoneal injection of rGDF11 (0.1 mg/kg) increased circulating levels of GDF11 above endogenous plasma levels, which were below the detection limit of the assay (Smith *et al.* 2015). Therefore, considering that our objective was to restore progeroid GDF11 plasma levels to a wild-type condition, we were confident that this dose was adequate to test our hypothesis.
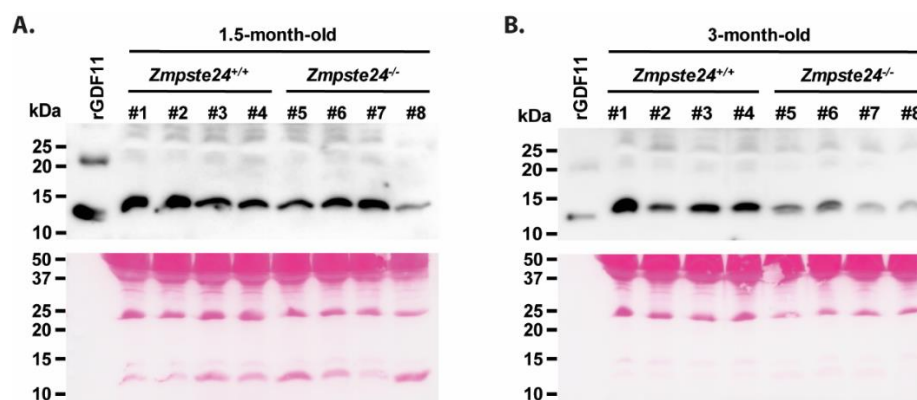
Figure 12. Progeroid *Zmpste24$^{-/-}$* mice show reduced GDF11/8 plasma levels. Western-blot analysis of GDF11/8 plasma levels of young (1.5-month-old) (**A**) and aged (3-month-old) (**B**) *Zmpste24$^{-/-}$* and wild-type mice. Note that plasma samples were obtained from the same individuals at the two time points. 2 ng of rGDF11 were loaded as a positive control. Ponceau S stained membranes of the corresponding western-blots are shown to demonstrate equivalent loading (bottom). # indicates mouse number.

Hence, male and female *Zmpste24$^{-/-}$* mice received a daily intraperitoneal injection of rGDF11 (0.1 mg/kg) or vehicle, starting at the age of 2.5 months, once the accelerated ageing symptoms started to manifest. rGDF11 treatment did not increase survival of *Zmpste24$^{-/-}$* mice compared with vehicle-treated animals (**Figure 14A, B**).

Figure 13. **rGDF11 intraperitoneal administration increases GDF11/8 plasma levels in *Zmpste24*^{-/-} mice.** GDF11/8 plasma levels of 3-month-old *Zmpste24*^{-/-} mice were evaluated by Western-blot analysis before and 2 h after a single intraperitoneal injection of 0.1 mg/kg of rGDF11. GDF11/8 plasma levels of wild-type littermate mice are shown as a reference. 2 ng of rGDF11 loaded as a positive contr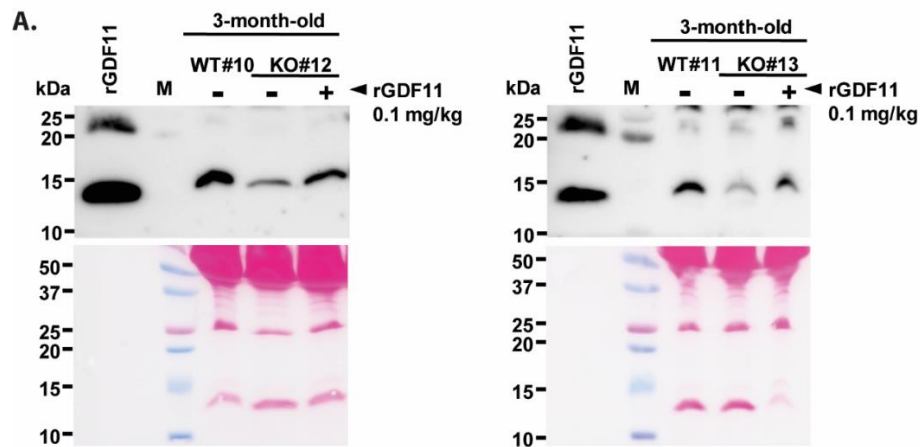ol. Ponceau S stained membranes of the corresponding western-blots are shown to demonstrate equivalent loading (bottom). # indicates mouse number. M indicates molecular weight marker.

These results were in line with recent reports showing no effect of GDF11 on cardiac or skeletal muscle function, arguing against the "rejuvenating" potential of this protein (Egerman *et al.* 2015; Smith *et al.* 2015; Hammers *et al.* 2017; Zimmers *et al.* 2017; Harper *et al.* 2018). Likewise, it had been reported that high doses (0.5 mg/kg) of rGDF11 could decrease body weight (Poggioli *et al.* 2016). However, we only observed a slight decrease in the body weight of *Zmpste24*^{-/-} mice treated daily with rGDF11 at a dose of 0.1 mg/kg compared with vehicle-treated littermates, being this difference statistically significant at some points of the treatment period in female mice (**Figure 14C, D**).

Altogether, our results demonstrate that circulating GDF11/8 levels are reduced in our mouse model of premature ageing, which resemble most of the symptoms occurring in physiological ageing. However, GDF11 protein administration is not enough to extend the longevity of these progeroid mice.
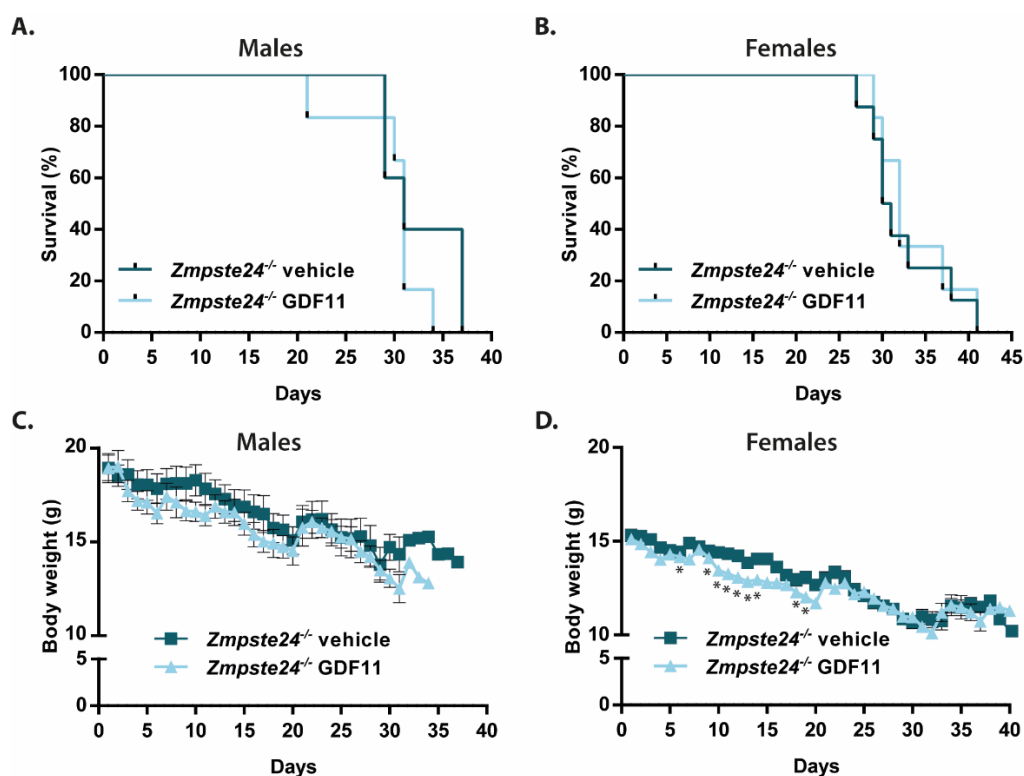
Figure 14. rGDF11 therapy neither extends longevity nor prevents body weight loss of *Zmpste24*^{-/-} mice. **A**. Kaplan-Meier survival plot of rGDF11-treated (n=5) and vehicle-treated (n=6) male *Zmpste24*^{-/-} mice. **B.** Kaplan-Meier survival plot of rGDF11-treated (n=8) and vehicle-treated (n=6) female *Zmpste24*^{-/-} mice. Mice received a daily intraperitoneal dose of rGDF11 (0.1 mg/kg) or vehicle. Body weights of rGDF11- and vehicle-treated male **C**. and female **D.** *Zmpste24*^{-/-} mice. Data are mean ± SEM. *P*-values were calculated by Student's t-test (*$P \leq 0.05$).

Conditional deletion of osteocyte-derived RANKL prevents bone resorption and increases survival of progeroid mice

On the basis of the putative broad effect that bone resorption may have on the ageing process, as a consequence of the mineral and extracellular matrix components that are released to the bloodstream, we decided to delete the membrane-bound cytokine and key regulator of the osteoclast activity RANKL (*Tnfsf11*) in our progeroid mouse model *Zmpste24*^{-/-}, in which one of the classical outcomes is the manifestation of numerous skeletal abnormalities (Pendás *et al.* 2002; Bergo *et al.* 2002). To this end, we chose to eliminate the production of RANKL specifically in osteocyte cells given that mice carrying a germline deletion of this cytokine displayed a severe phenotype of osteopetrosis (Yasuda *et al.* 1998; Kong *et al.* 1999). In addition, several studies have

recently suggested that osteocyte-derived RANKL deletion does not affect bone resorption occurring during bone development, but it can modulate bone remodelling during adulthood (Xiong *et al.* 2011; Nakashima *et al.* 2011). Therefore, we employed a Cre-loxP technology to specifically delete *Tnfsf11* gene in the osteocyte population, avoiding the deleterious effects of its germline deficiency. Thus, we first generated a new mouse model by crossing a murine strain harbouring *Tnfsf11* allele flanked by loxP sites with transgenic mice expressing Cre recombinase under the control of *Dmp1* promoter, which allows *Tnfsf11* specific deletion in osteocytes. After that, we crossed the resulting mouse strain *RANKL^{fl/fl}/Dmp1-Cre* with our progeroid animal model deficient in the protease Zmpste24, generating a new mouse strain hereafter called *RANKL^{fl/fl}/Zmpste24^{-/-}/Dmp1-Cre* mice. Prior to describing our results, it is necessary to clarify that all progeroid mice used in this study were checked daily for good physical condition and provided with softened food pellets to facilitate their feeding. To further investigate whether osteocyte secreted RANKL plays a significant role in the bone mass loss observed in *Zmpste24^{-/-}* mice, we performed µCT analysis of tibias obtained from *RANKL^{fl/fl}/Zmpste24^{+/+}*, *RANKL^{fl/fl} /Zmpste24^{-/-}* and *RANKL^{fl/fl}/Zmpste24^{-/-} /Dmp1-Cre* 6-6.5-month-old mice. µCT was used to measure morphometric bone parameters of trabecular and cortical regions in order to assess the microstructural bone organization in all experimental mice. This analysis revealed that *RANKL^{fl/fl}/Zmpste24^{-/-}* showed an exacerbated bone resorption compared with their wild-type littermates (*RANKL^{fl/fl}/Zmpste24^{+/+}*), which was characterized by a decrease of trabecular bone parameters, including bone volume fraction (BV/TV), trabecular thickness (Tb.Th), trabecular number (Tb.N) and bone mineral density (BMD), with a concomitant increase in trabecular space (Tb.Sp) (**Figure 15A, B**). Interestingly, deletion of osteocyte-produced RANKL in *Zmpste24^{-/-}* mice resulted in a significant reversion of the cancellous bone resorption observed in these mice. In addition, we also observed the same tendency in some of the morphometric cortical bone parameters analysed (**Supplementary Figure S1**). This analysis also revealed significant differences in some of the trabecular parameters between *RANKL^{fl/fl}/Zmpste24^{-/-}/Dmp1-Cre* and *RANKL^{fl/fl}/Zmpste24^{+/+}* mice (**Figure 15A, B**). Altogether, these results demonstrate that RANKL contributes to the development of the osteoporotic phenotype characteristic of these progeroid mice.
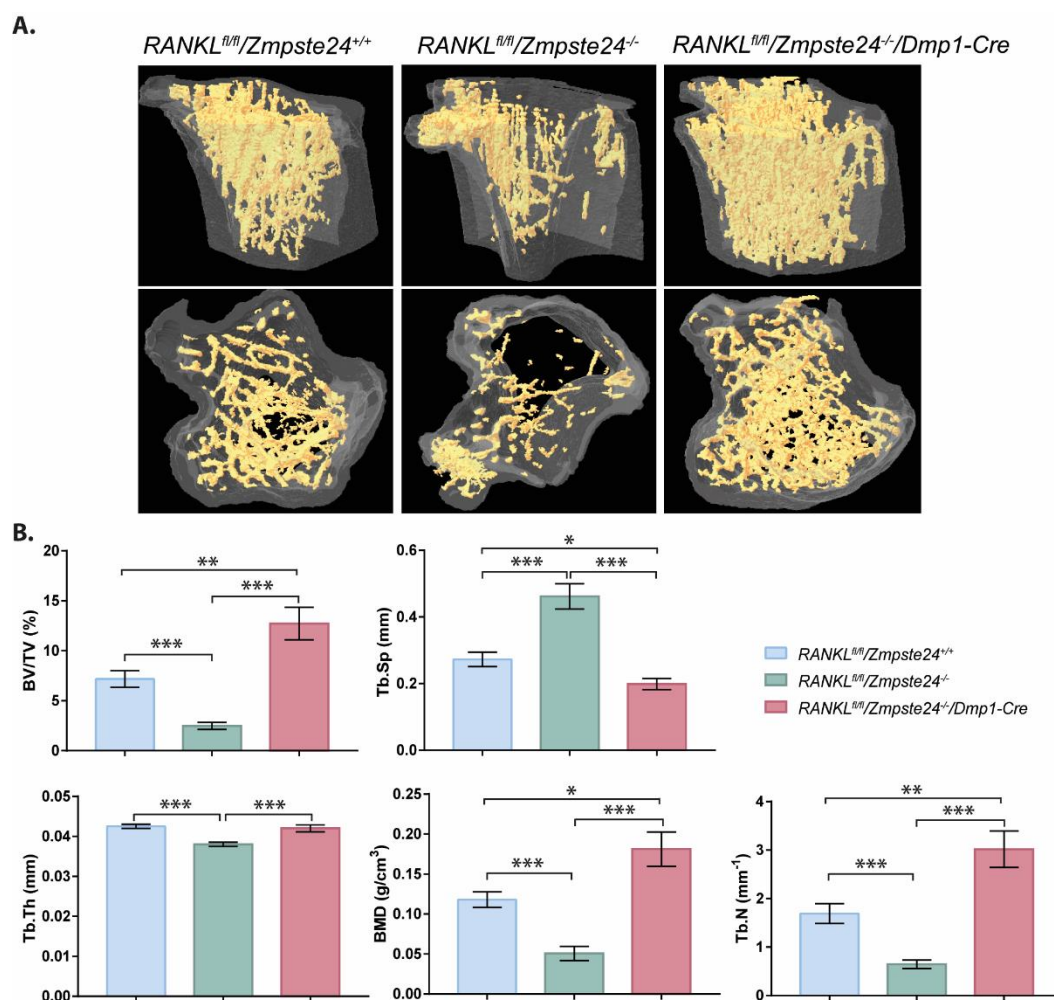
Figure 15. Deletion of RANKL in the osteocyte population of *Zmpste24*-deficient mice reduces cancellous bone resorption. A. Representative μCT images of proximal tibia from 6-month-old *RANKL^{fl/fl}/Zmpste24^{+/+}*, *RANKL^{fl/fl}/Zmpste24^{-/-}* and *RANKL^{fl/fl}/Zmpste24^{-/-}/Dmp1-Cre* littermates. **B.** Trabecular bone parameters in μCT analysis (BV/TV, bone volume/tissue volume ratio; Tb.Sp, trabecular spacing; Tb.Th, trabecular thickness; BMD, bone mineral density; Tb.N, trabecular number). *RANKL^{fl/fl}/Zmpste24^{+/+}* (n=14), *RANKL^{fl/fl}/Zmpste24^{-/-}* (n=12), *RANKL^{fl/fl}/Zmpste24^{-/-}/Dmp1-Cre* (n=12). Data shown are mean ± SEM. *$P<0.05$, **$P<0.01$, ***$P<0.001$, unpaired two-tailed Student's t-test with Welch's correction and Mann–Whitney tests were used to determine statistical significance.

Bone and skeletal muscle are two tightly coupled tissues involved in the correct function of the musculoskeletal system. Therefore, given the increased bone mass observed in *Zmpste24*-deficient mice upon RANKL deletion, we next wondered whether the improvement of this condition would impact on the motor skills of this progeroid mouse model. To address this question, we performed a treadmill exhaustion

test to evaluate *in vivo* the skeletal muscle function, as well as the exercise capacity and endurance of *RANKL^{fl/fl}/Zmpste24^{-/-}/Dmp1-Cre* mice. Exercise measurements were performed on 6-month-old mice, and all mice were adapted for 5 days before experimentation. Notably, the treadmill exercise test revealed that both duration of exercise and distance travelled were significantly diminished in *RANKL^{fl/fl}/Zmpste24^{-/-}* animals compared with their wild-type littermates (**Figure 16**). However, *RANKL^{fl/fl}/Zmpste24^{-/-}/Dmp1-Cre* mice exhibited an improved capacity in all parameters analysed when compared with *RANKL^{fl/fl}/Zmpste24^{-/-}* mice. Together, these results indicate that the reduced bone resorption observed in *Zmpste24^{-/-}* mice upon deletion of RANKL produced by osteocytes leads to an improved endurance capacity in a treadmill exhaustion test, suggesting that this strategy also ameliorates the skeletal muscle function of *Zmpste24^{-/-}* progeroid mice.
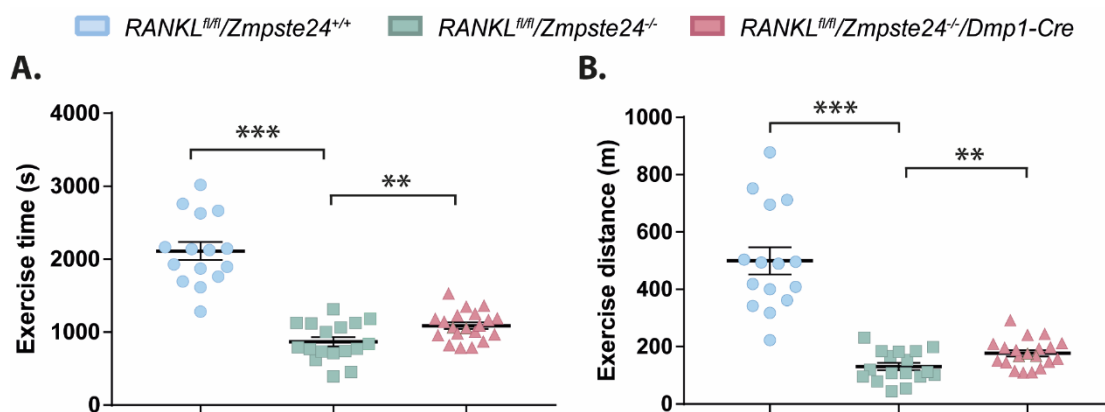
Figure 16. Improved exercise ability of *RANKL^{fl/fl}/Zmpste24^{-/-}/Dmp1-Cre* mice. Time-to-exhaustion (**A**) and distance travelled (**B**) during a treadmill exercise test. *RANKL^{fl/fl}/Zmpste24^{+/+}* (n=15), *RANKL^{fl/fl}/Zmpste24^{-/-}* (n=17), *RANKL^{fl/fl}/Zmpste24^{-/-}/Dmp1-Cre* (n=20). Data shown are mean ± SEM. **$P<0.01$, ***$P<0.001$, unpaired two-tailed Student's t-test was used to determine statistical significance.

Based on the aforementioned observations regarding the pathogenic relationship between bone resorption and vascular calcification, we hypothesized that the improvement of the osteoporotic phenotype might also impact on the healthspan and lifespan of these mice by ameliorating vascular stiffness. Although we did not observe any differences in body weight over time between experimental groups, *RANKL^{fl/fl}/Zmpste24^{-/-}/Dmp1-Cre* mice showed an increased survival, particularly at

early stages, when compared to *RANKL$^{fl/fl}$/Zmpste24$^{-/-}$*, with a median lifespan of 276 days *versus* 206 days respectively, which represents a 34% increment (*P*=0.0586) (**Figure 17A, B**). Thus, the percentage of alive *RANKL$^{fl/fl}$/Zmpste24$^{-/-}$/Dmp1-Cre* mice at the age of 200 days was 90.5% compared to 55.2% of *RANKL$^{fl/fl}$/Zmpste24$^{-/-}$* mice (*P*=0.0071) (**Figure 17B**). Nevertheless, further experiments aimed at evaluating the cardiovascular function and vascular calcification in *RANKL$^{fl/fl}$/Zmpste24$^{-/-}$/Dmp1-Cre* will determine whether the impaired production of osteocyte-derived RANKL might impinge on the development of these pathologies in *Zmpste24*-deficient mice, being this one of the possible explanations for the increased survival observed using this genetic approach.
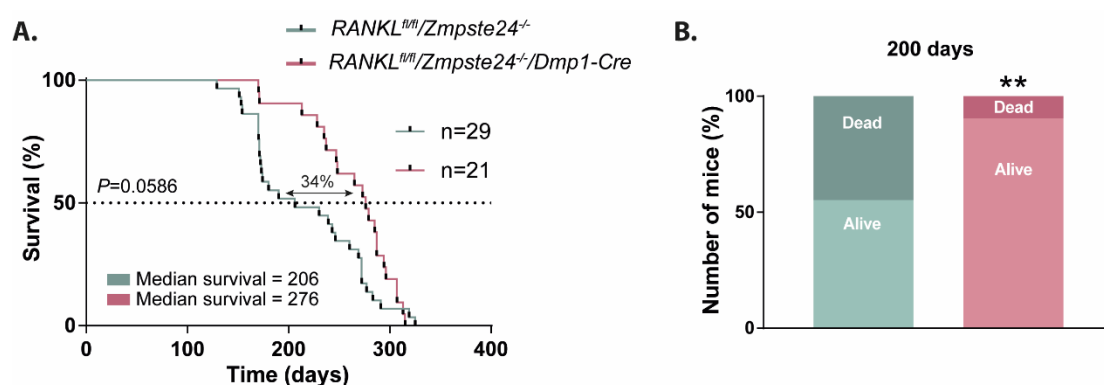
Figure 17. Depletion of RANKL in osteocytes leads to a marked increase in the median survival of *Zmpste24$^{-/-}$* mice. A. Kaplan-Meir survival plot. Median survival, percentage of median lifespan extension and animal number are indicated in the graph. **B.** Comparison of the number of dead and alive mice between *RANKL$^{fl/fl}$/Zmpste24$^{-/-}$* and *RANKL$^{fl/fl}$/Zmpste24$^{-/-}$ /Dmp1-Cre* groups at the age corresponding to 200 days of lifespan in the joint survival distribution. **P<0.01, one-tailed Fisher's exact test was used to determine statistical significance.

III.- Exploring the role of the hepcidin modulator matriptase-2 on the development of HFD-induced obesity in mice

Multiple studies have reported a close link between ageing and obesity, since age-associated decline is associated with the accumulation of abdominal WAT or the fat deposition in skeletal muscle, among others (Miard and Picard 2008; Slawik and Vidal-Puig 2006; Barzilai *et al.* 2012). The increase of WAT usually leads to serious alterations in endocrine signalling pathways, affecting for instance insulin sensitivity (Jura and Kozak 2016). On the other hand, as we previously summarized in the **Introduction** section, metabolic regulation plays a crucial role of in the initiation and establishment of the ageing process. Indeed, multiple anti-ageing approaches, as caloric restriction, have probed their efficiency alleviating ageing symptoms and lengthen life expectancy by targeting critical endocrine pathways such as insulin/IGF1 axis (Galluzzi *et al.* 2014; López-Otín *et al.* 2016). Interestingly, it has also been described that alterations in iron homeostasis have been related to obesity and other metabolic disorders such as diabetes (Pihan-Le Bars *et al.* 2016; Miranda and Lawson 2018). In this regard, obesity has been associated to elevated levels on hepcidin (Bekri *et al.* 2006; Pihan-Le Bars *et al.* 2016), a peptide hormone which has been identified as the major regulator of iron metabolism (Bogdan *et al.* 2016). Our previous findings demonstrating that the serine protease matriptase-2 (*Tmprss6*) is a negative regulator of hepcidin levels based on the generation and functional characterization of a KO mouse model lacking this enzyme (Velasco *et al.* 2002; Folgueras *et al.* 2008), gave us an excellent opportunity to further determine whether the loss of this negative regulator of hepcidin plays a significant role in the development of an obese phenotype.

Matriptase-2 loss protects against HFD-induced obesity

To this purpose, we fed wild-type and *Tmprss6*^{-/-} mice a high-fat diet (HFD) for 20 weeks after weaning. In addition, to evaluate the specific contribution of the hypoferremic phenotype of *Tmprss6*^{-/-} mice in the outcome of the experiment, we treated *Tmprss6*^{-/-} mice with intraperitoneal injections of iron-dextran to revert their plasma iron deficiency. This treatment resulted in a marked rescue of most of the hematologic parameters characteristic of IRIDA, which are found in *Tmprss6*^{-/-} mice (**Supplementary Figure S2**). However, iron-treated *Tmprss6*^{-/-} mice showed systemic

and tissue iron levels above those found in wild-type mice (**Figure 18A and Supplementary Figure S3**). Therefore, as a control for iron overload in obesity and metabolic analysis, we also treated wild-type mice with intraperitoneal injections of iron-dextran in order to obtain similar iron levels to those observed in iron-treated $Tmprss6^{-/-}$ mice.

Consistent with hepcidin regulation by iron (Kautz *et al.* 2008; Daba *et al.* 2013), the higher circulating iron levels found in both iron-treated $Tmprss6^{-/-}$ and $Tmprss6^{+/+}$ mice further increased hepcidin expression over the abnormally high levels found in the absence of matriptase-2 (**Figure 18B**). Interestingly, we observed that all experimental models showing high hepcidin levels ($Tmprss6^{-/-}$ and iron-treated $Tmprss6^{-/-}$ mice, as well as iron-treated $Tmprss6^{+/+}$ mice) showed significantly less body weight than wild-type controls (**Figure 18C**) upon HFD. Body weight of iron-treated $Tmprss6^{-/-}$ and $Tmprss6^{-/-}$ mice was decreased by 35% when normalized to their length, since the size of $Tmprss6^{-/-}$ mice is slightly smaller (Folgueras *et al.* 2008) and it is partially recovered after iron administration (**Supplementary Figure S4A, B**). Thus, iron-treated $Tmprss6^{-/-}$ and $Tmprss6^{-/-}$ mice gained 50% less weight than wild-type mice when challenged with a HFD (**Supplementary Figure S4C**). Moreover, analysis of body composition by MRI showed a significant decrease in the percentage of body fat in $Tmprss6^{-/-}$ mice, which was further exacerbated by iron administration (**Figure 18D, E**). Further, analysis of fat deposits demonstrated that fat pad weights normalized to total body weight were reduced in all compartments analysed, including brown adipose tissue (BAT), in $Tmprss6^{-/-}$ mice and in both $Tmprss6^{-/-}$ and $Tmprs6^{+/+}$ mice treated with iron compared with wild-type animals (**Figure 18F**).

In agreement with MRI analyses, the reduction in fat deposits was more pronounced in both iron-treated $Tmprss6^{-/-}$ and $Tmprs6^{+/+}$ mice than in $Tmprss6^{-/-}$ mice. Opposite to fat pads, the weight of other tissues normalized to total body weight was higher in $Tmprss6^{-/-}$ mice and in both iron-treated $Tmprss6^{-/-}$ and $Tmprss6^{+/+}$ mice than in wild-type mice (**Supplementary Figure S4D**). Altogether, our results indicate that the reduced weight gain observed in $Tmprss6^{-/-}$ mice and in both $Tmprss6^{-/-}$ and $Tmprss6^{+/+}$ mice treated with iron compared to wild-type mice is attributed to a lower fat content. Moreover, the analysis of lipid levels, frequently altered in obesity, showed a significant reduction in the concentration of plasma cholesterol in $Tmprss6^{-/-}$ mice and in both $Tmprss6^{-/-}$ and $Tmprss6^{+/+}$ mice treated with iron compared with controls

(**Figure 18G**). However, we found that plasma triglycerides were lower in *Tmprss6⁻/⁻* mice, but not in both iron-treated *Tmprss6⁻/⁻* and *Tmprss6⁺/⁺* mice, compared to wild-type mice (**Figure 18G**).
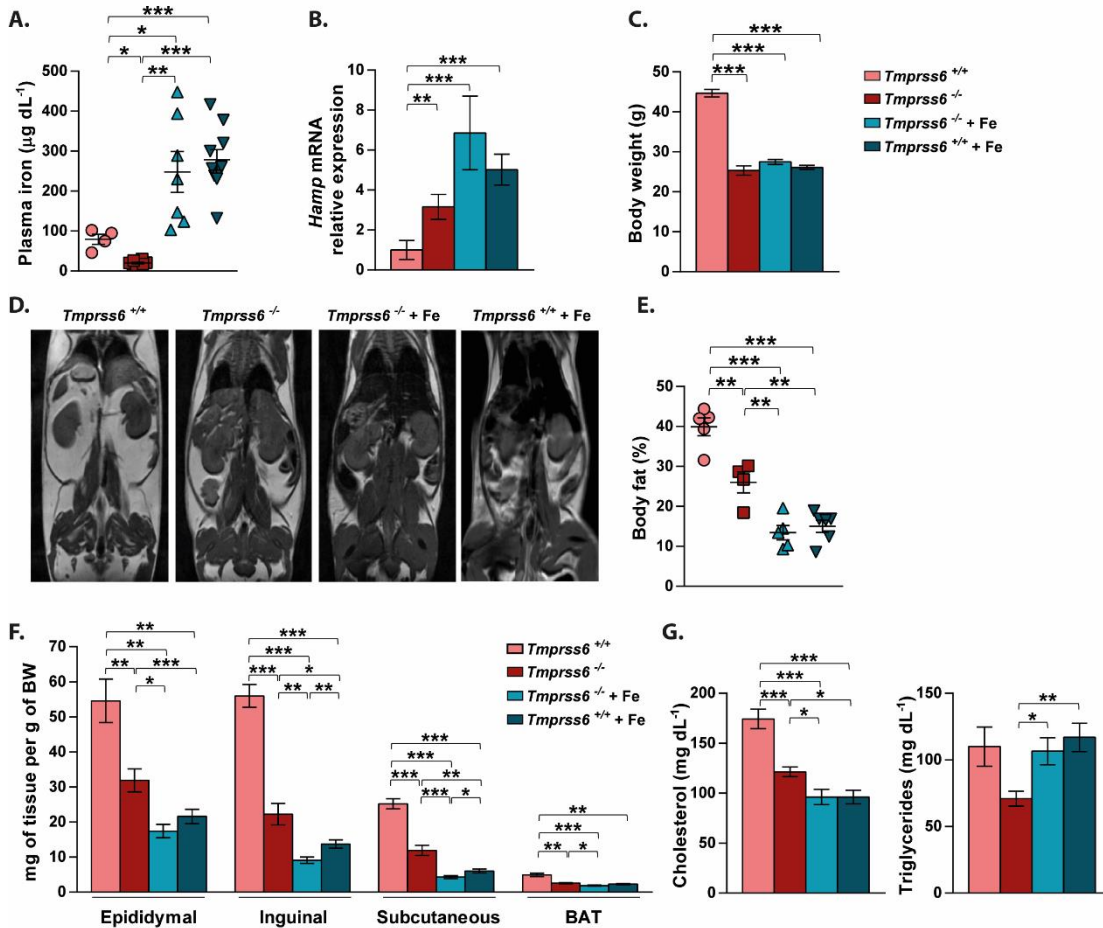
Figure 18. Loss of matriptase-2 induces resistance to high-fat diet-induced obesity. **A.** Fasting plasma concentration of iron in *Tmprss6⁺/⁺* (n=4), *Tmprss6⁻/⁻* (n=8), and both iron-treated *Tmprss6⁻/⁻* and *Tmprss6⁺/⁺* (n=7 and n=10, respectively) mice fed a HFD for 20 weeks. **B.** Relative gene expression of hepcidin (*Hamp*) in liver samples from HFD-fed *Tmprss6⁺/⁺* (n=11), *Tmprss6⁻/⁻* (n=10), and both iron-treated *Tmprss6⁻/⁻* and *Tmprss6⁺/⁺* mice (n=10 and n=8, respectively). **C.** Body weight of *Tmprss6⁺/⁺* (n=7), *Tmprss6⁻/⁻* (n=10), and both iron-treated *Tmprss6⁻/⁻* and *Tmprss6⁺/⁺* mice (n=13 and n=10 respectively) fed a HFD for 20 weeks. **D.** Representative MRI images across the body of *Tmprss6⁺/⁺* (n=5), *Tmprss6⁻/⁻* (n=4), and both iron-treated *Tmprss6⁻/⁻* and *Tmprss6⁺/⁺* mice (n=5 and n=6 respectively) fed a HFD. White areas denote fat. **E.** Body fat percentage was quantified by image analysis of MRI data on the same mice. **F.** White adipose (epididymal, subcutaneous and inguinal) and brown adipose tissue (BAT) masses were determined relative to body weight from HFD-fed *Tmprss6⁺/⁺* (n=7), *Tmprss6⁻/⁻* (n=10), and both iron-treated *Tmprss6⁻/⁻* and *Tmprss6⁺/⁺* mice (n=12-13 and n=10 respectively). **G.** Fasting plasma levels of cholesterol and triglycerides from HFD-fed

Tmprss6^{+/+} (n=7–9), *Tmprss6*^{-/-} (n=8–9), and both iron-treated *Tmprss6*^{-/-} and *Tmprss6*^{+/+} mice (n=9 and n=9–10 respectively). Data shown are mean ± SEM. *$P<0.05$, **$P<0.01$, ***$P<0.001$, two-tailed Student's t-test and Mann–Whitney test.

Reduced adipocyte hypertrophy in the absence of matriptase-2

To improve our understanding of the observed reduction in fat deposits in *Tmprss6*^{-/-} mice upon high-fat feeding, we performed histological analyses of white (WAT) and brown adipose tissues. WAT analysis revealed a significant decrease in adipocyte cell size in *Tmprss6*^{-/-} mice and in both iron-treated *Tmprss6*^{-/-} and *Tmprss6*^{+/+} mice compared with wild-type animals (**Figure 19A, B**). Accordingly, this reduction in adipocyte hypertrophy was accompanied by a concomitant increase in the number of adipocytes per area (**Figure 19A, B**). Moreover, histological analysis of BAT also showed a significant reduction in fat content in the absence of matriptase-2. Thus, iron-treated *Tmprss6*^{-/-} and *Tmprss6*^{-/-} mice showed smaller and multilocular lipid droplets compared to wild-type controls (**Figure 19A, C**), indicating that the observed resistance to the obesity-induced phenotype in *Tmprss6*^{-/-} mice was not only related to a decrease in WAT hypertrophy, but also to a reduction in the lipid content of BAT. This phenotype was also observed in iron-treated *Tmprss6*^{+/+} mice (**Figure 19A–C**). Notably, analysis of the expression levels of genes involved in adipocyte differentiation, such as *Cebpa*, *Srebf1*, and *Pparg*, showed no major differences between wild-type and *Tmprss6*^{-/-} mice, suggesting that the observed changes in adipocyte size were not due to alterations in the main adipocyte differentiation program (**Supplementary Figure S5A, B**). Of note, the expression of some of these genes was down-regulated in those experimental groups in which the reduction in body fat was more exacerbated, as in both *Tmprss6*^{-/-} and *Tmprss6*^{+/+} mice treated with iron.

To further explore those metabolic parameters that could be influenced by the loss of fat mass, we analysed the levels of leptin, a key adipokine produced by the adipose tissue. These analyses revealed a remarkable reduction in plasma leptin concentration in the absence of matriptase-2 and in the iron-treated experimental groups, all of them showing a lean phenotype, compared to wild-type mice (**Figure 19D**). Hence, consistent with low leptin levels, *Tmprss6*^{-/-} mice and both iron-treated *Tmprss6*^{-/-} and *Tmprss6*^{+/+} mice showed increased food intake compared with wild-type controls (**Supplementary Figure S4E**). Therefore, these results demonstrated that the

reduced weight gain observed in the absence of matriptase-2 was not due to a lower appetite.
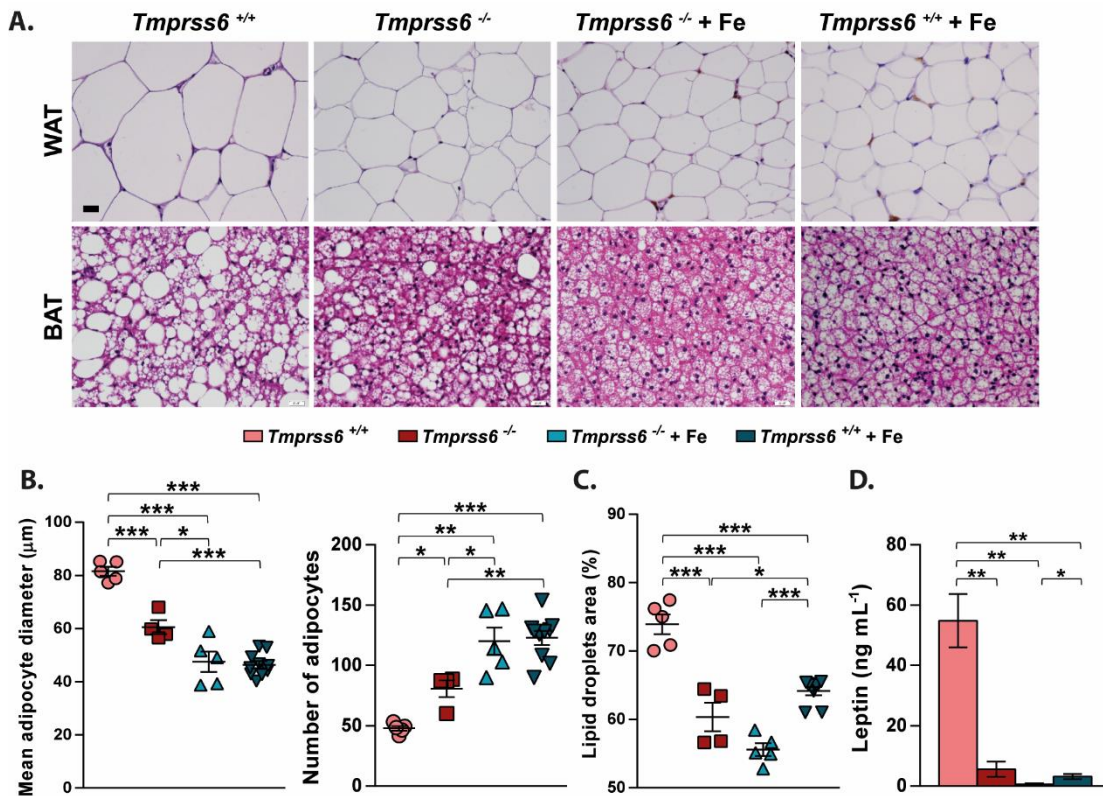
Figure 19. Matriptase-2 deficiency prevents diet-induced adipocyte hypertrophy. A. Representative images of epididymal fat pad and BAT sections stained with H&E from *Tmprss6*^{+/+} (n=5), *Tmprss6*^{-/-} (n=4), and both iron-treated *Tmprss6*^{-/-} and *Tmprss6*^{+/+} mice (n=5 and n=9–10 respectively) fed a HFD for 20 weeks. **B.** Size and number of epididymal adipocytes in *Tmprss6*^{+/+} (n=5), *Tmprss6*^{-/-} (n=4), and both iron-treated *Tmprss6*^{-/-} and *Tmprss6*^{+/+} mice (n=5 and n=10, respectively). **C.** Percentage of total area occupied by all lipid droplets in BAT sections stained with H&E in *Tmprss6*^{+/+} (n=5), *Tmprss6*^{-/-} (n=4), and both iron-treated *Tmprss6*^{-/-} and *Tmprss6*^{+/+} mice (n=5 and n=9, respectively). **D.** Fasting plasma concentration of leptin in *Tmprss6*^{+/+} (n=6), *Tmprss6*^{-/-} (n=6), and both iron-treated *Tmprss6*^{-/-} and *Tmprss6*^{+/+} mice (n=6 and n=9, respectively) fed a HFD. Scale bar 20 µm. Data shown are mean ± SEM. *$P<0.05$, **$P<0.01$, ***$P<0.001$, two-tailed Student's t-test and Mann–Whitney test.

Decreased hepatic steatosis in *Tmprss6*^{-/-} mice fed a HFD

Next, we analysed whether matriptase-2 deficiency also prevented the development of hepatic steatosis, a common disease frequently associated with obesity. Thus, Oil Red O staining of liver sections of HFD-fed mice showed a marked macrovesicular pattern of steatosis in wild-type mice (**Figure 20A**). However, this

macrovesicular pattern was not detected in *Tmprss6*$^{-/-}$ nor in both iron-treated *Tmprss6*$^{-/-}$ and *Tmprss6*$^{+/+}$ mice, indicating a clear reduction in liver lipid accumulation in the absence of matriptase-2 (**Figure 20A**). Consistent with these findings, quantification of liver triglyceride content showed a significant reduction in triglyceride levels in *Tmprss6*$^{-/-}$ mice and in both *Tmprss6*$^{-/-}$ and *Tmprss6*$^{+/+}$ mice treated with iron compared with wild-type animals (**Figure 20B**). To examine whether the observed reduction in lipid content was due to alterations in the hepatic lipid metabolism, we analysed the expression levels of key genes involved in lipid synthesis and fatty acid oxidation. Surprisingly, we found a significant up-regulation in the expression levels of genes involved in *de novo* lipid synthesis, such as *Fasn* and *Acaca*, in *Tmprss6*$^{-/-}$ mice compared to wild-type mice (**Figure 20C**). Furthermore, we found that the expression of one of the main regulators of fatty acid oxidation, such it is *Cpt1a*, was also increased in *Tmprss6*$^{-/-}$ mice (**Figure 20D**). Interestingly, this up-regulation was not observed in iron-treated *Tmprss6*$^{-/-}$ animals, suggesting that the increased expression of diverse metabolic enzymes with opposite functions in the absence of matriptase-2 is mainly caused by their hypoferremic phenotype, since iron treatment completely reverted the observed changes to wild-type levels. Nevertheless, in agreement with the observed histological and biochemical data, we found that the expression level of *Pparg*, a key driver of hepatic triglyceride storage (Matsusue *et al.* 2008), was markedly down-regulated in *Tmprss6*$^{-/-}$ mice and in both iron-treated *Tmprss6*$^{-/-}$ and *Tmprss6*$^{+/+}$ mice compared to wild-type animals (**Figure 20E**). This reduction was accompanied by a decrease in the expression level of the *Pparg* downstream target *Fsp27/CIDEC*, encoding a lipid-droplet associated protein that promotes lipid accumulation, in both iron-treated *Tmprss6*$^{-/-}$ and *Tmprss6*$^{+/+}$ mice compared to wild-type animals (**Figure 20E**).
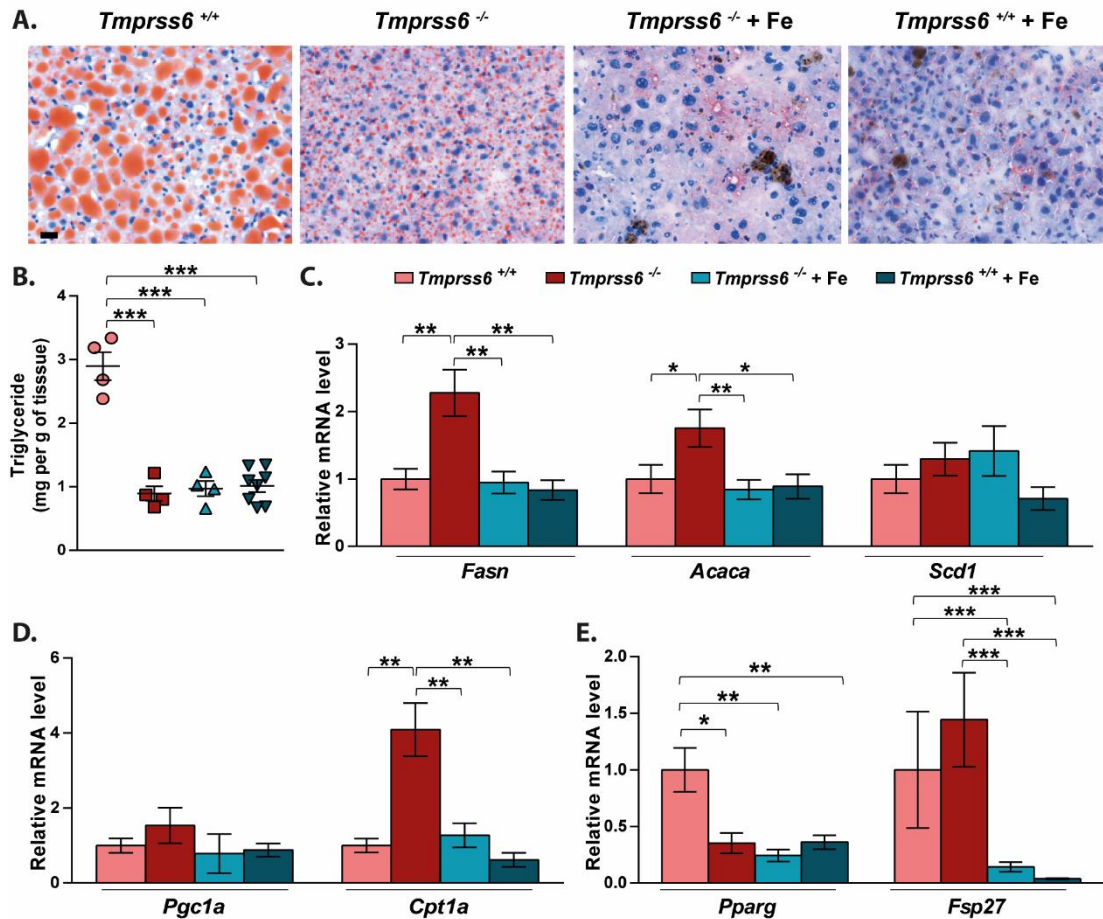
Figure 20. Matriptase-2 loss impairs hepatic steatosis upon HFD feeding. A. Representative Oil Red O staining of liver sections from *Tmprss6*^{+/+} (n=4), *Tmprss6*^{-/-} (n=4), and both iron-treated *Tmprss6*^{-/-} and *Tmprss6*^{+/+} mice (n=4 and n=8, respectively) fed a HFD. **B.** Triglyceride content of liver samples from HFD-fed *Tmprss6*^{+/+} (n=4), *Tmprss6*^{-/-} (n=4), and both iron-treated *Tmprss6*^{-/-} and *Tmprss6*^{+/+} mice (n=4 and n=8, respectively). Relative expression levels of genes related to lipogenesis (**C**), β-oxidation (**D**), and lipid storage (**E**) in liver samples from HFD-fed *Tmprss6*^{+/+} (n=11), *Tmprss6*^{-/-} (n=8–10), and both iron-treated *Tmprss6*^{-/-} and *Tmprss6*^{+/+} mice (n=9-10 and n=7–8 respectively). Scale bar 20 µm. Data shown are mean ± SEM. *$P<0.05$, **$P<0.01$, ***$P<0.001$, two-tailed Student's t-test and Mann–Whitney test.

Improved glucose homeostasis in *Tmprss6*^{−/−} mice fed a HFD.

The striking resistance to the development of an obese phenotype observed in the absence of matriptase-2, prompted us to evaluate whether matriptase-2 deficiency also affected glucose homeostasis. Thus, consistent with the reduced fat content, we found lower plasma insulin levels in *Tmprss6*^{-/-} mice and in both iron-treated *Tmprss6*^{-/-} and *Tmprss6*^{+/+} mice compared with wild-type mice, suggesting the possibility of

improved insulin sensitivity in the absence of matriptase-2 (**Figure 21A**). Accordingly, the concentration of fasting blood glucose was significantly reduced in both iron-treated *Tmprss6⁻/⁻* and *Tmprss6⁺/⁺* mice, in which the resistance to diet-induced obesity was more exacerbated, but not in *Tmprss6⁻/⁻* mice compared with WT mice (**Figure 21B**). Interestingly, analysis of the expression levels of key hepatic gluconeogenic and glycolytic genes, such as *Pck1* and *Pfk1*, revealed a significant up-regulation of these genes in *Tmprss6⁻/⁻* mice compared to those found in wild-type mice (**Figure 21C, D**). However, similarly to what we observed in the analysis of genes involved in the regulation of lipid metabolism, this up-regulation of enzymes belonging to opposite metabolic routes was ameliorated or completely reverted in iron-treated *Tmprss6⁻/⁻* mice (**Figure 21C, D**). Altogether, these results suggest that the observed deregulation in the expression levels of both gluconeogenic and glycolytic genes in *Tmprss6⁻/⁻* mice is a consequence of their iron deficiency, which may explain why glucose levels are not decreased in these mice compared with wild-type animals despite their leaner phenotype.
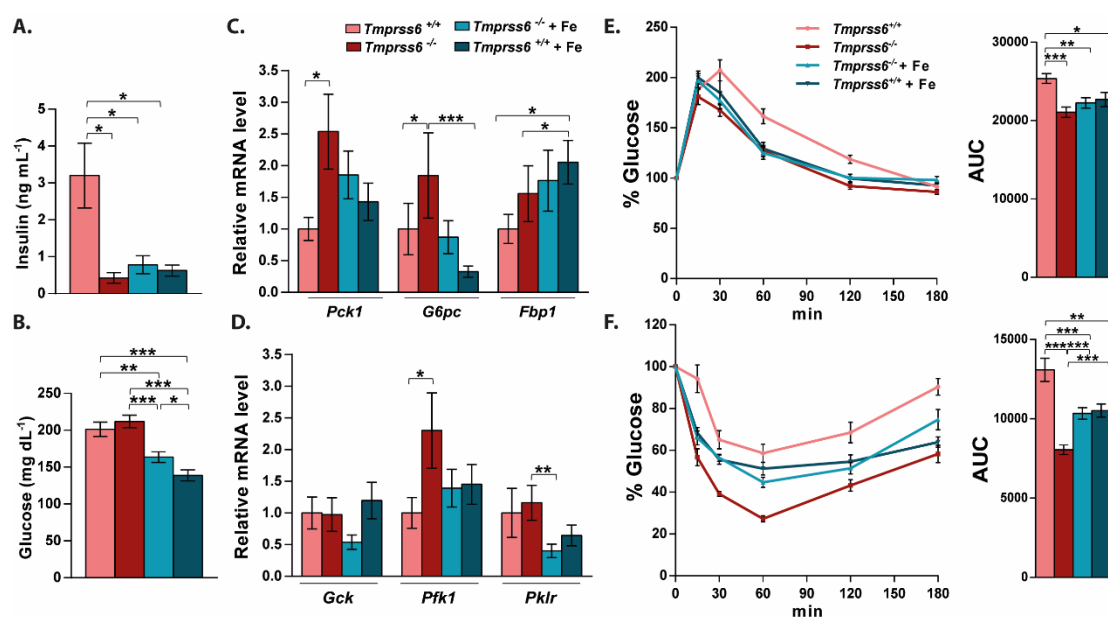
Figure 21. Improved glucose metabolism in HFD-fed *Tmprss6*-deficient mice. **A**. Fasting plasma concentration of insulin in HFD-fed *Tmprss6⁺/⁺* (n=10), *Tmprss6⁻/⁻* (n=6), and both iron-treated *Tmprss6⁻/⁻* and *Tmprss6⁺/⁺* mice (n=8 and n=6 respectively). **B.** Fasting blood glucose concentration in HFD-fed *Tmprss6⁺/⁺* (n=11), *Tmprss6⁻/⁻* (n=13), and both iron-treated *Tmprss6⁻/⁻* and *Tmprss6⁺/⁺* mice (n=13 and n=10 respectively). Relative expression levels of genes related to gluconeogenesis (**C**) and glycolysis (**D**) in liver samples from HFD-fed *Tmprss6⁺/⁺* (n=11), *Tmprss6⁻/⁻* (n=8–9), and both iron-treated *Tmprss6⁻/⁻* and *Tmprss6⁺/⁺* mice (n=10-11 and n=8 respectively). **E.** Glucose tolerance test after overnight fasting in HFD-fed Tmprss6 +/+

(n=11), *Tmprss6*^-/- (n=12), and both iron-treated *Tmprss6*^-/- and *Tmprss6*^+/+ mice (n=9 and n=9 respectively). **F.** Insulin tolerance test after overnight fasting in HFD-fed Tmprss6 +/+ (n=11), *Tmprss6*^-/- (n=12), and both iron-treated *Tmprss6*^-/- and *Tmprss6*^+/+ mice (n=13 and n=11 respectively). AUC, area under the curve. Data shown are mean ± SEM. *$P<0.05$, **$P<0.01$, ***$P<0.001$, two-tailed Student's t-test and Mann–Whitney test.

Nonetheless, to further explore glucose homeostasis in the absence of matriptase-2, we performed glucose tolerance tests by intraperitoneal administration of glucose to the mice. These experiments revealed a significant improved glucose clearance in *Tmprss6*^-/- and iron treated *Tmprss6*^-/- mice compared with wild-type animals (**Figure 21E**). Similarly, blood glucose levels decreased more rapidly in knock-out mice upon insulin injection, indicating increased insulin sensitivity in these mice, which is consistent with their lower insulin levels (**Figure 21F**). Remarkably, iron treatment partially increased insulin resistance of *Tmprss6*^-/- mice, although this resistance did not reach wild-type levels. Similar results were also observed in iron treated *Tmprss6*^+/+ mice. These findings are in agreement with a deleterious role of iron on adipose tissue function (Dongiovanni *et al.* 2013). Altogether, these results demonstrate that matriptase-2-deficiency protects against the development of glucose intolerance and insulin resistance associated with diet-induced obesity, probably as a consequence of their decreased fat mass.

Increased fat lipolysis in *Tmprss6*^–/– mice fed a HFD

To determine the possible causes of the reduced adiposity observed in the absence of matriptase-2, we next analysed mice energy expenditure by using indirect calorimetry. These experiments showed higher rates of oxygen consumption and CO_2 production adjusted for lean mass in *Tmprss6*^-/- mice compared with wild-type mice during both light and dark phases (**Supplementary Figure S6A, B**). Accordingly, energy expenditure was significantly increased in these mice (**Supplementary Figure S6C**). Remarkably, iron treatment completely reverted this phenotype. Thus, iron treated *Tmprss6*^-/- mice showed similar energy expenditure than wild-type mice (**Supplementary Figure S6C**), suggesting that the observed alterations in the absence of matriptase-2 could be a consequence of the hypoferremic phenotype. These changes occurred in the absence of a significant increase in the locomotor activity or the

expression levels of thermogenic genes in BAT samples of *Tmprss6*^{-/-} mice compared to those found in wild-type mice (**Supplementary Figure S6D, 7**). Taken together, these data suggest that energy balance might not be the main mechanism responsible for the observed resistance to diet-induced obesity in the absence of matriptase-2, since iron-treated *Tmprss6*^{-/-} mice behave similar to wild-type mice in this regard but show a marked lean phenotype. Therefore, to get further insights into the mechanisms that could explain the reduced fat content of *Tmprss6*^{-/-} and iron-treated *Tmprss6*^{-/-} mice, we analysed the expression levels of the main genes responsible for the hydrolysis of stored lipids in adipocytes in WAT samples. Notably, we found a significant increase in *Pnpla2* (adipose triglyceride lipase, ATGL) gene expression in *Tmprss6*^{-/-} mice compared to those in wild-type mice (**Figure 22A**), which was further confirmed at the protein level (**Figure 22B**). ATGL protein concentration was also significantly elevated in iron-treated *Tmprss6*^{-/-} mice (**Figure 22B**). No differences were detected in the expression level of the lipolytic gene *Lipe* (hormone-sensitive lipase, HSL), but we observed a significant increase in the expression level of *Adrb3* (β3-adrenergic receptor) in *Tmprss6*^{-/-} and iron-treated *Tmprss6*^{-/-} mice compared to wild-type mice (**Figure 22A**), being β-adrenergic signalling one of the main pathways responsible for the control of HSL activity and fat mobilization in the adipose tissue (Mottillo *et al.* 2007). Thus, β-adrenergic stimulation leads to the phosphorylation of HSL, which increases the hydrolytic activity of the enzyme against triacylglycerol substrate (Kraemer and Shen 2002).

Considering that HSL is primarily regulated by post-translational mechanisms rather than at the mRNA level, we were prompted to analyse the phosphorylation status of HSL in WAT samples. Western-blot analysis revealed a striking increase in phospho-HSL levels versus total HSL protein in *Tmprss6*^{-/-} and iron-treated *Tmprss6*^{-/-} mice compared with wild-type mice (**Figure 22B**). Interestingly, HSL phosphorylation was also significantly elevated in iron treated *Tmprss6*^{+/+} mice (**Figure 22B**). Taken together, these results suggest that the reduced adiposity observed in matriptase-2 deficient mice, with and without iron supplementation, is due to an increased lipolysis triggered by the two main lipolytic enzymes, HSL and ATGL. In addition, we found that HSL phosphorylation and ATGL concentration were increased in iron-treated *Tmprss6*^{+/+} mice, suggesting a relevant role for the lipolytic pathway in these mice that also show a significant reduction in their fat mass compared to wild-type mice.

A.

B.
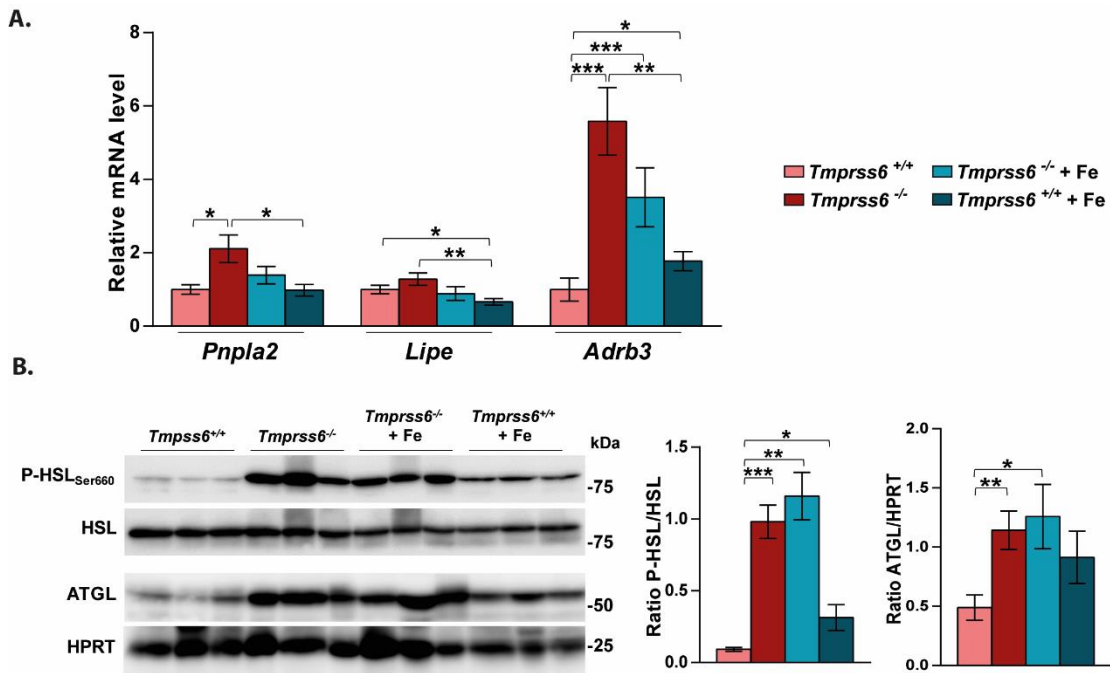
Figure 22. Increased WAT lipolysis in mice lacking matriptase-2 upon HFD feeding. **A.** Relative expression levels of genes related to lipolysis in WAT samples from HFD-fed *Tmprss6*^{+/+} (n=11), *Tmprss6*^{-/-} (n=7), and both iron-treated *Tmprss6*^{-/-} and *Tmprss6*^{+/+} mice (n=11 and n=8, respectively). **B.** Western-blot analysis of phospho-HSL(Ser660), total HSL and ATGL protein expression in WAT samples from HFD-fed *Tmprss6*^{+/+} (n=6), *Tmprss6*^{-/-} (n=6), and both iron-treated *Tmprss6*^{-/-} and *Tmprss6*^{+/+} mice (n=6 and n=7 respectively). (left) A representative result showing increased phospho-HSL and ATGL protein levels in *Tmprss6*^{-/-} and both iron-treated *Tmprss6*^{-/-} and *Tmprss6*^{+/+} mice compared to wild-type mice. (right) Quantification of phospho-HSL protein levels relative to total HSL levels and ATGL protein levels relative to loading control HPRT (hypoxanthine-guanine phosphoribosyltransferase). Note that phospho-HSL and the corresponding loading control, the total HSL protein, were detected on the same samples run in parallel in two identical blots. Data shown are mean ± SEM. *$P<0.05$, **$P<0.01$, ***$P<0.001$, two-tailed Student's t-test and Mann–Whitney test.

Hepcidin down-regulation induces obesity in *Tmprss6*^{–/–} mice

Considering that adipocyte iron deregulation has recently been associated to alterations in adipokine secretion and insulin resistance (Dongiovanni *et al.* 2013; Gabrielsen *et al.* 2012; Gao *et al.* 2015), we next asked if variations in adipocyte iron content may also influence the lipolytic program of the adipose tissue of matriptase-2 deficient mice. To this end, we measured iron levels in adipocytes isolated from WAT samples obtained from all experimental groups. No differences were observed in the iron content of adipocytes from *Tmprss6*^{-/-} and iron-treated *Tmprss6*^{-/-} mice compared

to wild-type mice. Remarkably, the excess of iron of both *Tmprss6*^{-/-} and *Tmprss6*^{+/+} mice treated with iron was mostly accumulated in the stromal-vascular fraction (SVF) of the adipose tissue, which contains a high percentage of infiltrating macrophages, rather than in the adipocytes themselves (**Supplementary Figure S8**). On the basis of the high hepcidin levels found in the three experimental groups with a leaner phenotype, *Tmprss6*^{-/-} and both iron-treated *Tmprss6*^{-/-} and *Tmprss6*^{+/+} mice, we further investigated whether hepcidin up-regulation might be responsible for the induction of lipolysis and the HFD-obesity resistance phenotype observed in matriptase-2 deficient mice. To test this hypothesis, we aimed at blocking hepcidin up-regulation in *Tmprss6*^{-/-} mice by using a neutralizing antibody against hemojuvelin (HJV), a molecule that acts as a co-receptor of the BMP (bone morphogenetic protein) signalling pathway that promotes hepcidin transcription (Babitt *et al.* 2006). We treated weekly *Tmprss6*^{-/-} mice with an anti-HJV neutralizing antibody or control anti-IgG for 18 weeks. Thus, mice were treated for the first time at the age of 6 weeks, two weeks after weaning and the onset of HFD administration, and the treatment lasted until the time of sacrifice. As shown in **Supplementary Figure S9**, the monitoring of plasma hematologic parameters over time showed a rapid rescue of haemoglobin (Hgb) levels in anti-HJV-treated *Tmprss6*^{-/-} mice compared to those injected with control anti-IgG after two weeks of treatment. This recovery was also observed in the rest of hematologic parameters analysed, which peaked 4 weeks after the onset of the antibody therapy and it was sustained during the whole treatment period, reaching wild-type levels in anti-HJV-treated *Tmprss6*^{-/-} mice (**Table 1**).

Table 1. Hematologic parameters of HFD-fed *Tmprss6*^{+/+} and *Tmprss6*^{-/-} mice treated with anti-IgG or anti-HJV antibodies.

	Hgb (g dL^{-1})	Hct (%)	MCV (fL)	MCH (pg)	MCHC (g dL^{-1})	RDW (%)
Tmprss6^{+/+}	11.9 ± 0.4	35.1 ± 0.8	39.5 ± 0.4	13.4 ± 0.1	33.9 ± 0.4	18.8 ± 0.2[‡‡‡]
Tmprss6^{-/-} + anti-IgG	7.8 ± 0.3 [***]	24.5 ± 0.8 [***]	24.2 ± 0.5 [***]	7.7 ± 0.2 [***]	31.7 ± 0.7 [*]	29.8 ± 0.7 [***]
Tmprss6^{-/-} + anti-HJV	12.2 ± 0.5[†††]	36.5 ± 1.5[†††]	40.5 ± 0.5[†††]	13.5 ± 0.3[†††]	33.5 ± 0.6	21.2 ± 0.6[††]

Complete blood counts were measured from whole blood of HFD-fed *Tmprss6*^{+/+} (n=8), *Tmprss6*^{-/-} + anti-IgG (n=5) and *Tmprss6*^{-/-} + anti-HJV (n=8) male mice after 18 weeks of antibody therapy upon overnight fasting. Data are presented as mean ± SEM. Hgb, haemoglobin; Hct, haematocrit; MCV, mean corpuscular volume; MCH, mean corpuscular

haemoglobin; MCHC, mean corpuscular haemoglobin concentration; RDW, red cell distribution width. $^{*}P<0.05$; $^{***}P<0.001$, two-tailed Student's t-test and Mann-Whitney test *Tmprss6$^{-/-}$ + anti-IgG versus Tmprss6$^{+/+}$* mice. $^{††}P<0.01$; $^{†††}P<0.001$, two-tailed Student's t-test and Mann-Whitney test *Tmprss6$^{-/-}$ + anti-HJV versus Tmprss6$^{-/-}$ + anti-IgG* mice. $^{‡‡‡}P<0.001$, two-tailed Student's t-test and Mann-Whitney test *Tmprss6$^{-/-}$ + anti-HJV versus Tmprss6$^{+/+}$* mice.

Consistent with these data, anti-HJV therapy also restored the hair coat of *Tmprss6$^{-/-}$* mice as a result of the recovery of plasma iron levels (Folgueras *et al.* 2008) (**Figure 23A, C**). The analysis of liver samples from this experimental setting allowed us to confirm the significant reduction of hepcidin expression in anti-HJV-treated *Tmprss6$^{-/-}$* mice compared to anti-IgG-treated *Tmprss6$^{-/-}$* mice, thereby demonstrating the efficacy of the anti-HJV therapy (**Figure 23B**). Consistent with the restoration of systemic iron levels upon hepcidin down-regulation, the concentration of plasma ferritin significantly increased in anti-HJV-treated *Tmprss6$^{-/-}$* mice compared to anti-IgG-treated *Tmprss6$^{-/-}$* mice, reaching wild-type levels (**Supplementary Figure S10A**). In agreement, we observed a significant increase in the liver iron content of anti-HJV-treated *Tmprss6$^{-/-}$* mice compared to the anti-IgG control group, which was accompanied by a down-regulation of the transferrin receptor 1 (*Tfrc*, *TfR1*) mRNA levels and protein expression in this tissue (**Supplementary Figure S10B–D**). More important, hepcidin down-regulation in anti-HJV-treated *Tmprss6$^{-/-}$* mice completely abolished the obesity-resistant phenotype observed in matriptase-2 deficient mice on HFD diet. Thus, anti-HJV-treated *Tmprss6$^{-/-}$* mice gain significantly more weight than anti-IgG-treated *Tmprss6$^{-/-}$* mice (**Figure 23D**).
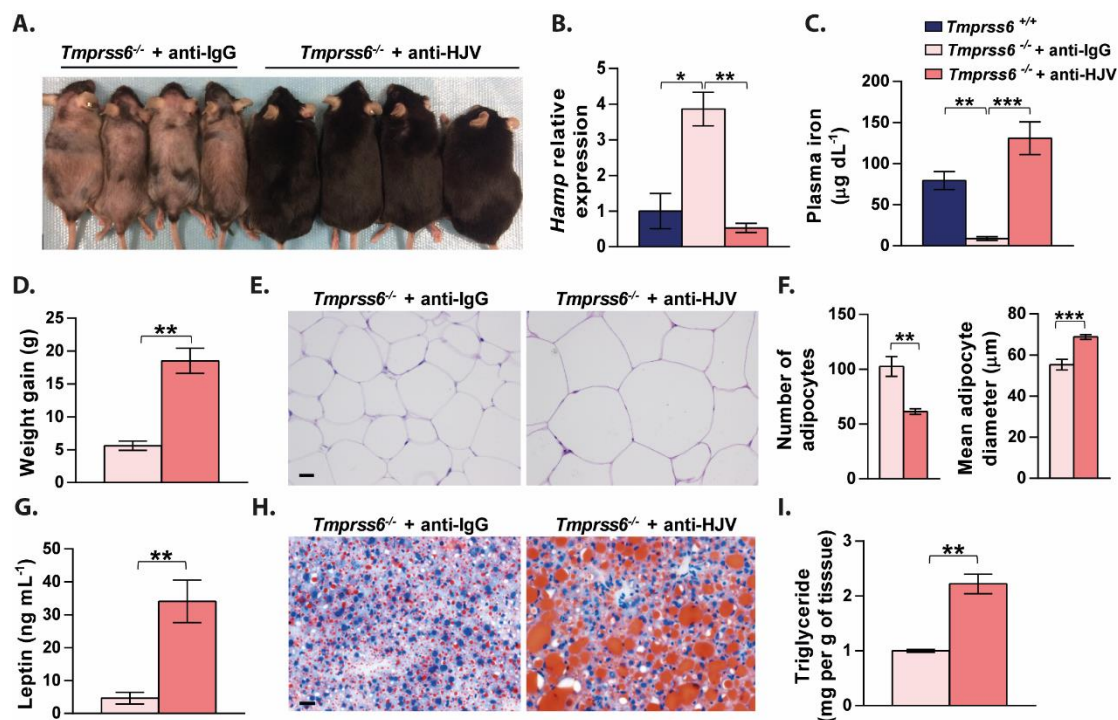
Figure 23. Hepcidin down-regulation in *Tmprss6*-deficient mice reverts the obesity-resistant phenotype. **A.** Representative image of HFD-fed *Tmprss6$^{-/-}$* mice treated weekly with anti-HJV neutralizing antibody or control anti-IgG for 18 weeks. The image shows the hair coat recovery and the increased body weight of anti-HJV-treated *Tmprss6$^{-/-}$* mice compared to *Tmprss6$^{-/-}$* mice treated with control anti-IgG. **B.** Relative gene expression of hepcidin (*Hamp*) in liver samples from HFD-fed *Tmprss6$^{+/+}$* (n=7), anti-IgG-treated *Tmprss6$^{-/-}$* (n=5), and anti-HJV-treated *Tmprss6$^{-/-}$* (n=8) mice. **C.** Fasting plasma concentration of iron in HFD-fed *Tmprss6$^{+/+}$* (n=4), anti-IgG-treated *Tmprss6$^{-/-}$* (n=5), and anti-HJV-treated *Tmprss6$^{-/-}$* (n=8) mice. **D.** Weight gain of anti-IgG-treated *Tmprss6$^{-/-}$* (n=5), and anti-HJV-treated *Tmprss6$^{-/-}$* (n=8) HFD-fed mice after 18 weeks of antibody administration. **E.** Representative images of epididymal fat pad sections stained with H&E from HFD-fed anti-IgG-treated *Tmprss6$^{-/-}$* (n=5) and anti-HJV-treated *Tmprss6$^{-/-}$* (n=8) mice. **F.** Number and size of epididymal adipocytes in HFD-fed anti-IgG-treated *Tmprss6$^{-/-}$* (n=5), and anti-HJV-treated *Tmprss6$^{-/-}$* (n=8) mice. **G.** Fasting plasma concentration of leptin in anti-IgG-treated *Tmprss6$^{-/-}$* (n=5), and anti-HJV-treated *Tmprss6$^{-/-}$* (n=8) mice fed a HFD. **H.** Representative Oil Red O staining of liver sections from anti-IgG-treated *Tmprss6$^{-/-}$* (n=5), and anti-HJV-treated *Tmprss6$^{-/-}$* (n=8) mice fed a HFD. **I.** Triglyceride content of liver samples from HFD-fed anti-IgG-treated *Tmprss6$^{-/-}$* (n=5), and anti-HJV-treated *Tmprss6$^{-/-}$* (n=8) mice. Scale bar 20 µm. Data shown are mean ± SEM. *$P<0.05$, **$P<0.01$, ***$P<0.001$, two-tailed Student's t-test and Mann–Whitney test.

Further, analysis of fat deposits in these mice demonstrated that the weight gain was due to a significant increase in the adiposity of anti-HJV-treated *Tmprss6$^{-/-}$* versus anti-IgG-treated mice (**Supplementary Figure S11**). This increase in the adiposity was

accompanied by a marked adipocyte hypertrophy of WAT samples and a significant increase in leptin production in anti-HJV-treated $Tmprss6^{-/-}$ mice compared to anti-IgG treated $Tmprss6^{-/-}$ mice (**Figure 23E–G**). Hepcidin down-regulation also resulted in a marked liver steatosis in anti-HJV-treated $Tmprss6^{-/-}$ mice (**Figure 23H, I**). Furthermore, we found that hepcidin down-regulation in matriptase-2 deficient mice through anti-HJV therapy completely reverted the lipolytic program of the adipose tissue to wild-type levels (**Figure 24A, B**). Altogether, these data yield insights into the mechanism responsible for the obesity-resistant phenotype of matripase-2 deficient mice, providing functional evidence of the prominent role of hepcidin in the regulation of lipid metabolism (**Supplementary Table S4**).
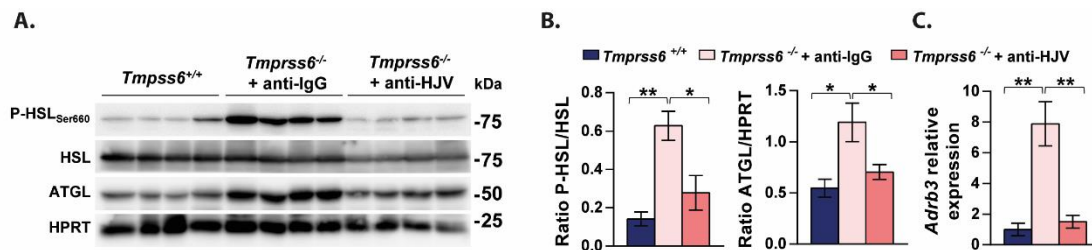
Figure 24. Hepcidin down-regulation in *Tmprss6*-deficient mice impairs WAT lipolysis.
A. Western-blot analysis of phospho-HSL(Ser660), total HSL and ATGL protein expression in WAT samples from HFD-fed T $Tmprss6^{+/+}$ (n=5), anti-IgG-treated $Tmprss6^{-/-}$ (n=5), and anti-HJV-treated $Tmprss6^{-/-}$ (n=8) mice. A representative result showing decreased phospho-HSL and ATGL protein levels in anti- HJV-treated $Tmprss6^{-/-}$ mice compared to anti-IgG-treated $Tmprss6^{-/-}$ mice. **B.** Quantification of phospho-HSL protein levels relative to total HSL levels and ATGL protein levels relative to loading control HPRT. Note that phospho-HSL and the corresponding loading control, the total HSL protein, were detected on the same samples run in parallel in two identical blots. **C.** Relative gene expression of Adrb3 in WAT samples from HFD-fed $Tmprss6^{+/+}$ (n=8), anti-IgG-treated $Tmprss6^{-/-}$ (n=5), and anti-HJV-treated $Tmprss6^{-/-}$ (n=8) mice. Scale bar 20µm. Data shown are mean ± SEM. *$P<0.05$, **$P<0.01$, two-tailed Student's t-test and Mann–Whitney test.

Discussion

Ageing can be defined as an inexorable process that causes a progressive functional deterioration of the organisms over time, leading to reduced reproduction and increased probability of suffering a number of pathological conditions and death (Jones *et al.* 2014; Kennedy *et al.* 2014). Due to its social and economic impact, an increased interest in ageing-related research has exponentially grown over the last 30 years. During this time, many studies have focused on exploring the role of cell-intrinsic alterations in the ageing process and longevity, paying special attention to those changes occurring at the intercellular, tissue, and organism level as a result of this intrinsic cellular deterioration (Gude *et al.* 2018; Pluvinage and Wyss-Coray 2020; Zhang *et al.* 2020). Interestingly, systemic interventions such as exercise or caloric restriction have been shown to modulated ageing-related phenotypes in a variety of tissues (Clark-Matott *et al.* 2015; Hou *et al.* 2016), and even lifespan (Wood *et al.* 2004; Fontana *et al.* 2010; Mattison *et al.* 2012; Bárcena *et al.* 2018), highlighting the relevance of understanding this process as a global phenomenon. These findings raise the important question of which is the relative contribution of cell-intrinsic and -extrinsic mechanisms to the emergence and development of ageing and age-related diseases. Hence, in this Doctoral Thesis we have studied how genomic specific changes and other interesting age-related cell-extrinsic alterations, which may encompass biophysical fluctuations in secreted factors, may be sufficient to modulate the ageing process as a whole, also impacting on the development of frequent age-associated disorders such as obesity.

As longevity is an inherent complex process that is, at least, partially coded in our genome, an interesting approach to identify key players in age-associated organismal decline is to analyse specific genetic variants in species that, from an evolutionary perspective, have evolved longer lifespans. This analysis may help to unveil the molecular mechanisms of healthy ageing that have been developed by long-lived species, including those changes related to protection against early manifestations of age-related disorders such as cancer. For this reason, the first objective of this Doctoral Thesis has been the "Identification of cell-intrinsic determinants of longevity in the genome of two long-lived giant tortoises by means of a manual annotation approach" (**I**). In this context, we reported the preliminary characterization of the Lonesome George's genome, which belongs to the subspecies *Chelonoidis abingdonii*, along with a low-coverage version of the genome of *Aldabrachelys gigantea*. We have

manually annotated a large set of genes related to multiple physiological processes following a hypothesis-driven strategy, which allowed the identification of changes affecting relevant residues of pivotal proteins that, otherwise, might have been overlooked by automatic methods. Hence, the results presented in this Doctoral Thesis provide evidence of selective pressure towards mechanisms aimed at maintaining genome stability in giant tortoises, along with improved function of the immune system and tumour protecting capabilities, among others (**I**). This evidence comes from considering the presumed function of pivotal gene expansions and gene-specific variants, compared with their close related species, as putative adaptations of the giant tortoise lineage to an exceptional and healthy longevity.

Thus, by comparing the genome of related tortoise species, we have identified specific lineage variants that could potentially affect six of the nine hallmarks of ageing (López-Otín *et al.* 2013). First, we identified changes in three candidate factors (NEIL1, RMI2, and XRCC6) related to the maintenance of genome integrity, one of the primary characteristics of ageing, as well as in proteins related to telomere maintenance and proteostasis (DCLRE1B and EEF1A1) (**I**). Causal evidences of the role of genome maintenance in the aging process have been provided by exploring human progeroid syndromes and genetically engineered mouse models that exhibit DNA damage accumulation, accelerated ageing phenotypes, and shortened lifespan (Moskalev *et al.* 2013). Moreover, multiple genome sequencing studies have pointed towards several putative strategies for lifespan modulation and low disease incidence based on these mechanisms. In agreement with our findings, it has recently been described that other large, long-lived vertebrates have developed specific adaptations associated with DNA repair and maintenance of genome instability, as well as proteostasis preservation. For instance, the analysis of the bowhead whale genome – a huge mammal whose lifespan is over 200 years – revealed a duplication in *proliferating cell nuclear antigen* (*PCNA*), a gene involved in DNA replication and damage repair processes that acts as a cofactor of DNA polymerase δ and increases its processivity during replication. This work also pointed out positively selected genes implicated in DNA repair, such as *ERCC1*, along with an enrichment in genes associated with translation processes, which could be ultimately linked to improved proteostasis (Keane *et al.* 2015; Toren *et al.* 2020). Likewise, similar findings were observed in the genome of the white shark, a large Elasmobranchii characterised by a large genome

size and a lifespan of 73 years, in which many of the genes found to be under positive selection participate in DNA damage response, DNA repair, and translation synthesis, such as *CHEK2*, *RFC5* or *DTL* (Marra *et al.* 2019). Of note, these mechanisms seem to be also involved in the modulation of longevity in small, long-lived mammals (Kim *et al.* 2011; Zhang *et al.* 2013; Huang *et al.* 2019). Indeed, a recent study has shed light into the relevance of double-strand break (DSB) repair in long-lived rodents, whose longevity is associated with specific aminoacidic-changes that optimize the efficacy of SIRT6, a protein that regulates DNA repair and maintains epigenomic stability (Tian *et al.* 2019b). The fact that these adaptations are well conserved across phylogenetically distant species that share exceptional lifespans suggests a process of convergent evolution and reinforces the critical relevance of these genetic changes in the ageing process.

Furthermore, we uncovered variants in genes that are relevant for cellular nutrient detection systems (*IGF1R*, *GSK3A*, and *NLN*), but also for the mitochondrial function (*ALDH2*, *NLN*, and *GAPDH*) and intercellular communication (*ITGA* and *MIF*) (**I**). Classically, decreased insulin/insulin-like growth factor 1 (IGF1) signalling (IIS) has been related to longevity in an evolutionarily conserved manner (Fontana *et al.* 2010). Besides, other modifications putatively involved in a metabolic adjustment towards longer lifespans have been observed across mammals (Ma *et al.* 2015), highlighting the influence of nutrient sensing mechanisms in the systemic regulation of health and longevity (López-Otín *et al.* 2016). In this context, mutations that significantly impair the function of IGF1R have been reported in human centenarians (Suh *et al.* 2008). Moreover, other specific sequence changes affecting this receptor were also described in *Myotis brandtii*, a species of microbat that can live more than 41 years (Seim *et al.* 2013). Likewise, other works have revealed altered transcriptional regulation of the insulin/IGF-1 axis in other small mammals, such as the naked mole rat, which is the longest-lived rodent with a lifespan of over 30 years (Kim *et al.* 2011). However, evidences of positive selection affecting classical regulators of metabolic homeostasis, such as *INSRA*, *IGF1RA* or *IRS1*, have also been found in the genomic analysis of the African turquoise killifish, which unlike other species mentioned above, displays an exceptional short lifespan (Valenzano *et al.* 2015). Although the physiological effects of these genomic changes in some of these species are still unexplored, this fact emphasizes that longevity modulation may implicate the same

mechanisms but regulated in opposite directions in both long- and short-lived species. Notably, the genetic variants and copy-number variations found in the giant tortoise genome involve the same gene sets and signalling networks as those described in other long-lived organisms, such as GH/IGF-1 axis or DNA damage response pathways. These similarities reinforce the convergence of diverse cell-intrinsic modifications affecting the genome of numerous species towards systemic nodes that modulate longevity across evolution.

Besides some of the above-mentioned exceptions, it is widely accepted that larger animals of different species live longer than their smaller counterparts. For example, elephants and humans live longer than mice, but they live less than bowhead whales, which can reach 100 tons and may live up to 200 years. Despite the benefits of living longer, an important consequence of gigantism is a potential increase in the risk of cancer development. Hypothetically, a larger number of cells together with an extended lifespan would provide cells more time to accumulate mutations, increasing the probability of carcinogenesis. However, the relationship between these biological processes seems to be much more complex than expected. Thus, there are long-lived metazoans, such as giant tortoises, that very rarely exhibit malignant tumours, suggesting the occurrence of natural determinants of both cancer protection and longevity in large organisms (Peto's paradox) (Albanes 1998; Caulin *et al.* 2011).

In an attempt to further explore these questions, we found a number of gene specific changes in giant tortoises that might contribute to explain the low prevalence of cancer in Chelonians, which is remarkably lower than in the other reptilians (2.7% in Chelonians vs. 15% in snakes) (Garner *et al.* 2004). Indeed, when Chelonians are split into turtles and tortoises, the prevalence of neoplasia in the last group is even lower, around 1.4%. In this regard, the aforementioned changes affecting *NEIL1, RMI2* and *XRCC6* suggest a differential regulation of DNA integrity in this lineage, which may be critical for their exceptional lifespan, but it also provides protection against cancer (**I**). It is well known that most cancers are characterized by the accumulation of a high frequency of genomic mutations, which finally triggers DNA damage and jeopardize genome integrity (Hanahan *et al.* 2011). The result of this continual selective pressure has been the development of protective mechanisms to counteract the detrimental effects of these mutations and safeguard the genetic information, especially in those organisms that have evolved towards longer lifespans and larger bodies. Thus,

the relevance of DNA repair mechanisms in cancer resistance has also been highlighted by other works. For example, the comparative analysis of telomere dynamics among different species of bats has suggested that the changes observed in several genes involved in telomere maintenance and DNA repair could underlie the low level of cancer incidence reported in these species (Foley *et al.* 2018). Further, the above-mentioned comparative genomic and transcriptomic studies in the bowhead whale identified notable examples of positively selected genes implicated in DNA repair, such as *ERCC1* and *ERCC3*, which, together with the duplication of *PCNA*, might also contribute to cancer resistance in this specie (Keane *et al.* 2015). Likewise, evidences of positive selection were also observed in the DNA repair enzyme XRCC5 of African killifish, putatively affecting the role of this protein (Valenzano *et al.* 2015).

Moreover, we found that several known tumour suppressor genes, like *PRDM1* and *SMAD4*, were expanded in a common ancestor of both giant tortoises, Lonesome George and Aldabra tortoise, which results in a very interesting finding since gene duplication is one of the principal mechanisms that generate phenotypic innovations in evolution (Kaessmann 2010). Notably, some of these genes also play a pivotal role in the immune response, which, together with the expansions observed in other key players of this process (*PRF1* and *GZMA*), suggests an enhanced immunosurveillance in turtles that might confer an extra capability to suppress oncogenic processes in these animals (**I**). Gene expansions associated with the immune response in a cancer protective context were also found in small, long-lived mammals, such as microbats or the blind mole rat (Zhang *et al.* 2013; Seim *et al.* 2013; Fang *et al.* 2014).

These proposals related to the evolution of giant-tortoise-specific anticancer mechanisms need to be further evaluated by functional studies. However, other large, long-lived mammals, such as elephants, have evolved similar mechanisms to avoid their hypothetical increased risk to suffer cancer, such as harbouring in their genome multiple copy variants of *TP53*, an essential gene for genome stability that is considered the tumour suppressor par excellence (Abegglen *et al.* 2015). Although we did not observe any copy-number variation affecting this tumour suppressor gene, we found a specific modification at codon 106 (p.S106E) of *TP53* in turtles, which was also found in root voles (*Microtus oeconomus*). Initially, this variant was described in a stress-dependent context as an adaptation to hypoxia and cold, in which p.S106E hinders p53 from activating apoptotic genes under stress conditions, without affecting cell-cycle

genes (Zhao *et al.* 2013). Thus, the presence of this change in the amino acid sequence of p53 in the genome of terrestrial giant tortoises suggests a convergent evolutionary process in the adaptation to hypoxia, probably driven by an ancestral aquatic environment. Furthermore, other mechanism regarding p53 pathway has been evolved by blind mole rats, which present a specific change in p53 (R174K) that seems to promote its binding to promoters of cell cycle arrest genes instead of apoptotic targets (Kim *et al.* 2011; Fang *et al.* 2014). Together, these findings suggest that the same pathway may be regulated in different manners depending on the evolutionary context in order to adapt successfully to the changing environmental conditions, as well as to prevent pathologic processes that might be triggered by those unfavourable circumstances.

All above-mentioned findings further support the usefulness of hypothesis-driven approaches to unveil those genomic changes that may contribute to disentangle which molecular pathways are relevant for healthy ageing in long-lived species. Therefore, the first objective of this Doctoral Thesis has been accomplished through the identification of candidate genes and pathways that may underlie the extraordinary characteristics of two giant tortoise species, such as cancer resistance and their exceptional longevity. Nevertheless, much work remains to be done in order to decipher the intrinsic mechanisms of longevity, being one of the major challenges to understand how these specific genetic changes may encompass the systemic modulation of the ageing process and determine that some species live much longer than others.

An interesting feature of the functional decline associated to ageing is that it is systematically coordinated in different tissues and organs that are exposed to disparate microenvironments and stresses. Currently, numerous evidences support the idea that changes produced in an aged tissue can lead to the functional decay of other healthy tissues (López-Otín *et al.* 2013). In this regard, experiments based on heterochronic parabiosis have demonstrated that secreted factors in the young blood of healthy individuals can revert age-related features of their older counterparts and *vice versa* (Conboy *et al.* 2005; Brack *et al.* 2007; Villeda *et al.* 2011; Loffredo *et al.* 2013). As a further step to previous studies of our laboratory, highlighting the role of cell-extrinsic

mechanisms in the achievement of premature ageing phenotypes (de la Rosa *et al.* 2013), a second objective of this Doctoral Thesis has been the "Assessment of the functional relevance of cell-extrinsic mechanisms to the development of the progeroid phenotype in murine models of premature ageing" (**II**).

Numerous studies have pointed to GDF11 as a powerful anti-ageing candidate based on the observation that its levels in blood decrease with age, and that its supplementation in old mice improved the features and function of a number of age-deteriorated tissues, including cardiac and skeletal muscle and the cerebral vasculature (Loffredo *et al.* 2013; Katsimpardi *et al.* 2014; Sinha *et al.* 2014). As a result of these initial evidence, GDF11 became the focus of study as a presumed systemic modulator of the ageing process with broad benefits across multiple tissues. Indeed, recent findings have also established a relationship between rGDF11 treatment and the maintenance of metabolic homeostasis in aged mice (Walker *et al.* 2020; Katsimpardi *et al.* 2020), increasing the list of systems that may be putatively modulated by this circulating factor and establishing a connection between caloric restriction intervention and GDF11 regulation with age. Thus, this apparent pleiotropy prompted us to hypothesize that this factor might contribute to increase the lifespan of our progeroid mouse model, taking into consideration the number of key tissues/organs that could benefit.

To this end, we investigate the effect of the presumed anti-ageing factor GDF11 on the longevity of *Zmpste24* KO mice, given that this mouse model shares many of the phenotypes characteristic of natural ageing. Interestingly, we observed that *Zmpste24*$^{-/-}$ mice exhibited a marked decrease in the circulating pool of GDF11/8 proteins compared with their wild-type littermates when progeroid symptoms had already started to manifest, as no differences were observed when comparing plasma samples obtained from the same individuals at an early age (**II**). At this point, it is important to clarify that previous studies reported that the immunoreagents used when these experiments were carried out could not discriminate between GDF11 and GDF8, two closely related members of the TGF-β superfamily, in plasma samples (Egerman *et al.* 2015). Therefore, this preliminary conclusion regarding the reduction of GDF11 plasmatic levels must also include GDF8. Despite this fact, these results further support the similarities between the phenotype of our mouse model of premature ageing and the process of physiological ageing, since GDF11/8 decrease was first observed in

naturally aged mice and humans (Loffredo *et al.* 2013; Olson *et al.* 2015). However, rGDF11 daily treatment did not extend the lifespan of progeroid mice compared with vehicle-treated *Zmpste24*^{-/-} littermates (**II**). Nevertheless, this experiment allowed us to evaluate for the first time the effect of rGDF11 administration on longevity, a question that needed to be addressed considering its broad impact over other age-related phenotypes.

These findings emerged in a very controverted scenario in which GDF11 capacity to reverse age-associated decline and tissue dysfunction were called into question. As mentioned above, the initial observation regarding the decrease of GDF11 levels with age in mouse plasma samples (Loffredo *et al.* 2013) has recently been reinforced by additional reports working with aged mice but also with human samples (Zhang *et al.* 2015; Tian *et al.* 2019a; Añón-Hidalgo *et al.* 2019; Hudobenko *et al.* 2020; Katsimpardi *et al.* 2020). Nevertheless, the controversy about GDF11 age-dependent decline arises from the studies of Egerman *et al.*, who pointed out that the methods used in the initiall study by Loffredo *et al.* to detect GDF11 were nonspecific, as they could not discriminate between GDF11 and GDF8 cytokines. In addition, Egerman *et al.* were unable to detect a decrease in circulating GDF11 levels with age in human samples using a GDF11-specific immunoassay (Egerman *et al.* 2015), which raised the first doubts about the original observation about a GDF11 decline in aged organisms. Furthermore, using a similar immunoassay, another work found increased GDF11 serum levels in aged women (Chen *et al.* 2016), and comparable results were recently reported in mice, in which GDF11 serum levels were higher in aged mice compared with their younger counterparts (Liu *et al.* 2016). Considering all these data is difficult to reach an agreement on the circulating level dynamics of GDF11 over time, being this conflict probably based on the reliability of the detection methods used to recognize specifically GDF11 in plasma samples. However, regarding our experiments, we checked by Western-blot the levels of GDF11/8 in the blood of the same individual prior and 1 to 2 h after rGDF11 injection. Thus, even though we used an antibody able to recognize both GDF11 and GDF8, it is reasonable to speculate that the protein increase detected corresponded to rGDF11.

Along with our results showing no effect of rGDF11 administration on progeroid mice longevity (**II**), several works have also called into question the presumed capacity of this circulating factor to reverse tissue age-related decline. Thus, in addition to the controversy related to the decrease of GDF11 levels with age, there are also contradictory data with regards to GDF11 anti-ageing properties. Over the last years, several works have supported the initial observation about the positive effects of GDF11 supplementation on cardiac muscle hypertrophy (Poggioli *et al.* 2016; Duran *et al.* 2018). However, other recent studies have also shown the opposite effect (Zimmers *et al.* 2017; Harper *et al.* 2018). Moreover, it has been suggested that some of the original conclusions about GDF11 cardioprotective effects could be due to the decrease in body weight observed as a secondary effect of rGDF11 daily administration, directly related with a dose-dependent effect (Smith *et al.* 2015; Poggioli *et al.* 2016). Our results showed that rGDF11 treatment only caused a slight reduction in the body weight of female *Zmpste24*^{-/-} mice compared with vehicle-treated littermates during the first days of the experiment, whereas no significant differences were observed in the male cohort (**II**). Nevertheless, it is not clear whether any decrease in body weight would have resulted in longevity extension in our model, since one of the progeroid features is the reduction of body weight with age. In addition, contradictory data have also been reported regarding skeletal muscle regeneration (Sinha *et al.* 2014; Egerman *et al.* 2015; Schafer *et al.* 2016). Both dosing and the source of the recombinant protein have been claimed as possible factors explaining the discrepancies between the data obtained by different researchers (Poggioli *et al.* 2016; Walker *et al.* 2016). Nevertheless, such discrepancies cannot account for the dramatic differences in results obtained by two different groups that used equivalent amounts of rGDF11 (0.1mg/kg) (Sinha *et al.* 2014; Egerman *et al.* 2015). Therefore. additional effort is still needed in order to clarify the specific contribution of GDF11 in the development of age-related pathological conditions.

In summary, our findings demonstrate that although circulating GDF11/8 levels decrease in *Zmpste24*-deficient mice over time, rGDF11 protein administration is not sufficient to extend longevity in these progeroid mice (**II**). Although accelerated-ageing mouse models can serve as powerful tools to test and develop anti-ageing therapies common to both physiological and pathological ageing, the existence of certain differences between the two processes implies that further investigation is still

required to determine whether long-term GDF11 administration has a pro-survival effect on normal aged animals.

One of the main features of premature ageing syndromes, as well as natural ageing, is the loss of bone mass. This phenotype is recapitulated in *Zmpste24*-deficient mice, which exhibit a marked osteoporosis. In fact, mutations in its human orthologue *ZMPSTE24* cause mandibuloacral dysplasia, a form of progeria characterized by skeletal anomalies such as craniofacial abnormalities, hypoplasia of the mandible and clavicles and progressive osteolysis of the distal phalanges (Agarwal *et al.* 2003). Likewise, these patients, as those suffering from Hutchinson-Gilford progeria syndrome, develop cardiovascular disease characterized by atherosclerosis and arterial stiffness caused by vascular fibrosis and calcium deposition, which ultimately lead to myocardial infarction or stroke (Hamczyk *et al.* 2018a). Based on this background, we hypothesized that bone resorption might have a systemic effect on healthspan and even longevity of *Zmpste24*-deficient mice. Therefore, as part of the second objective of this Doctoral Thesis, we studied the organismal effect that the deletion of the cytokine RANKL, a master regulator of osteoclastogenesis (Yasuda *et al.* 1998; Kong *et al.* 1999), might have on these progeroid mice.

On this basis, we generated a new mouse strain in which *Zmpste24*$^{-/-}$ mice harbours a conditional deletion of RANKL in the osteocyte population, which has been postulated as the major source of this factor in bone after birth (Xiong *et al.* 2011; Nakashima *et al.* 2011). The specific elimination of RANKL in osteocytes prevented the development of a severe osteopetrosis phenotype (Xiong *et al.* 2011), as it has been described with the germline deletion of RANKL (Dougall *et al.* 1999). By using this approach, we demonstrated that the conditional elimination of osteocyte-produced RANKL totally recovers the microstructural trabecular bone parameters normally altered in *Zmpste24*$^{-/-}$ mice (**II**). Moreover, we also observed increased trabecular number or greater BMD referring cancellous bone in *RANKL*$^{fl/fl}$/*Zmpste24*$^{-/-}$/*Dmp1-Cre* mice compared to their WT littermates, which is in agreement with the results previously obtained with the generation of *RANKL*$^{fl/fl}$/*Dmp1-Cre* mice (Xiong *et al.* 2011). Thus, even though osteocyte-derived RANKL deletion leads to an increase in the femoral cancellous bone volume of about twofold when compared to WTs, no signs

of osteopetrosis were reported by Xiong *et al.* in these mice. Thus, we did not expect any detrimental impact because of the increased bone mass observed in our mouse model.

Interestingly, we have also observed an enhanced treadmill endurance in *RANKL^{fl/fl}/Zmpste24^{-/-}/Dmp1-Cre* mice compared with their *RANKL^{fl/fl}/Zmpste24^{-/-}* littermates, which was manifested as an improvement in both duration of exercise and distance travelled (**II**). Recently, it has been described that the induction of the RANK/RANKL pathway can inhibit myogenic differentiation, leading to skeletal muscle dysfunction (Dufresne *et al.* 2016). Likewise, it has been reported that human RANKL overexpression in mice (HuRANKL-Tg+) induced bone loss and diminished their muscle mass, as well as the maximal speed reached in treadmill (Bonnet *et al.* 2019). Moreover, it has been demonstrated that the treatment with denosumab, a neutralizing antibody against RANKL, was able to restore the muscle function in huRANKL mice (Bonnet *et al.* 2019). Although these works have employed approaches in which RANKL is modulated systemically and our strategy involves a specific osteocyte-derived RANKL deletion, their results are in line with our observations, therefore suggesting that local modulation of RANKL might also exert a broad impact on the musculoskeletal system. Nevertheless, given the ability of this membrane-bound cytokine to be processed by proteolytic cleavage, further experiments are needed to elucidate the relative effect of the membrane-bound and soluble forms of RANKL expressed by osteocytes on neighbour muscles.

Further, the remarkable extension on the median lifespan of *RANKL^{fl/fl}/ Zmpste24^{-/-}/Dmp1-Cre* compared with *RANKL^{fl/fl}/Zmpste24^{-/-}* mice becomes particularly evident at the age of 200 days of survival (**II**), demonstrating an organismal effect of the osteocyte-specific deletion of this cytokine. As hypothesized, this result may be a consequence of the reduced bone resorption achieved with this targeting strategy, which may impinge on the cardiovascular abnormalities observed in *Zmpste24^{-/-}* mice (Pendás *et al.* 2002; Rivera-Torres *et al.* 2016). The inverse correlation between bone mineral density and aortic calcification was established approximately 20 years ago, suggesting a close relationship between an excessive bone resorption, calcification of soft tissues and the onset of cardiovascular disease (Frye *et al.* 1992; Danilevicius *et al.* 2007; Caffarelli *et al.* 2017). Nonetheless, further experiments are required to determine the specific role of calcium metabolism in the

modulation of vascular calcification and its impact on the longevity of these progeroid mice.

Together, the results obtained in the second objective of this Thesis remark the relevance of cell-extrinsic mechanisms, acting either systemically or locally on neighbouring cells, in the control of specific pathologies and, more broadly, organismal ageing in a progeroid context. Along these lines, previous work of our laboratory have demonstrated that the coexistence of *Zmpste24*-deficient cells and *Zmpste24*-proficient cells (mosaic mice) completely prevented the development of the premature ageing phenotype, suggesting that cell-extrinsic mechanisms exerted by those "healthy" cells were responsible for the full reversion of progeroid features (de la Rosa *et al.* 2013). Moreover, additional experiments showed that the replicative defects of *Zmpste24*$^{-/-}$ fibroblasts grown *in vitro* were rescued by the presence of ECM produced by non-aged wild-type cells (de la Rosa *et al.* 2013). In this regard, it has been reported that many of the alterations observed in *Zmpste24*-null mice are caused by an impaired stem cell function (Espada *et al.* 2008; Liu *et al.* 2012; Song *et al.* 2013). Thus, these studies suggest that secreted proteins are able to boost tissue regeneration by promoting stem cell plasticity, also in a premature ageing context, contributing to the delay of organismal ageing and the onset of the pathologies observed in our progeroid model (Liu *et al.* 2012; Song *et al.* 2013; Kubben *et al.* 2017). In particular, previous reports have demonstrated that the exposure of muscle stem cells derived from *Zmpste24*-deficient mice to conditioned media from wild-type cells is able to restore *in vitro* their myogenic potential (Song *et al.* 2013). In this regard, it would be important to shed light on the impact of RANKL on stem cell function. Although significant progress has been made over the last years, much effort is still needed to identify additional systemic factors and signalling networks that may ameliorate the pathological conditions associated with accelerating ageing syndromes and natural ageing. Thus, understanding how the levels of these secreted factors are regulated will provide new insights into the organismal communication during ageing and how cell-intrinsic and extrinsic mechanisms integrate to drive this process.

It is well known that ageing is accompanied by quantitative changes in body composition over time, showing an increase in fat mass whereas lean mass declines.

These age-related changes in body composition commonly involve several metabolic alterations that are associated with each of the nine hallmarks of ageing (López-Otín *et al.* 2013; López-Otín *et al.* 2016). In an age-related context, obesity has emerged as a major health challenge because it significantly increases the vulnerability to diseases such as hypertension, T2DM, CV, and cancer, thereby contributing to reduced healthspan and lifespan (Bluher 2019). Remarkably, some authors have proposed that obesity impacts on organismal health in a similar manner to ageing, establishing that obesity may accelerate the process of ageing by underpinning the same molecular mechanisms from cellular to systemic level (Tam *et al.* 2020). Obesity condition is also associated with alterations in integrative networks that have an organismal effect on the individual, such as the promotion of systemic inflammation and the impairment of endocrine communication among different tissues (Bluher 2019; Tam *et al.* 2020).

Hepcidin is a major regulator of body iron balance at the systemic level, and numerous disorders have been related to an inappropriate iron and hepcidin regulation (Ganz and Nemeth 2015; Vela 2018; van Swelm *et al.* 2020). In this context, epidemiological studies have associated elevated hepcidin levels and iron deficiency with obesity (Bekri *et al.* 2006; Pihan-Le Bars *et al.* 2016). These studies suggest that increased hepcidin concentrations occur as a result of the chronic inflammatory condition linked to obese individuals, which ultimately leads to defective intestinal iron absorption and anaemia (Yanoff *et al.* 2007; Stoffel *et al.* 2020). On the other hand, iron overload, which also triggers hepcidin up-regulation, has been associated with fatty-liver disease, diabetes and insulin resistance, three common conditions frequently associated with obesity (Barisani *et al.* 2008; Martinelli *et al.* 2012). Therefore, in an attempt to shed light into the contribution of iron and the regulators of its homeostasis to the development of obesity and its pathogenic features, we developed the third objective of this Doctoral Thesis, which was focused on the "Characterization of the role of iron and matriptase-2, a negative regulator of the circulating factor hepcidin, in the development of HFD-induced obesity using a mouse model deficient in matriptase-2" (**III**).

We found that both *Tmprss6*$^{-/-}$ mice, which display a marked hypoferremic phenotype due to inadequate hepcidin upregulation, and iron-treated *Tmprss6*$^{-/-}$ mice, which are no longer hypoferremic but still preserve high hepcidin levels, were protected against body fat accumulation and the development of hepatic steatosis when

challenged with HFD. Furthermore, iron-treated wild-type mice, which also showed a significant hepcidin upregulation as a consequence of the exogenous iron administration, were equally protected against lipid accumulation (**III**). The fact that elevated hepcidin levels was the common mechanism shared by the three experimental groups, argued for a putative role of this peptide in the protection against the development of obesity and hepatic steatosis. Consistent with this hypothesis, our data demonstrated that blocking hepcidin up-regulation in *Tmprss6*$^{-/-}$ mice via anti-HJV therapy, completely reverted the lean phenotype as well as the hepatic steatosis resistance of matriptase-2 deficient mice (**III**). Moreover, we also observed that *Tmprss6*$^{-/-}$ mice displayed improved insulin sensitivity compared to wild-type mice, potentially accounting for their reduced adiposity (**III**). However, in agreement with previous data, both iron-treated *Tmprss6*$^{-/-}$ and *Tmprss6*$^{+/+}$ mice, which show higher levels of hepcidin compared to untreated *Tmprss6*$^{-/-}$ mice in addition to an iron overload phenotype, are more resistant to insulin signalling (**III**). These results are in line with the findings regarding the reduced visceral fat mass and insulin resistance observed in mice fed with an iron-enriched diet, which displayed a strong hepcidin up-regulation in the adipose tissue (Dongiovanni *et al.* 2013). Thus, further studies are needed to determine if hepcidin up-regulation alone is responsible for the observed phenotypes in the iron-treated mice or whether additional effects derived from iron deposition may account for the reduced adiposity, hepatic steatosis and the insulin resistance observed under iron overload conditions.

Recent findings also highlight the implication of iron overload in the control of adipokine production by adipose tissue. Thus, adipocyte specific ferroportin knock-out mice showed a significant reduction in both leptin and adiponectin plasma levels (Gabrielsen *et al.* 2012; Gao *et al.* 2015). Conversely, *Hfe*$^{-/-}$ mice, a model of hereditary hemochromatosis with decreased hepcidin levels and increased adipocyte ferroportin expression, showed enhanced leptin production (Gao *et al.* 2015). Although we have not found significant differences in the iron content of the adipocytes isolated from the different experimental groups, the finding of reduced leptin production in our mouse models with elevated hepcidin levels are compatible with the reported data mentioned above (**III**).

Further, our results suggest that the reduced adiposity observed in the absence of matriptase-2 is mainly due to the enhanced lipolysis we detected in the adipose tissue

of these mice, since no differences were observed in the expression levels of genes involved in adipocyte differentiation or thermogenesis compared with wild-type controls (**III**). Thus, the downregulation of the lipolytic program to wild-type levels, together with the recovery of the fat mass and the increased weight gain observed in anti-HJV-treated *Tmprss6*$^{-/-}$ mice, further supports the promoting role of hepcidin and lipolysis in the obesity-resistant phenotype of matriptase-2 deficient mice (**III**).

Altogether, the results obtained in the third objective demonstrate that the loss of matriptase-2 triggers lipolysis and prevents body fat accumulation upon nutrition overload, but also protects against obesity-associated pathological conditions such as hepatic steatosis and insulin resistance. Furthermore, we demonstrate that this phenotype is dependent on the inadequate hepcidin up-regulation characteristic of *Tmprss6*$^{-/-}$ mice. Our findings provide new insights regarding the role of hepcidin and iron regulation in metabolic homeostasis and adipocyte function, and suggest new strategies based on matriptase-2 inhibition for the treatment of obesity.

Interestingly, similar results to those presented in this Doctoral Thesis have been recently described regarding the function of other membrane-bound serine protease, hepsin, also highly expressed in the liver. Thus, this work has demonstrated that hepsin increases glycogen and lipid production in the liver and decreases metabolic rates and adipose tissue browning in mice by activating the hepatocyte growth factor (HGF) pathway in adipocytes and hepatocytes. Moreover, the authors described that hepsin-deficient mice exhibit a marked resistance to high-fat diet-induced obesity, as well as protection against hyperglycaemia and hyperlipidaemia. Further, hepsin deficiency in *db/db* mice, a classical animal model for T2DM, reduces the severity of their obesity and diabetes (Li *et al.* 2020). Since HGF is also a circulating factor produced by the liver with an emerging regulatory role on glucose transport and metabolism (Oliveira *et al.* 2018), these results emphasize the capacity of circulating factors to modulate the energy metabolism, and, thereby, impact on the development of metabolic diseases such obesity and diabetes.

Of note, the critical role of secreted factors in the maintenance of metabolic homeostasis has been extensively demonstrated. One of the best-established examples in this context is the role of interleukins in obesity and associated pathologies. Thus, a wide range of interleukins were identified as critical regulators of nutrient overload,

obesity and impaired insulin signalling, highlighting its contribution to the maintenance of energy balance (Hotamisligil 2017). Furthermore, several works have reported the regulation of energy homeostasis by secreted peptides derived from the central nervous system and peripheral tissues. Some of these peptides such as GLP-1, CCK, neuropeptide Y or leptin are involved in the modulation of metabolic disorders, including obesity (Kumar 2019). In this regard, numerous current studies are focused on developing anti-obesity treatments based on targeting these peptides (Coll 2018). Conversely, administration of recombinant fibroblast growth factor 21 (FGF21) corrects obesity and its pathological related conditions in mice, monkeys and even in humans, although the improvement was slight in this last experimental group (Coskun *et al.* 2008; Xu *et al.* 2009; Kharitonenkov *et al.* 2007; Talukdar *et al.* 2016). Of note, FGF21 overexpression is able to extend the lifespan of mice (Zhang *et al.* 2012), supporting the central role of metabolic homeostasis in the modulation of longevity, an evidence that was shown 30 years ago when targeting the insulin/IGF1 system in *Caenorhabditis elegans* (Kenyon *et al.* 1993). Further, the identification of other circulating factors, along with intracellular mediators, which potentially shift the energetic imbalance associated with pathological conditions like obesity, may provide new therapeutic opportunities to fight against metabolic diseases, improve the quality of life and promote a healthy ageing process.

In summary, the work presented in this Doctoral Thesis has focused on disentangling the complex interactions between intercellular pathways and cell-autonomous mechanisms that underlie the ageing process and age-related diseases (**Figure 25**). In the first part of this work, we have explored the genome of two long-lived giant tortoises in search of specific cell-intrinsic alterations that may be responsible for their extraordinary lifespan. Our study based on a detailed hypothesis-driven analysis has allowed us to identify genetic variants found in candidate genes involved in several of the hallmarks of ageing, as well as other related processes such as cancer resistance and immunosurveillance. Secondly, we have focused on studying the modulation of the ageing process through cell-extrinsic mechanisms by using a mouse model of premature ageing. Herein, we have provided new evidence regarding the complex function of GDF11 in age-dependent decline and have unveiled the pivotal contribution of osteocyte-derived RANKL to the pathological alterations associated with accelerated ageing syndromes. Finally, we have analysed the role of iron and

matriptase-2, a negative regulator of the circulating factor hepcidin, in the development of metabolic disorders frequently associated with age, such as obesity, by using *Tmprss6*-deficient mice challenged with HFD diet. Altogether, this work has intended to contribute to the better understanding of the regulatory cell-intrinsic and -extrinsic mechanisms that integrate the organismal communication during ageing and disease, and hopefully, may have shed some light on the development of novel therapeutic strategies aimed at improving the quality of life in a gradually aged world.
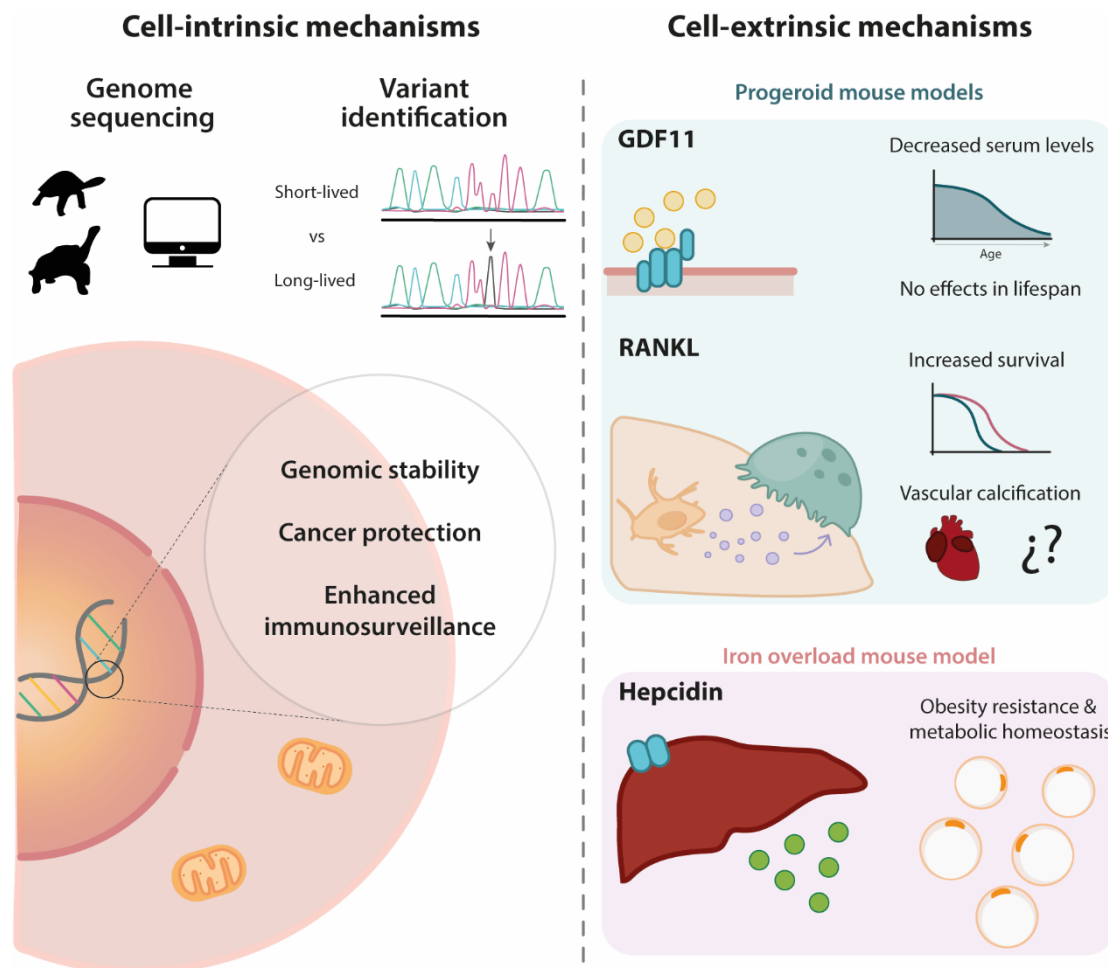
Figure 25. Putative cell-intrinsic and -extrinsic mechanisms involved in the process of normal and premature ageing, as well as in age-associated diseases, explored in the present Doctoral Thesis.

Conclusions

1. Hypothesis-driven manual annotation is an excellent tool to identify specific gene variants present in the genome of species with phenotypic characteristics of interest that could be overlooked using automatic annotation methods.

2. Giant-tortoise genome sequencing and manual annotation revealed lineage specific variants affecting DNA repair genes, inflammatory mediators and genes related to cancer resistance, which may contribute to the exceptional longevity of these species.

3. GDF11/8 plasma levels decrease with age in the mouse model deficient in the protease Zmpste24, which develops a premature ageing phenotype.

4. rGDF11 treatment is not sufficient to extend longevity of *Zmpste24*-deficient mice.

5. Osteocyte-specific RANKL elimination prevents osteoporotic phenotype in *Zmpste24*-deficient mice and improves their endurance capacity in a treadmill exhaustion test.

6. Conditional deletion of RANKL in osteocytes increases survival of *Zmpste24*-knockout mice.

7. The loss of matriptase-2 prevents body fat accumulation upon HFD administration and protects against obesity-associated pathological conditions such as hepatic steatosis and insulin resistance.

8. The phenotype of obesity-resistance observed in matriptase-2-deficient mice is triggered by a significant increase in fat lipolysis.

9. The phenotype of obesity-resistance observed in matriptase-2-deficient mice is dependent on the inadequate hepcidin up-regulation.

10. Down-regulation of hepcidin to wild-type levels using anti-HJV-based therapy completely reverts the obesity-resistant phenotype of matriptase-2-deficient mice.

1. La anotación manual dirigida por hipótesis es una excelente herramienta para identificar variantes génicas en el genoma de especies con características fenotípicas de interés que podrían pasar desapercibidas utilizando métodos de anotación automáticos.

2. La secuenciación y la anotación manual del genoma de las tortugas gigantes ha revelado variantes génicas específicas de linaje en genes involucrados en la reparación del daño en el ADN, en mediadores inflamatorios y en genes relacionados con la resistencia a cáncer, que pueden contribuir a la gran longevidad de estas especies.

3. Los niveles plasmáticos de GDF11/8 disminuyen con la edad en el modelo murino deficiente en la proteasa Zmpste24, el cual desarrolla un fenotipo de envejecimiento prematuro.

4. El tratamiento con GDF11 recombinante no es suficiente para aumentar la longevidad en el modelo murino deficiente en *Zmpste24*.

5. La eliminación especifica de RANKL en los osteocitos evita el desarrollo del fenotipo de osteoporosis observado en el modelo murino deficiente en *Zmpste24*, además de mejorar su capacidad de resistencia en una prueba de esfuerzo.

6. La eliminación condicional de RANKL en la población osteocítica aumenta la supervivencia de los ratones deficientes en *Zmpste24*.

7. La pérdida de la matriptasa-2 previene la acumulación de grasa tras la administración de una dieta rica en grasa y protege ante la aparición de patologías asociadas a la obesidad, como la esteatosis hepática o la resistencia a la insulina.

8. El fenotipo de resistencia a la obesidad observado en los ratones deficientes en matriptasa-2 es desencadenado por un aumento significativo de la lipólisis de la grasa.

9. El fenotipo de resistencia a la obesidad observado en los ratones deficientes en matriptasa-2 es dependiente de un aumento inadecuado en los niveles de hepcidina.

10. La reducción de la expresión de la hepcidina a los niveles propios los ratones silvestres, utilizando una terapia anti-HJV, revierte el fenotipo de resistencia a la obesidad observado en los ratones deficientes en matriptasa-2.

References

Abegglen, L. M., A. F. Caulin, A. Chan, K. Lee, R. Robinson, M. S. Campbell, W. K. Kiso, D. L. Schmitt, P. J. Waddell, S. Bhaskara, S. T. Jensen, et al. (2015). Potential mechanisms for cancer resistance in elephants and comparative cellular response to DNA damage in humans. *JAMA*, 314: 1850-60.

Agarwal, A. K., J. P. Fryns, R. J. Auchus, and A. Garg. (2003). Zinc metalloproteinase, ZMPSTE24, is mutated in mandibuloacral dysplasia. *Hum Mol Genet*, 12: 1995-2001.

Albanes, D. (1998). Height, early energy intake, and cancer. Evidence mounts for the relation of energy intake to adult malignancies. *BMJ*, 317: 1331-2.

Añón-Hidalgo, J., V. Catalán, A. Rodríguez, B. Ramírez, C. Silva, J. C. Galofré, J. Salvador, G. Fruhbeck, and J. Gómez-Ambrosi. (2019). Circulating GDF11 levels are decreased with age but are unchanged with obesity and type 2 diabetes. *Aging (Albany NY)*, 11: 1733-44.

Ashraf, A., M. Clark, and P. W. So. (2018). The aging of iron man. *Front Aging Neurosci*, 10: 65.

Babitt, J. L., F. W. Huang, D. M. Wrighting, Y. Xia, Y. Sidis, T. A. Samad, J. A. Campagna, R. T. Chung, A. L. Schneyer, C. J. Woolf, N. C. Andrews, et al. (2006). Bone morphogenetic protein signaling by hemojuvelin regulates hepcidin expression. *Nat Genet*, 38: 531-9.

Baker, D. J., T. Wijshake, T. Tchkonia, N. K. LeBrasseur, B. G. Childs, B. van de Sluis, J. L. Kirkland, and J. M. van Deursen. (2011). Clearance of p16Ink4a-positive senescent cells delays ageing-associated disorders. *Nature*, 479: 232-6.

Bárcena, C., P. M. Quirós, S. Durand, P. Mayoral, F. Rodríguez, X. M. Caravia, G. Mariño, C. Garabaya, M. T. Fernández-García, G. Kroemer, J. M. P. Freije, et al. (2018). Methionine restriction extends lifespan in progeroid mice and alters lipid and bile acid metabolism. *Cell Rep*, 24: 2392-403.

Bárcena, C., R. Valdés-Mas, P. Mayoral, C. Garabaya, S. Durand, F. Rodríguez, M. T. Fernández-García, N. Salazar, A. M. Nogacka, N. Garatachea, N. Bossut, et al. (2019). Healthspan and lifespan extension by fecal microbiota transplantation into progeroid mice. *Nat Med*, 25: 1234-42.

Barisani, D., S. Pelucchi, R. Mariani, S. Galimberti, P. Trombini, D. Fumagalli, R. Meneveri, E. Nemeth, T. Ganz, and A. Piperno. (2008). Hepcidin and iron-related gene expression in subjects with Dysmetabolic Hepatic Iron Overload. *J Hepatol*, 49: 123-33.

Baron, R., and M. Kneissel. (2013). WNT signaling in bone homeostasis and disease: from human mutations to treatments. *Nat Med*, 19: 179-92.

Barreiro, L. B., and L. Quintana-Murci. (2010). From evolutionary genetics to human immunology: how selection shapes host defence genes. *Nat Rev Genet*, 11: 17-30.

Barzilai, N., D. M. Huffman, R. H. Muzumdar, and A. Bartke. (2012). The critical role of metabolic pathways in aging. *Diabetes*, 61: 1315-22.

Bekri, S., P. Gual, R. Anty, N. Luciani, M. Dahman, B. Ramesh, A. Iannelli, A. Staccini-Myx, D. Casanova, I. Ben Amor, M. C. Saint-Paul, et al. (2006). Increased adipose tissue expression of hepcidin in severe obesity is independent from diabetes and NASH. *Gastroenterology*, 131: 788-96.

Bergo, M. O., B. Gavino, J. Ross, W. K. Schmidt, C. Hong, L. V. Kendall, A. Mohr, M. Meta, H. Genant, Y. Jiang, E. R. Wisner, et al. (2002). *Zmpste24* deficiency in mice causes

References

spontaneous bone fractures, muscle weakness, and a prelamin A processing defect. *Proc Natl Acad Sci U S A*, 99: 13049-54.

Birch, H. L. (2018). Extracellular matrix and ageing. *Subcell Biochem*, 90: 169-90.

Bitto, A., T. K. Ito, V. V. Pineda, N. J. LeTexier, H. Z. Huang, E. Sutlief, H. Tung, N. Vizzini, B. Chen, K. Smith, D. Meza, et al. (2016). Transient rapamycin treatment can increase lifespan and healthspan in middle-aged mice. *Elife*, 5.

Bitto, A., A. M. Wang, C. F. Bennett, and M. Kaeberlein. (2015). Biochemical Genetic Pathways that Modulate Aging in Multiple Species. *Cold Spring Harb Perspect Med*, 5.

Bluher, M. (2019). Obesity: global epidemiology and pathogenesis. *Nat Rev Endocrinol*, 15: 288-98.

Bluher, M., B. B. Kahn, and C. R. Kahn. (2003). Extended longevity in mice lacking the insulin receptor in adipose tissue. *Science*, 299: 572-4.

Bogdan, A. R., M. Miyazawa, K. Hashimoto, and Y. Tsuji. (2016). Regulators of iron homeostasis: new players in metabolism, cell death, and disease. *Trends Biochem Sci*, 41: 274-86.

Bonnet, N., L. Bourgoin, E. Biver, E. Douni, and S. Ferrari. (2019). RANKL inhibition improves muscle strength and insulin sensitivity and restores bone mass. *J Clin Invest*, 129: 3214-23.

Borghesan, M., W. M. H. Hoogaars, M. Varela-Eirin, N. Talma, and M. Demaria. (2020). A senescence-centric view of aging: implications for longevity and disease. *Trends Cell Biol*, 30: 777-91.

Brack, A. S., M. J. Conboy, S. Roy, M. Lee, C. J. Kuo, C. Keller, and T. A. Rando. (2007). Increased Wnt signaling during aging alters muscle stem cell fate and increases fibrosis. *Science*, 317: 807-10.

Brown, R. A. M., K. L. Richardson, T. D. Kabir, D. Trinder, R. Ganss, and P. J. Leedman. (2020). Altered iron metabolism and impact in cancer biology, metastasis, and immunology. *Front Oncol*, 10: 476.

Bustos, V., and L. Partridge. (2017). Good ol' fat: links between lipid signaling and longevity. *Trends Biochem Sci*, 42: 812-23.

Caffarelli, C., A. Montagnani, R. Nuti, and S. Gonnelli. (2017). Bisphosphonates, atherosclerosis and vascular calcification: update and systematic review of clinical studies. *Clin Interv Aging*, 12: 1819-28.

Carrero, D., C. Soria-Valles, and C. López-Otín. (2016). Hallmarks of progeroid syndromes: lessons from mice and reprogrammed cells. *Dis Model Mech*, 9: 719-35.

Castillo-Quan, J. I., L. Li, K. J. Kinghorn, D. K. Ivanov, L. S. Tain, C. Slack, F. Kerr, T. Nespital, J. Thornton, J. Hardy, I. Bjedov, et al. (2016). Lithium promotes longevity through GSK3/NRF2-dependent hormesis. *Cell Rep*, 15: 638-50.

Caulin, A. F., and C. C. Maley. (2011). Peto's Paradox: evolution's prescription for cancer prevention. *Trends Ecol Evol*, 26: 175-82.

Clark-Matott, J., A. Saleem, Y. Dai, Y. Shurubor, X. Ma, A. Safdar, M. F. Beal, M. Tarnopolsky, and D. K. Simon. (2015). Metabolomic analysis of exercise effects in the POLG mitochondrial DNA mutator mouse brain. *Neurobiol Aging*, 36: 2972-83.

Codina-Martínez, H., B. Fernández-García, C. Díez-Planelles, A. F. Fernández, S. G. Higarza, M. Fernández-Sanjurjo, S. Díez-Robles, E. Iglesias-Gutiérrez, and C. Tomás-Zapico.

(2020). Autophagy is required for performance adaptive response to resistance training and exercise-induced adult neurogenesis. *Scand J Med Sci Sports*, 30: 238-53.

Coll, A. P. (2018). Monogenic obesity; using drugs to bypass the problem. *Cell Metab*, 28: 1-2.

Compston, J. E., M. R. McClung, and W. D. Leslie. (2019). Osteoporosis. *Lancet*, 393: 364-76.

Conboy, I. M., M. J. Conboy, A. J. Wagers, E. R. Girma, I. L. Weissman, and T. A. Rando. (2005). Rejuvenation of aged progenitor cells by exposure to a young systemic environment. *Nature*, 433: 760-4.

Cornelissen, A., L. Guo, A. Sakamoto, R. Virmani, and A. V. Finn. (2019). New insights into the role of iron in inflammation and atherosclerosis. *EBioMedicine*, 47: 598-606.

Corti, P., J. Xue, J. Tejero, N. Wajih, M. Sun, D. B. Stolz, M. Tsang, D. B. Kim-Shapiro, and M. T. Gladwin. (2016). Globin X is a six-coordinate globin that reduces nitrite to nitric oxide in fish red blood cells. *Proc Natl Acad Sci U S A*, 113: 8538-43.

Coskun, T., H. A. Bina, M. A. Schneider, J. D. Dunbar, C. C. Hu, Y. Chen, D. E. Moller, and A. Kharitonenkov. (2008). Fibroblast growth factor 21 corrects obesity in mice. *Endocrinology*, 149: 6018-27.

Cremona, C. A., P. Sarangi, Y. Yang, L. E. Hang, S. Rahman, and X. Zhao. (2012). Extensive DNA damage-induced sumoylation contributes to replication and repair and acts in addition to the mec1 checkpoint. *Mol Cell*, 45: 422-32.

Cronin, S. J. F., C. J. Woolf, G. Weiss, and J. M. Penninger. (2019). The role of iron regulation in immunometabolism and immune-related disease. *Front Mol Biosci*, 6: 116.

Chen, X., Z. Wang, N. Duan, G. Zhu, E. M. Schwarz, and C. Xie. (2018). Osteoblast-osteoclast interactions. *Connect Tissue Res*, 59: 99-107.

Chen, Y., Q. Guo, M. Zhang, S. Song, T. Quan, T. Zhao, H. Li, L. Guo, T. Jiang, and G. Wang. (2016). Relationship of serum GDF11 levels with bone mineral density and bone turnover markers in postmenopausal Chinese women. *Bone Res*, 4: 16012.

Chen, Y., X. Zhao, and H. Wu. (2020). Arterial stiffness: a focus on vascular calcification and its link to bone mineralization. *Arterioscler Thromb Vasc Biol*, 40: 1078-93.

Cho, J. S., S. H. Kook, A. R. Robinson, L. J. Niedernhofer, and B. C. Lee. (2013). Cell autonomous and nonautonomous mechanisms drive hematopoietic stem/progenitor cell loss in the absence of DNA repair. *Stem Cells*, 31: 511-25.

Choudhury, A. R., Z. Ju, M. W. Djojosubroto, A. Schienke, A. Lechel, S. Schaetzlein, H. Jiang, A. Stepczynska, C. Wang, J. Buer, H. W. Lee, et al. (2007). Cdkn1a deletion improves stem cell function and lifespan of mice with dysfunctional telomeres without accelerating cancer formation. *Nat Genet*, 39: 99-105.

Daba, A., K. Gkouvatsos, G. Sebastiani, and K. Pantopoulos. (2013). Differences in activation of mouse hepcidin by dietary iron and parenterally administered iron dextran: compartmentalization is critical for iron sensing. *J Mol Med (Berl)*, 91: 95-102.

Daley, J. M., T. Chiba, X. Xue, H. Niu, and P. Sung. (2014). Multifaceted role of the Topo IIIalpha-RMI1-RMI2 complex and DNA2 in the BLM-dependent pathway of DNA break end resection. *Nucleic Acids Res*, 42: 11083-91.

Danilevicius, C. F., J. B. Lopes, and R. M. Pereira. (2007). Bone metabolism and vascular calcification. *Braz J Med Biol Res*, 40: 435-42.

References

de la Rosa, J., J. M. Freije, R. Cabanillas, F. G. Osorio, M. F. Fraga, M. S. Fernández-García, R. Rad, V. Fanjul, A. P. Ugalde, Q. Liang, H. M. Prosser, et al. (2013). Prelamin A causes progeria through cell-extrinsic mechanisms and prevents cancer invasion. *Nat Commun*, 4: 2268.

de Magalhaes, J. P., and J. Costa. (2009). A database of vertebrate longevity records and their relation to other life-history traits. *J Evol Biol*, 22: 1770-4.

de Magalhaes, J. P., C. E. Finch, and G. Janssens. (2010). Next-generation sequencing in aging research: emerging applications, problems, pitfalls and possible solutions. *Ageing Res Rev*, 9: 315-23.

De Sandre-Giovannoli, A., R. Bernard, P. Cau, C. Navarro, J. Amiel, I. Boccaccio, S. Lyonnet, C. L. Stewart, A. Munnich, M. Le Merrer, and N. Levy. (2003). Lamin a truncation in Hutchinson-Gilford progeria. *Science*, 300: 2055.

Dempster, D. W., J. E. Compston, M. K. Drezner, F. H. Glorieux, J. A. Kanis, H. Malluche, P. J. Meunier, S. M. Ott, R. R. Recker, and A. M. Parfitt. (2013). Standardized nomenclature, symbols, and units for bone histomorphometry: a 2012 update of the report of the ASBMR Histomorphometry Nomenclature Committee. *J Bone Miner Res*, 28: 2-17.

Dev, S., and J. L. Babitt. (2017). Overview of iron metabolism in health and disease. *Hemodial Int*, 21 Suppl 1: S6-S20.

Dongiovanni, P., A. L. Fracanzani, S. Fargion, and L. Valenti. (2011). Iron in fatty liver and in the metabolic syndrome: a promising therapeutic target. *J Hepatol*, 55: 920-32.

Dongiovanni, P., M. Ruscica, R. Rametta, S. Recalcati, L. Steffani, S. Gatti, D. Girelli, G. Cairo, P. Magni, S. Fargion, and L. Valenti. (2013). Dietary iron overload induces visceral adipose tissue insulin resistance. *Am J Pathol*, 182: 2254-63.

Dotiwala, F., S. Mulik, R. B. Polidoro, J. A. Ansara, B. A. Burleigh, M. Walch, R. T. Gazzinelli, and J. Lieberman. (2016). Killer lymphocytes use granulysin, perforin and granzymes to kill intracellular parasites. *Nat Med*, 22: 210-6.

Dougall, W. C., M. Glaccum, K. Charrier, K. Rohrbach, K. Brasel, T. De Smedt, E. Daro, J. Smith, M. E. Tometsko, C. R. Maliszewski, A. Armstrong, et al. (1999). RANK is essential for osteoclast and lymph node development. *Genes Dev*, 13: 2412-24.

Dufresne, S. S., N. A. Dumont, A. Boulanger-Piette, V. A. Fajardo, D. Gamu, S. A. Kake-Guena, R. O. David, P. Bouchard, E. Lavergne, J. M. Penninger, P. C. Pape, et al. (2016). Muscle RANK is a key regulator of Ca2+ storage, SERCA activity, and function of fast-twitch skeletal muscles. *Am J Physiol Cell Physiol*, 310: C663-72.

Duran, J., M. F. Troncoso, D. Lagos, S. Ramos, G. Marin, and M. Estrada. (2018). GDF11 modulates Ca^{2+}-dependent Smad2/3 signaling to prevent cardiomyocyte hypertrophy. *Int J Mol Sci*, 19.

Durham, A. L., M. Y. Speer, M. Scatena, C. M. Giachelli, and C. M. Shanahan. (2018). Role of smooth muscle cells in vascular calcification: implications in atherosclerosis and arterial stiffness. *Cardiovasc Res*, 114: 590-600.

Egerman, M. A., S. M. Cadena, J. A. Gilbert, A. Meyer, H. N. Nelson, S. E. Swalley, C. Mallozzi, C. Jacobi, L. L. Jennings, I. Clay, G. Laurent, et al. (2015). GDF11 increases with age and inhibits skeletal muscle regeneration. *Cell Metab*, 22: 164-74.

Eriksson, M., W. T. Brown, L. B. Gordon, M. W. Glynn, J. Singer, L. Scott, M. R. Erdos, C. M. Robbins, T. Y. Moses, P. Berglund, A. Dutra, et al. (2003). Recurrent de novo point

mutations in lamin A cause Hutchinson-Gilford progeria syndrome. *Nature*, 423: 293-8.

Ermolaeva, M., F. Neri, A. Ori, and K. L. Rudolph. (2018). Cellular and epigenetic drivers of stem cell ageing. *Nat Rev Mol Cell Biol*, 19: 594-610.

Espada, J., I. Varela, I. Flores, A. P. Ugalde, J. Cadiñanos, A. M. Pendás, C. L. Stewart, K. Tryggvason, M. A. Blasco, J. M. Freije, and C. López-Otín. (2008). Nuclear envelope defects cause stem cell dysfunction in premature-aging mice. *J Cell Biol*, 181: 27-35.

Fan, C., D. Rajasekaran, M. A. Syed, L. Leng, J. P. Loria, V. Bhandari, R. Bucala, and E. J. Lolis. (2013). MIF intersubunit disulfide mutant antagonist supports activation of CD74 by endogenous MIF trimer at physiologic concentrations. *Proc Natl Acad Sci U S A*, 110: 10994-9.

Fang, X., E. Nevo, L. Han, E. Y. Levanon, J. Zhao, A. Avivi, D. Larkin, X. Jiang, S. Feranchuk, Y. Zhu, A. Fishman, et al. (2014). Genome-wide adaptive complexes to underground stresses in blind mole rats Spalax. *Nat Commun*, 5: 3966.

Ferrucci, L., and E. Fabbri. (2018). Inflammageing: chronic inflammation in ageing, cardiovascular disease, and frailty. *Nat Rev Cardiol*, 15: 505-22.

Finerty, J. C. (1952). Parabiosis in physiological studies. *Physiol Rev*, 32: 277-302.

Foley, N. M., G. M. Hughes, Z. Huang, M. Clarke, D. Jebb, C. V. Whelan, E. J. Petit, F. Touzalin, O. Farcy, G. Jones, R. D. Ransome, et al. (2018). Growing old, yet staying young: The role of telomeres in bats' exceptional longevity. *Sci Adv*, 4: eaao0926.

Folgueras, A. R., F. M. de Lara, A. M. Pendás, C. Garabaya, F. Rodríguez, A. Astudillo, T. Bernal, R. Cabanillas, C. López-Otín, and G. Velasco. (2008). Membrane-bound serine protease matriptase-2 (*Tmprss6*) is an essential regulator of iron homeostasis. *Blood*, 112: 2539-45.

Folgueras, A. R., S. Freitas-Rodríguez, G. Velasco, and C. López-Otín. (2018). Mouse models to disentangle the hallmarks of human aging. *Circ Res*, 123: 905-24.

Fontana, L., L. Partridge, and V. D. Longo. (2010). Extending healthy life span--from yeast to humans. *Science*, 328: 321-6.

Freitas-Rodríguez, S., A. R. Folgueras, and C. López-Otín. (2017). The role of matrix metalloproteinases in aging: Tissue remodeling and beyond. *Biochim Biophys Acta Mol Cell Res*, 1864: 2015-25.

Frye, M. A., L. J. 3rd Melton, S. C. Bryant, L. A. Fitzpatrick, H. W. Wahner, R. S. Schwartz, and B. L. Riggs. (1992). Osteoporosis and calcification of the aorta. *Bone Miner*, 19: 185-94.

Futreal, P. A., L. Coin, M. Marshall, T. Down, T. Hubbard, R. Wooster, N. Rahman, and M. R. Stratton. (2004). A census of human cancer genes. *Nat Rev Cancer*, 4: 177-83.

Gabrielsen, J. S., Y. Gao, J. A. Simcox, J. Huang, D. Thorup, D. Jones, R. C. Cooksey, D. Gabrielsen, T. D. Adams, S. C. Hunt, P. N. Hopkins, et al. (2012). Adipocyte iron regulates adiponectin and insulin sensitivity. *J Clin Invest*, 122: 3529-40.

Galaris, D., A. Barbouti, and K. Pantopoulos. (2019). Iron homeostasis and oxidative stress: An intimate relationship. *Biochim Biophys Acta Mol Cell Res*, 1866: 118535.

Galluzzi, L., F. Pietrocola, B. Levine, and G. Kroemer. (2014). Metabolic control of autophagy. *Cell*, 159: 1263-76.

References

Gamer, L. W., K. A. Cox, C. Small, and V. Rosen. (2001). Gdf11 is a negative regulator of chondrogenesis and myogenesis in the developing chick limb. *Dev Biol*, 229: 407-20.

Ganz, T., and E. Nemeth. (2015). Iron homeostasis in host defence and inflammation. *Nat Rev Immunol*, 15: 500-10.

Gao, Y., Z. Li, J. S. Gabrielsen, J. A. Simcox, S. H. Lee, D. Jones, B. Cooksey, G. Stoddard, W. T. Cefalu, and D. A. McClain. (2015). Adipocyte iron regulates leptin and food intake. *J Clin Invest*, 125: 3681-91.

Garner, M. M., S. M. Hernandez-Divers, and J. T. Raymond. (2004). Reptile neoplasia: a retrospective study of case submissions to a specialty diagnostic service. *Vet Clin North Am Exot Anim Pract*, 7: 653-71, vi.

Gorbunova, V., A. Seluanov, Z. Zhang, V. N. Gladyshev, and J. Vijg. (2014). Comparative genetics of longevity and cancer: insights from long-lived rodents. *Nat Rev Genet*, 15: 531-40.

Gordon, L. B., J. Massaro, R. B. D'Agostino, Sr., S. E. Campbell, J. Brazier, W. T. Brown, M. E. Kleinman, M. W. Kieran, and Collaborative Progeria Clinical Trials. (2014a). Impact of farnesylation inhibitors on survival in Hutchinson-Gilford progeria syndrome. *Circulation*, 130: 27-34.

Gordon, L. B., F. G. Rothman, C. López-Otín, and T. Misteli. (2014b). Progeria: a paradigm for translational medicine. *Cell*, 156: 400-7.

Gude, N. A., K. M. Broughton, F. Firouzi, and M. A. Sussman. (2018). Cardiac ageing: extrinsic and intrinsic factors in cellular renewal and senescence. *Nat Rev Cardiol*, 15: 523-42.

Hajer, G. R., T. W. van Haeften, and F. L. Visseren. (2008). Adipose tissue dysfunction in obesity, diabetes, and vascular diseases. *Eur Heart J*, 29: 2959-71.

Hamczyk, M. R., L. del Campo, and V. Andrés. (2018a). Aging in the cardiovascular system: lessons from Hutchinson-Gilford progeria syndrome. *Annu Rev Physiol*, 80: 27-48.

Hamczyk, M. R., R. Villa-Bellosta, P. Gonzalo, M. J. Andrés-Manzano, P. Nogales, J. F. Bentzon, C. López-Otín, and V. Andrés. (2018b). Vascular smooth muscle-specific progerin expression accelerates atherosclerosis and death in a mouse nodel of Hutchinson-Gilford progeria syndrome. *Circulation*, 138: 266-82.

Hammers, D. W., M. Merscham-Banda, J. Y. Hsiao, S. Engst, J. J. Hartman, and H. L. Sweeney. (2017). Supraphysiological levels of GDF11 induce striated muscle atrophy. *EMBO Mol Med*, 9: 531-44.

Han, Y., X. You, W. Xing, Z. Zhang, and W. Zou. (2018). Paracrine and endocrine actions of bone-the functions of secretory proteins from osteoblasts, osteocytes, and osteoclasts. *Bone Res*, 6: 16.

Hanahan, D., and R. A. Weinberg. (2011). Hallmarks of cancer: the next generation. *Cell*, 144: 646-74.

Harper, S. C., J. Johnson, G. Borghetti, H. Zhao, T. Wang, M. Wallner, H. Kubo, E. A. Feldsott, Y. Yang, Y. Joo, X. Gou, et al. (2018). GDF11 decreases pressure overload-induced hypertrophy, but can cause severe cachexia and premature death. *Circ Res*, 123: 1220-31.

Hoffmann, F. G., M. W. Vandewege, J. F. Storz, and J. C. Opazo. (2018). Gene turnover and diversification of the alpha- and beta-globin gene families in sauropsid vertebrates. *Genome Biol Evol*, 10: 344-58.

Hotamisligil, G. S. (2017). Inflammation, metaflammation and immunometabolic disorders. *Nature*, 542: 177-85.

Hou, L., D. Wang, D. Chen, Y. Liu, Y. Zhang, H. Cheng, C. Xu, N. Sun, J. McDermott, W. B. Mair, and J. D. Han. (2016). A systems approach to reverse engineer lifespan extension by dietary restriction. *Cell Metab*, 23: 529-40.

Hu, T., A. Kitano, V. Luu, B. Dawson, K. A. Hoegenauer, B. H. Lee, and D. Nakada. (2019). Bmi1 suppresses adipogenesis in the hematopoietic stem cell niche. *Stem Cell Reports*, 13: 545-58.

Huang, Z., C. V. Whelan, N. M. Foley, D. Jebb, F. Touzalin, E. J. Petit, S. J. Puechmaille, and E. C. Teeling. (2019). Longitudinal comparative transcriptomics reveals unique mechanisms underlying extended healthspan in bats. *Nat Ecol Evol*, 3: 1110-20.

Hubler, M. J., K. R. Peterson, and A. H. Hasty. (2015). Iron homeostasis: a new job for macrophages in adipose tissue? *Trends Endocrinol Metab*, 26: 101-9.

Huby, A. C., G. Antonova, J. Groenendyk, C. E. Gomez-Sanchez, W. B. Bollag, J. A. Filosa, and E. J. Belin de Chantemele. (2015). Adipocyte-derived hormone leptin is a direct regulator of aldosterone secretion, which promotes endothelial dysfunction and cardiac fibrosis. *Circulation*, 132: 2134-45.

Hudobenko, J., B. P. Ganesh, J. Jiang, E. C. Mohan, S. Lee, S. Sheth, D. Morales, L. Zhu, J. K. Kofler, R. G. Pautler, L. D. McCullough, et al. (2020). Growth differentiation factor-11 supplementation improves survival and promotes recovery after ischemic stroke in aged mice. *Aging (Albany NY)*, 12.

Imura, A., A. Iwano, O. Tohyama, Y. Tsuji, K. Nozaki, N. Hashimoto, T. Fujimori, and Y. Nabeshima. (2004). Secreted Klotho protein in sera and CSF: implication for post-translational cleavage in release of Klotho protein from cell membrane. *FEBS Lett*, 565: 143-7.

Jacobsen, S. B., M. N. Hansen, F. B. Jensen, N. Skovgaard, T. Wang, and A. Fago. (2012). Circulating nitric oxide metabolites and cardiovascular changes in the turtle Trachemys scripta during normoxia, anoxia and reoxygenation. *J Exp Biol*, 215: 2560-6.

Jones, O. R., A. Scheuerlein, R. Salguero-Gómez, C. G. Camarda, R. Schaible, B. B. Casper, J. P. Dahlgren, J. Ehrlén, M. B. García, E. S. Menges, P. F. Quintana-Ascencio, et al. (2014). Diversity of ageing across the tree of life. *Nature*, 505: 169-73.

Jura, M., and L. P. Kozak. (2016). Obesity and related consequences to ageing. *Age (Dordr)*, 38: 23.

Kaessmann, H. (2010). Origins, evolution, and phenotypic impact of new genes. *Genome Res*, 20: 1313-26.

Katsimpardi, L., N. Kuperwasser, C. Camus, C. Moigneu, A. Chiche, V. Tolle, H. Li, E. Kokovay, and P. M. Lledo. (2020). Systemic GDF11 stimulates the secretion of adiponectin and induces a calorie restriction-like phenotype in aged mice. *Aging Cell*, 19: e13038.

Katsimpardi, L., N. K. Litterman, P. A. Schein, C. M. Miller, F. S. Loffredo, G. R. Wojtkiewicz, J. W. Chen, R. T. Lee, A. J. Wagers, and L. L. Rubin. (2014). Vascular and neurogenic rejuvenation of the aging mouse brain by young systemic factors. *Science*, 344: 630-4.

Kautz, L., D. Meynard, A. Monnier, V. Darnaud, R. Bouvet, R. H. Wang, C. Deng, S. Vaulont, J. Mosser, H. Coppin, and M. P. Roth. (2008). Iron regulates phosphorylation of

References

Smad1/5/8 and gene expression of Bmp6, Smad7, Id1, and Atoh8 in the mouse liver. *Blood*, 112: 1503-9.

Keane, M., J. Semeiks, A. E. Webb, Y. I. Li, V. Quesada, T. Craig, L. B. Madsen, S. van Dam, D. Brawand, P. I. Marques, P. Michalak, et al. (2015). Insights into the evolution of longevity from the bowhead whale genome. *Cell Rep*, 10: 112-22.

Kennedy, B. K., S. L. Berger, A. Brunet, J. Campisi, A. M. Cuervo, E. S. Epel, C. Franceschi, G. J. Lithgow, R. I. Morimoto, J. E. Pessin, T. A. Rando, et al. (2014). Geroscience: linking aging to chronic disease. *Cell*, 159: 709-13.

Kenyon, C., J. Chang, E. Gensch, A. Rudner, and R. Tabtiang. (1993). A *C. elegans* mutant that lives twice as long as wild type. *Nature*, 366: 461-4.

Kharitonenkov, A., V. J. Wroblewski, A. Koester, Y. F. Chen, C. K. Clutinger, X. T. Tigno, B. C. Hansen, A. B. Shanafelt, and G. J. Etgen. (2007). The metabolic state of diabetic monkeys is regulated by fibroblast growth factor-21. *Endocrinology*, 148: 774-81.

Kim, E. B., X. Fang, A. A. Fushan, Z. Huang, A. V. Lobanov, L. Han, S. M. Marino, X. Sun, A. A. Turanov, P. Yang, S. H. Yim, et al. (2011). Genome sequencing reveals insights into physiology and longevity of the naked mole rat. *Nature*, 479: 223-7.

Kimura, K. D., H. A. Tissenbaum, Y. Liu, and G. Ruvkun. (1997). daf-2, an insulin receptor-like gene that regulates longevity and diapause in *Caenorhabditis elegans*. *Science*, 277: 942-6.

Klass, M. R. (1983). A method for the isolation of longevity mutants in the nematode Caenorhabditis elegans and initial results. *Mech Ageing Dev*, 22: 279-86.

Kong, Y. Y., H. Yoshida, I. Sarosi, H. L. Tan, E. Timms, C. Capparelli, S. Morony, A. J. Oliveira-dos-Santos, G. Van, A. Itie, W. Khoo, et al. (1999). OPGL is a key regulator of osteoclastogenesis, lymphocyte development and lymph-node organogenesis. *Nature*, 397: 315-23.

Kraemer, F. B., and W. J. Shen. (2002). Hormone-sensitive lipase: control of intracellular tri-(di-)acylglycerol and cholesteryl ester hydrolysis. *J Lipid Res*, 43: 1585-94.

Kratz, M., B. R. Coats, K. B. Hisert, D. Hagman, V. Mutskov, E. Peris, K. Q. Schoenfelt, J. N. Kuzma, I. Larson, P. S. Billing, R. W. Landerholm, et al. (2014). Metabolic dysfunction drives a mechanistically distinct proinflammatory phenotype in adipose tissue macrophages. *Cell Metab*, 20: 614-25.

Krishnan, V., M. Z. Chow, Z. Wang, L. Zhang, B. Liu, X. Liu, and Z. Zhou. (2011). Histone H4 lysine 16 hypoacetylation is associated with defective DNA repair and premature senescence in Zmpste24-deficient mice. *Proc Natl Acad Sci U S A*, 108: 12325-30.

Kroemer, G., C. López-Otín, F. Madeo, and R. de Cabo. (2018). Carbotoxicity-noxious effects of carbohydrates. *Cell*, 175: 605-14.

Kubben, N., and T. Misteli. (2017). Shared molecular and cellular mechanisms of premature ageing and ageing-associated diseases. *Nat Rev Mol Cell Biol*, 18: 595-609.

Kular, J. K., S. Basu, and R. I. Sharma. (2014). The extracellular matrix: Structure, composition, age-related differences, tools for analysis and applications for tissue engineering. *J Tissue Eng*, 5: 2041731414557112.

Kumar, M. S. (2019). Peptides and peptidomimetics as potential antiobesity agents: overview of current status. *Front Nutr*, 6: 11.

Kumar, S., G. Stecher, M. Suleski, and S. B. Hedges. (2017). TimeTree: a resource for timelines, timetrees, and divergence Times. *Mol Biol Evol*, 34: 1812-19.

Kuro, O. M. (2019). The Klotho proteins in health and disease. *Nat Rev Nephrol*, 15: 27-44.

Kuro, O. M., Y. Matsumura, H. Aizawa, H. Kawaguchi, T. Suga, T. Utsugi, Y. Ohyama, M. Kurabayashi, T. Kaname, E. Kume, H. Iwasaki, et al. (1997). Mutation of the mouse *klotho* gene leads to a syndrome resembling ageing. *Nature*, 390: 45-51.

Kurosu, H., M. Yamamoto, J. D. Clark, J. V. Pastor, A. Nandi, P. Gurnani, O. P. McGuinness, H. Chikuda, M. Yamaguchi, H. Kawaguchi, I. Shimomura, et al. (2005). Suppression of aging in mice by the hormone Klotho. *Science*, 309: 1829-33.

Lans, H., J. H. J. Hoeijmakers, W. Vermeulen, and J. A. Marteijn. (2019). The DNA damage response to transcription stress. *Nat Rev Mol Cell Biol*, 20: 766-84.

Lei, P., S. Ayton, D. I. Finkelstein, L. Spoerri, G. D. Ciccotosto, D. K. Wright, B. X. Wong, P. A. Adlard, R. A. Cherny, L. Q. Lam, B. R. Roberts, et al. (2012). Tau deficiency induces parkinsonism with dementia by impairing APP-mediated iron export. *Nat Med*, 18: 291-5.

Lerner, U. H., E. Kindstedt, and P. Lundberg. (2019). The critical interplay between bone resorbing and bone forming cells. *J Clin Periodontol*, 46 Suppl 21: 33-51.

Li, S., J. Peng, H. Wang, W. Zhang, J. M. Brown, Y. Zhou, and Q. Wu. (2020). Hepsin enhances liver metabolism and inhibits adipocyte browning in mice. *Proc Natl Acad Sci U S A*, 117: 12359-67.

Lin, Y., K. Wong, and K. Calame. (1997). Repression of c-*myc* transcription by Blimp-1, an inducer of terminal B cell differentiation. *Science*, 276: 596-9.

Lira, V. A., M. Okutsu, M. Zhang, N. P. Greene, R. C. Laker, D. S. Breen, K. L. Hoehn, and Z. Yan. (2013). Autophagy is required for exercise training-induced skeletal muscle adaptation and improvement of physical performance. *FASEB J*, 27: 4184-93.

Liu, B., S. Ghosh, X. Yang, H. Zheng, X. Liu, Z. Wang, G. Jin, B. Zheng, B. K. Kennedy, Y. Suh, M. Kaeberlein, et al. (2012). Resveratrol rescues SIRT1-dependent adult stem cell decline and alleviates progeroid features in laminopathy-based progeria. *Cell Metab*, 16: 738-50.

Liu, B., Z. Wang, L. Zhang, S. Ghosh, H. Zheng, and Z. Zhou. (2013a). Depleting the methyltransferase Suv39h1 improves DNA repair and extends lifespan in a progeria mouse model. *Nat Commun*, 4: 1868.

Liu, W., L. Zhou, C. Zhou, S. Zhang, J. Jing, L. Xie, N. Sun, X. Duan, W. Jing, X. Liang, H. Zhao, et al. (2016). GDF11 decreases bone mass by stimulating osteoclastogenesis and inhibiting osteoblast differentiation. *Nat Commun*, 7: 12794.

Liu, Y., I. Drozdov, R. Shroff, L. E. Beltran, and C. M. Shanahan. (2013b). Prelamin A accelerates vascular calcification via activation of the DNA damage response and senescence-associated secretory phenotype in vascular smooth muscle cells. *Circ Res*, 112: e99-109.

Liu, Z., K. K. L. Wu, X. Jiang, A. Xu, and K. K. Y. Cheng. (2020). The role of adipose tissue senescence in obesity- and ageing-related metabolic disorders. *Clin Sci (Lond)*, 134: 315-30.

Loffredo, F. S., M. L. Steinhauser, S. M. Jay, J. Gannon, J. R. Pancoast, P. Yalamanchi, M. Sinha, C. Dall'Osso, D. Khong, J. L. Shadrach, C. M. Miller, et al. (2013). Growth

differentiation factor 11 is a circulating factor that reverses age-related cardiac hypertrophy. *Cell*, 153: 828-39.

López-Otín, C., M. A. Blasco, L. Partridge, M. Serrano, and G. Kroemer. (2013). The hallmarks of aging. *Cell*, 153: 1194-217.

López-Otín, C., L. Galluzzi, J. M. P. Freije, F. Madeo, and G. Kroemer. (2016). Metabolic control of longevity. *Cell*, 166: 802-21.

Lutz, P. L., H. M. Prentice, and S. L. Milton. (2003). Is turtle longevity linked to enhanced mechanisms for surviving brain anoxia and reoxygenation? *Exp Gerontol*, 38: 797-800.

Ma, S., and V. N. Gladyshev. (2017). Molecular signatures of longevity: Insights from cross-species comparative studies. *Semin Cell Dev Biol*, 70: 190-203.

Ma, S., S. H. Yim, S. G. Lee, E. B. Kim, S. R. Lee, K. T. Chang, R. Buffenstein, K. N. Lewis, T. J. Park, R. A. Miller, C. B. Clish, et al. (2015). Organization of the mammalian metabolome according to organ function, lineage specialization, and longevity. *Cell Metab*, 22: 332-43.

MacRae, S. L., M. M. Croken, R. B. Calder, A. Aliper, B. Milholland, R. R. White, A. Zhavoronkov, V. N. Gladyshev, A. Seluanov, V. Gorbunova, Z. D. Zhang, et al. (2015). DNA repair in species with extreme lifespan differences. *Aging (Albany NY)*, 7: 1171-84.

Mariño, G., A. P. Ugalde, A. F. Fernández, F. G. Osorio, A. Fueyo, J. M. Freije, and C. López-Otín. (2010). Insulin-like growth factor 1 treatment extends longevity in a mouse model of human premature aging by restoring somatotroph axis function. *Proc Natl Acad Sci U S A*, 107: 16268-73.

Mariño, G., A. P. Ugalde, N. Salvador-Montoliu, I. Varela, P. M. Quirós, J. Cadiñanos, I. van der Pluijm, J. M. Freije, and C. López-Otín. (2008). Premature aging in mice activates a systemic metabolic response involving autophagy induction. *Hum Mol Genet*, 17: 2196-211.

Marra, N. J., M. J. Stanhope, N. K. Jue, M. Wang, Q. Sun, P. Pavinski Bitar, V. P. Richards, A. Komissarov, M. Rayko, S. Kliver, B. J. Stanhope, et al. (2019). White shark genome reveals ancient elasmobranch adaptations associated with wound healing and the maintenance of genome stability. *Proc Natl Acad Sci U S A*, 116: 4446-55.

Martinelli, N., M. Traglia, N. Campostrini, G. Biino, M. Corbella, C. Sala, F. Busti, C. Masciullo, D. Manna, S. Previtali, A. Castagna, et al. (2012). Increased serum hepcidin levels in subjects with the metabolic syndrome: a population study. *PLoS One*, 7: e48250.

Matsusue, K., T. Kusakabe, T. Noguchi, S. Takiguchi, T. Suzuki, S. Yamano, and F. J. González. (2008). Hepatic steatosis in leptin-deficient mice is promoted by the PPARgamma target gene Fsp27. *Cell Metab*, 7: 302-11.

Mattison, J. A., R. J. Colman, T. M. Beasley, D. B. Allison, J. W. Kemnitz, G. S. Roth, D. K. Ingram, R. Weindruch, R. de Cabo, and R. M. Anderson. (2017). Caloric restriction improves health and survival of rhesus monkeys. *Nat Commun*, 8: 14063.

Mattison, J. A., G. S. Roth, T. M. Beasley, E. M. Tilmont, A. M. Handy, R. L. Herbert, D. L. Longo, D. B. Allison, J. E. Young, M. Bryant, D. Barnard, et al. (2012). Impact of caloric restriction on health and survival in rhesus monkeys from the NIA study. *Nature*, 489: 318-21.

Melzer, D., L. C. Pilling, and L. Ferrucci. (2020). The genetics of human ageing. *Nat Rev Genet*, 21: 88-101.

Miard, S., and F. Picard. (2008). Obesity and aging have divergent genomic fingerprints. *Int J Obes (Lond)*, 32: 1873-4.

Miranda, M. A., and H. A. Lawson. (2018). Ironing out the details: untangling dietary iron and genetic background in diabetes. *Nutrients*, 10.

Mitchell, S. J., M. Scheibye-Knudsen, D. L. Longo, and R. de Cabo. (2015). Animal models of aging research: implications for human aging and age-related diseases. *Annu Rev Anim Biosci*, 3: 283-303.

Molofsky, A. V., S. He, M. Bydon, S. J. Morrison, and R. Pardal. (2005). Bmi-1 promotes neural stem cell self-renewal and neural development but not mouse growth and survival by repressing the p16Ink4a and p19Arf senescence pathways. *Genes Dev*, 19: 1432-7.

Moskalev, A. A., M. V. Shaposhnikov, E. N. Plyusnina, A. Zhavoronkov, A. Budovsky, H. Yanai, and V. E. Fraifeld. (2013). The role of DNA damage and repair in aging through the prism of Koch-like criteria. *Ageing Res Rev*, 12: 661-84.

Mottillo, E. P., X. J. Shen, and J. G. Granneman. (2007). Role of hormone-sensitive lipase in beta-adrenergic remodeling of white adipose tissue. *Am J Physiol Endocrinol Metab*, 293: E1188-97.

Muckenthaler, M. U., S. Rivella, M. W. Hentze, and B. Galy. (2017). A red carpet for iron metabolism. *Cell*, 168: 344-61.

Nakashima, T., M. Hayashi, T. Fukunaga, K. Kurata, M. Oh-Hora, J. Q. Feng, L. F. Bonewald, T. Kodama, A. Wutz, E. F. Wagner, J. M. Penninger, et al. (2011). Evidence for osteocyte regulation of bone homeostasis through RANKL expression. *Nat Med*, 17: 1231-4.

Naves, M., M. Rodriguez-Garcia, J. B. Diaz-Lopez, C. Gomez-Alonso, and J. B. Cannata-Andia. (2008). Progression of vascular calcifications is associated with greater bone loss and increased bone fractures. *Osteoporos Int*, 19: 1161-6.

Neufer, P. D., M. M. Bamman, D. M. Muoio, C. Bouchard, D. M. Cooper, B. H. Goodpaster, F. W. Booth, W. M. Kohrt, R. E. Gerszten, M. P. Mattson, R. T. Hepple, et al. (2015). Understanding the cellular and molecular mechanisms of physical activity-induced health benefits. *Cell Metab*, 22: 4-11.

Novelli, G., A. Muchir, F. Sangiuolo, A. Helbling-Leclerc, M. R. D'Apice, C. Massart, F. Capon, P. Sbraccia, M. Federici, R. Lauro, C. Tudisco, et al. (2002). Mandibuloacral dysplasia is caused by a mutation in LMNA-encoding lamin A/C. *Am J Hum Genet*, 71: 426-31.

Oguro, H., A. Iwama, Y. Morita, T. Kamijo, M. van Lohuizen, and H. Nakauchi. (2006). Differential impact of Ink4a and Arf on hematopoietic stem cells and their bone marrow microenvironment in Bmi1-deficient mice. *J Exp Med*, 203: 2247-53.

Ohta, S., I. Ohsawa, K. Kamino, F. Ando, and H. Shimokata. (2004). Mitochondrial ALDH2 deficiency as an oxidative stress. *Ann N Y Acad Sci*, 1011: 36-44.

Olive, M., I. Harten, R. Mitchell, J. K. Beers, K. Djabali, K. Cao, M. R. Erdos, C. Blair, B. Funke, L. Smoot, M. Gerhard-Herman, et al. (2010). Cardiovascular pathology in Hutchinson-Gilford progeria: correlation with the vascular pathology of aging. *Arterioscler Thromb Vasc Biol*, 30: 2301-9.

Oliveira, A. G., T. G. Araujo, B. M. Carvalho, G. Z. Rocha, A. Santos, and M. J. A. Saad. (2018). The role of hepatocyte growth factor (HGF) in insulin resistance and diabetes. *Front Endocrinol (Lausanne)*, 9: 503.

References

Olson, K. A., A. L. Beatty, B. Heidecker, M. C. Regan, E. N. Brody, T. Foreman, S. Kato, R. E. Mehler, B. S. Singer, K. Hveem, H. Dalen, et al. (2015). Association of growth differentiation factor 11/8, putative anti-ageing factor, with cardiovascular outcomes and overall mortality in humans: analysis of the Heart and Soul and HUNT3 cohorts. *Eur Heart J*, 36: 3426-34.

Osorio, F. G., C. Bárcena, C. Soria-Valles, A. J. Ramsay, F. de Carlos, J. Cobo, A. Fueyo, J. M. Freije, and C. López-Otín. (2012). Nuclear lamina defects cause ATM-dependent NF-kappaB activation and link accelerated aging to a systemic inflammatory response. *Genes Dev*, 26: 2311-24.

Osorio, F. G., C. L. Navarro, J. Cadiñanos, I. C. López-Mejía, P. M. Quirós, C. Bartoli, J. Rivera, J. Tazi, G. Guzmán, I. Varela, D. Depetris, et al. (2011). Splicing-directed therapy in a new mouse model of human accelerated aging. *Sci Transl Med*, 3: 106ra07.

Osorio, F. G., I. Varela, E. Lara, X. S. Puente, J. Espada, R. Santoro, J. M. Freije, M. F. Fraga, and C. López-Otín. (2010). Nuclear envelope alterations generate an aging-like epigenetic pattern in mice deficient in Zmpste24 metalloprotease. *Aging Cell*, 9: 947-57.

Peinado, J. R., P. M. Quirós, M. R. Pulido, G. Mariño, M. L. Martínez-Chantar, R. Vázquez-Martínez, J. M. Freije, C. López-Otín, and M. M. Malagon. (2011). Proteomic profiling of adipose tissue from *Zmpste24$^{-/-}$* mice, a model of lipodystrophy and premature aging, reveals major changes in mitochondrial function and vimentin processing. *Mol Cell Proteomics*, 10: M111 008094.

Pendás, A. M., Z. Zhou, J. Cadiñanos, J. M. Freije, J. Wang, K. Hultenby, A. Astudillo, A. Wernerson, F. Rodríguez, K. Tryggvason, and C. López-Otín. (2002). Defective prelamin A processing and muscular and adipocyte alterations in Zmpste24 metalloproteinase-deficient mice. *Nat Genet*, 31: 94-9.

Pérez-Silva, J. G., M. Araujo-Voces, and V. Quesada. (2018). nVenn: generalized, quasi-proportional Venn and Euler diagrams. *Bioinformatics*, 34: 2322-24.

Pérez-Silva, J. G., Y. Español, G. Velasco, and V. Quesada. (2016). The Degradome database: expanding roles of mammalian proteases in life and disease. *Nucleic Acids Res*, 44: D351-5.

Pignolo, R. J., J. F. Passos, S. Khosla, T. Tchkonia, and J. L. Kirkland. (2020). Reducing senescent cell burden in aging and disease. *Trends Mol Med*, 26: 630-38.

Pihan-Le Bars, F., F. Bonnet, O. Loreal, A. G. Le Loupp, M. Ropert, E. Letessier, X. Prieur, K. Bach, Y. Deugnier, B. Fromenty, and B. Cariou. (2016). Indicators of iron status are correlated with adiponectin expression in adipose tissue of patients with morbid obesity. *Diabetes Metab*, 42: 105-11.

Pluvinage, J. V., and T. Wyss-Coray. (2020). Systemic factors as mediators of brain homeostasis, ageing and neurodegeneration. *Nat Rev Neurosci*, 21: 93-102.

Poggioli, T., A. Vujic, P. Yang, C. Macias-Trevino, A. Uygur, F. S. Loffredo, J. R. Pancoast, M. Cho, J. Goldstein, R. M. Tandias, E. Gonzalez, et al. (2016). Circulating growth differentiation factor 11/8 levels decline with age. *Circ Res*, 118: 29-37.

Puente, X. S., L. M. Sánchez, C. M. Overall, and C. López-Otín. (2003). Human and mouse proteases: a comparative genomic approach. *Nat Rev Genet*, 4: 544-58.

Quesada, V., G. Velasco, X. S. Puente, W. C. Warren, and C. López-Otín. (2010). Comparative genomic analysis of the zebra finch degradome provides new insights into evolution of proteases in birds and mammals. *BMC Genomics*, 11: 220.

Quirós, P. M., T. Langer, and C. López-Otín. (2015). New roles for mitochondrial proteases in health, ageing and disease. *Nat Rev Mol Cell Biol*, 16: 345-59.

Raggi, P., C. Giachelli, and A. Bellasi. (2007). Interaction of vascular and bone disease in patients with normal renal function and patients undergoing dialysis. *Nat Clin Pract Cardiovasc Med*, 4: 26-33.

Ragnauth, C. D., D. T. Warren, Y. Liu, R. McNair, T. Tajsic, N. Figg, R. Shroff, J. Skepper, and C. M. Shanahan. (2010). Prelamin A acts to accelerate smooth muscle cell senescence and is a novel biomarker of human vascular aging. *Circulation*, 121: 2200-10.

Ramsay, A. J., J. D. Hooper, A. R. Folgueras, G. Velasco, and C. López-Otín. (2009). Matriptase-2 (*TMPRSS6*): a proteolytic regulator of iron homeostasis. *Haematologica*, 94: 840-9.

Ribes-Zamora, A., S. M. Indiviglio, I. Mihalek, C. L. Williams, and A. A. Bertuch. (2013). TRF2 interaction with Ku heterotetramerization interface gives insight into c-NHEJ prevention at human telomeres. *Cell Rep*, 5: 194-206.

Rivera-Torres, J., C. J. Calvo, A. Llach, G. Guzmán-Martínez, R. Caballero, C. González-Gómez, L. J. Jiménez-Borreguero, J. A. Guadix, F. G. Osorio, C. López-Otín, A. Herraiz-Martínez, et al. (2016). Cardiac electrical defects in progeroid mice and Hutchinson-Gilford progeria syndrome patients with nuclear lamina alterations. *Proc Natl Acad Sci U S A*, 113: E7250-E59.

Rossi, D. J., D. Bryder, J. M. Zahn, H. Ahlenius, R. Sonu, A. J. Wagers, and I. L. Weissman. (2005). Cell intrinsic alterations underlie hematopoietic stem cell aging. *Proc Natl Acad Sci U S A*, 102: 9194-9.

Roy, C. N. (2011). Anemia in frailty. *Clin Geriatr Med*, 27: 67-78.

Russell, S. J., and C. R. Kahn. (2007). Endocrine regulation of ageing. *Nat Rev Mol Cell Biol*, 8: 681-91.

Santiago-Fernández, O., F. G. Osorio, V. Quesada, F. Rodríguez, S. Basso, D. Maeso, L. Rolas, A. Barkaway, S. Nourshargh, A. R. Folgueras, J. M. P. Freije, et al. (2019). Development of a CRISPR/Cas9-based therapy for Hutchinson-Gilford progeria syndrome. *Nat Med*, 25: 423-26.

Scaffidi, P., and T. Misteli. (2006). Lamin A-dependent nuclear defects in human aging. *Science*, 312: 1059-63.

Schafer, M. J., E. J. Atkinson, P. M. Vanderboom, B. Kotajarvi, T. A. White, M. M. Moore, C. J. Bruce, K. L. Greason, R. M. Suri, S. Khosla, J. D. Miller, et al. (2016). Quantification of GDF11 and myostatin in human aging and cardiovascular disease. *Cell Metab*, 23: 1207-15.

Schindelin, J., I. Arganda-Carreras, E. Frise, V. Kaynig, M. Longair, T. Pietzsch, S. Preibisch, C. Rueden, S. Saalfeld, B. Schmid, J. Y. Tinevez, et al. (2012). Fiji: an open-source platform for biological-image analysis. *Nat Methods*, 9: 676-82.

Schmeer, C., A. Kretz, D. Wengerodt, M. Stojiljkovic, and O. W. Witte. (2019). Dissecting aging and senescence-current concepts and open lessons. *Cells*, 8.

Seim, I., X. Fang, Z. Xiong, A. V. Lobanov, Z. Huang, S. Ma, Y. Feng, A. A. Turanov, Y. Zhu, T. L. Lenz, M. V. Gerashchenko, et al. (2013). Genome analysis reveals insights into physiology and longevity of the Brandt's bat *Myotis brandtii*. *Nat Commun*, 4: 2212.

References

Shanahan, C. M., M. H. Crouthamel, A. Kapustin, and C. M. Giachelli. (2011). Arterial calcification in chronic kidney disease: key roles for calcium and phosphate. *Circ Res*, 109: 697-711.

Shikama, N., R. Ackermann, and C. Brack. (1994). Protein synthesis elongation factor EF-1 alpha expression and longevity in *Drosophila melanogaster*. *Proc Natl Acad Sci U S A*, 91: 4199-203.

Shiraki-Iida, T., H. Aizawa, Y. Matsumura, S. Sekine, A. Iida, H. Anazawa, R. Nagai, M. Kuro-o, and Y. Nabeshima. (1998). Structure of the mouse *klotho* gene and its two transcripts encoding membrane and secreted protein. *FEBS Lett*, 424: 6-10.

Simcox, J. A., and D. A. McClain. (2013). Iron and diabetes risk. *Cell Metab*, 17: 329-41.

Sims, N. A., and N. C. Walsh. (2012). Intercellular cross-talk among bone cells: new factors and pathways. *Curr Osteoporos Rep*, 10: 109-17.

Singh, P. P., B. A. Demmitt, R. D. Nath, and A. Brunet. (2019). The genetics of aging: a vertebrate perspective. *Cell*, 177: 200-20.

Sinha, M., Y. C. Jang, J. Oh, D. Khong, E. Y. Wu, R. Manohar, C. Miller, S. G. Regalado, F. S. Loffredo, J. R. Pancoast, M. F. Hirshman, et al. (2014). Restoring systemic GDF11 levels reverses age-related dysfunction in mouse skeletal muscle. *Science*, 344: 649-52.

Slawik, M., and A. J. Vidal-Puig. (2006). Lipotoxicity, overnutrition and energy metabolism in aging. *Ageing Res Rev*, 5: 144-64.

Smith, S. C., X. Zhang, X. Zhang, P. Gross, T. Starosta, S. Mohsin, M. Franti, P. Gupta, D. Hayes, M. Myzithras, J. Kahn, et al. (2015). GDF11 does not rescue aging-related pathological hypertrophy. *Circ Res*, 117: 926-32.

Song, M., M. Lavasani, S. D. Thompson, A. Lu, B. Ahani, and J. Huard. (2013). Muscle-derived stem/progenitor cell dysfunction in *Zmpste24*-deficient progeroid mice limits muscle regeneration. *Stem Cell Res Ther*, 4: 33.

Spinelli, R., L. Parrillo, M. Longo, P. Florese, A. Desiderio, F. Zatterale, C. Miele, G. A. Raciti, and F. Beguinot. (2020). Molecular basis of ageing in chronic metabolic diseases. *J Endocrinol Invest*, 43: 1373-89.

Stauder, R., P. Valent, and I. Theurl. (2018). Anemia at older age: etiologies, clinical implications, and management. *Blood*, 131: 505-14.

Stoffel, N. U., C. El-Mallah, I. Herter-Aeberli, N. Bissani, N. Wehbe, O. Obeid, and M. B. Zimmermann. (2020). The effect of central obesity on inflammation, hepcidin, and iron metabolism in young women. *Int J Obes (Lond)*, 44: 1291-300.

Suh, Y., G. Atzmon, M. O. Cho, D. Hwang, B. Liu, D. J. Leahy, N. Barzilai, and P. Cohen. (2008). Functionally significant insulin-like growth factor I receptor mutations in centenarians. *Proc Natl Acad Sci U S A*, 105: 3438-42.

Tacutu, R., D. Thornton, E. Johnson, A. Budovsky, D. Barardo, T. Craig, E. Diana, G. Lehmann, D. Toren, J. Wang, V. E. Fraifeld, et al. (2018). Human ageing genomic resources: new and updated databases. *Nucleic Acids Res*, 46: D1083-D90.

Talukdar, S., Y. Zhou, D. Li, M. Rossulek, J. Dong, V. Somayaji, Y. Weng, R. Clark, A. Lanba, B. M. Owen, M. B. Brenner, et al. (2016). A long-acting FGF21 molecule, PF-05231023, decreases body weight and improves lipid profile in non-human primates and type 2 diabetic subjects. *Cell Metab*, 23: 427-40.

Tam, B. T., J. A. Morais, and S. Santosa. (2020). Obesity and ageing: two sides of the same coin. *Obes Rev*, 21: e12991.

Tian, J., X. X. Lei, L. Xuan, J. B. Tang, and B. Cheng. (2019a). The effects of aging, diabetes mellitus, and antiplatelet drugs on growth factors and anti-aging proteins in platelet-rich plasma. *Platelets*, 30: 773-92.

Tian, X., D. Firsanov, Z. Zhang, Y. Cheng, L. Luo, G. Tombline, R. Tan, M. Simon, S. Henderson, J. Steffan, A. Goldfarb, et al. (2019b). SIRT6 is responsible for more efficient DNA double-strand break repair in long-lived species. *Cell*, 177: 622-38 e22.

Tong, A. S., J. L. Stern, A. Sfeir, M. Kartawinata, T. de Lange, X. D. Zhu, and T. M. Bryan. (2015). ATM and ATR signaling regulate the recruitment of human telomerase to telomeres. *Cell Rep*, 13: 1633-46.

Toren, D., A. Kulaga, M. Jethva, E. Rubin, A. V. Snezhkina, A. V. Kudryavtseva, D. Nowicki, R. Tacutu, A. A. Moskalev, and V. E. Fraifeld. (2020). Gray whale transcriptome reveals longevity adaptations associated with DNA repair and ubiquitination. *Aging Cell*, 19.

Toyokuni, S. . (2011). Iron as a target of chemoprevention for longevity in humans. *Free Radic Res*, 45: 906-17.

Unamuno, X., J. Gómez-Ambrosi, A. Rodríguez, S. Becerril, G. Frühbeck, and V. Catalán. (2018). Adipokine dysregulation and adipose tissue inflammation in human obesity. *Eur J Clin Invest*, 48: e12997.

Valenzano, D. R., B. A. Benayoun, P. P. Singh, E. Zhang, P. D. Etter, C. K. Hu, M. Clement-Ziza, D. Willemsen, R. Cui, I. Harel, B. E. Machado, et al. (2015). The african turquoise killifish genome provides insights into evolution and genetic architecture of lifespan. *Cell*, 163: 1539-54.

van Deursen, J. M. (2014). The role of senescent cells in ageing. *Nature*, 509: 439-46.

van Swelm, R. P. L., J. F. M. Wetzels, and D. W. Swinkels. (2020). The multifaceted role of iron in renal health and disease. *Nat Rev Nephrol*, 16: 77-98.

Varela, I., J. Cadiñanos, A. M. Pendás, A. Gutiérrez-Fernández, A. R. Folgueras, L. M. Sánchez, Z. Zhou, F. J. Rodríguez, C. L. Stewart, J. A. Vega, K. Tryggvason, et al. (2005). Accelerated ageing in mice deficient in Zmpste24 protease is linked to p53 signalling activation. *Nature*, 437: 564-8.

Varela, I., S. Pereira, A. P. Ugalde, C. L. Navarro, M. F. Suárez, P. Cau, J. Cadiñanos, F. G. Osorio, N. Foray, J. Cobo, F. de Carlos, et al. (2008). Combined treatment with statins and aminobisphosphonates extends longevity in a mouse model of human premature aging. *Nat Med*, 14: 767-72.

Vela, D. (2018). Balance of cardiac and systemic hepcidin and its role in heart physiology and pathology. *Lab Invest*, 98: 315-26.

Velasco, G., S. Cal, V. Quesada, L. M. Sánchez, and C. López-Otín. (2002). Matriptase-2, a membrane-bound mosaic serine proteinase predominantly expressed in human liver and showing degrading activity against extracellular matrix proteins. *J Biol Chem*, 277: 37637-46.

Vermeij, W. P., J. H. Hoeijmakers, and J. Pothof. (2016). Genome integrity in aging: human syndromes, mouse models, and therapeutic options. *Annu Rev Pharmacol Toxicol*, 56: 427-45.

References

Villa-Bellosta, R., J. Rivera-Torres, F. G. Osorio, R. Acín-Pérez, J. A. Enriquez, C. López-Otín, and V. Andrés. (2013). Defective extracellular pyrophosphate metabolism promotes vascular calcification in a mouse model of Hutchinson-Gilford progeria syndrome that is ameliorated on pyrophosphate treatment. *Circulation*, 127: 2442-51.

Villeda, S. A., J. Luo, K. I. Mosher, B. Zou, M. Britschgi, G. Bieri, T. M. Stan, N. Fainberg, Z. Ding, A. Eggel, K. M. Lucin, et al. (2011). The ageing systemic milieu negatively regulates neurogenesis and cognitive function. *Nature*, 477: 90-4.

Vitale, G., G. Pellegrino, M. Vollery, and L. J. Hofland. (2019). Role of IGF-1 system in the modulation of longevity: controversies and new insights from a centenarians' perspective. *Front Endocrinol (Lausanne)*, 10: 27.

Voskoboinik, I., J. C. Whisstock, and J. A. Trapani. (2015). Perforin and granzymes: function, dysfunction and human pathology. *Nat Rev Immunol*, 15: 388-400.

Walker, R. G., O. Barrandon, T. Poggioli, S. Dagdeviren, S. H. Carroll, M. J. Mills, K. R. Mendello, Y. Gomez, F. S. Loffredo, J. R. Pancoast, C. Macias-Trevino, et al. (2020). Exogenous GDF11, but not GDF8, reduces body weight and improves glucose homeostasis in mice. *Sci Rep*, 10: 4561.

Walker, R. G., T. Poggioli, L. Katsimpardi, S. M. Buchanan, J. Oh, S. Wattrus, B. Heidecker, Y. W. Fong, L. L. Rubin, P. Ganz, T. B. Thompson, et al. (2016). Biochemistry and biology of GDF11 and myostatin: similarities, differences, and questions for future investigation. *Circ Res*, 118: 1125-41; discussion 42.

Wang, H., D. Diao, Z. Shi, X. Zhu, Y. Gao, S. Gao, X. Liu, Y. Wu, K. L. Rudolph, G. Liu, T. Li, et al. (2016). SIRT6 controls hematopoietic stem cell homeostasis through epigenetic regulation of Wnt signaling. *Cell Stem Cell*, 18: 495-507.

Warren, W. C., L. Kuderna, A. Alexander, J. Catchen, J. G. Pérez-Silva, C. López-Otín, V. Quesada, P. Minx, C. Tomlinson, M. J. Montague, F. H. G. Farias, et al. (2017). The novel evolution of the sperm whale genome. *Genome Biol Evol*, 9: 3260-64.

Weiss, G., T. Ganz, and L. T. Goodnough. (2019). Anemia of inflammation. *Blood*, 133: 40-50.

White, C. R., D. J. Marshall, L. A. Alton, P. A. Arnold, J. E. Beaman, C. L. Bywater, C. Condon, T. S. Crispin, A. Janetzki, E. Pirtle, H. S. Winwood-Smith, et al. (2019). The origin and maintenance of metabolic allometry in animals. *Nat Ecol Evol*, 3: 598-603.

Whittaker, J., A. V. Groth, D. C. Mynarcik, L. Pluzek, V. L. Gadsboll, and L. J. Whittaker. (2001). Alanine scanning mutagenesis of a type 1 insulin-like growth factor receptor ligand binding site. *J Biol Chem*, 276: 43980-6.

Wood, J. G., B. Rogina, S. Lavu, K. Howitz, S. L. Helfand, M. Tatar, and D. Sinclair. (2004). Sirtuin activators mimic caloric restriction and delay ageing in metazoans. *Nature*, 430: 686-9.

Wu, M., G. Chen, and Y. P. Li. (2016). TGF-beta and BMP signaling in osteoblast, skeletal development, and bone formation, homeostasis and disease. *Bone Res*, 4: 16009.

Xiong, J., K. Cawley, M. Piemontese, Y. Fujiwara, H. Zhao, J. J. Goellner, and C. A. O'Brien. (2018). Soluble RANKL contributes to osteoclast formation in adult mice but not ovariectomy-induced bone loss. *Nat Commun*, 9: 2909.

Xiong, J., M. Onal, R. L. Jilka, R. S. Weinstein, S. C. Manolagas, and C. A. O'Brien. (2011). Matrix-embedded cells control osteoclast formation. *Nat Med*, 17: 1235-41.

Xu, J., D. J. Lloyd, C. Hale, S. Stanislaus, M. Chen, G. Sivits, S. Vonderfecht, R. Hecht, Y. S. Li, R. A. Lindberg, J. L. Chen, et al. (2009). Fibroblast growth factor 21 reverses hepatic

steatosis, increases energy expenditure, and improves insulin sensitivity in diet-induced obese mice. *Diabetes*, 58: 250-9.

Yang, S. H., M. Meta, X. Qiao, D. Frost, J. Bauch, C. Coffinier, S. Majumdar, M. O. Bergo, S. G. Young, and L. G. Fong. (2006). A farnesyltransferase inhibitor improves disease phenotypes in mice with a Hutchinson-Gilford progeria syndrome mutation. *J Clin Invest*, 116: 2115-21.

Yang, T. L., H. Shen, A. Liu, S. S. Dong, L. Zhang, F. Y. Deng, Q. Zhao, and H. W. Deng. (2020). A road map for understanding molecular and genetic determinants of osteoporosis. *Nat Rev Endocrinol*, 16: 91-103.

Yang, Z., H. Jun, C. I. Choi, K. H. Yoo, C. H. Cho, S. M. Q. Hussaini, A. J. Simmons, S. Kim, J. M. van Deursen, D. J. Baker, and M. H. Jang. (2017). Age-related decline in BubR1 impairs adult hippocampal neurogenesis. *Aging Cell*, 16: 598-601.

Yanoff, L. B., C. M. Menzie, B. Denkinger, N. G. Sebring, T. McHugh, A. T. Remaley, and J. A. Yanovski. (2007). Inflammation and iron deficiency in the hypoferremia of obesity. *Int J Obes (Lond)*, 31: 1412-9.

Yasuda, H., N. Shima, N. Nakagawa, K. Yamaguchi, M. Kinosaki, S. Mochizuki, A. Tomoyasu, K. Yano, M. Goto, A. Murakami, E. Tsuda, et al. (1998). Osteoclast differentiation factor is a ligand for osteoprotegerin/osteoclastogenesis-inhibitory factor and is identical to TRANCE/RANKL. *Proc Natl Acad Sci U S A*, 95: 3597-602.

Zhang, G., C. Cowled, Z. Shi, Z. Huang, K. A. Bishop-Lilly, X. Fang, J. W. Wynne, Z. Xiong, M. L. Baker, W. Zhao, M. Tachedjian, et al. (2013). Comparative analysis of bat genomes provides insight into the evolution of flight and immunity. *Science*, 339: 456-60.

Zhang, W., J. Qu, G. H. Liu, and J. C. I. Belmonte. (2020). The ageing epigenome and its rejuvenation. *Nat Rev Mol Cell Biol*, 21: 137-50.

Zhang, Y., J. Shao, Z. Wang, T. Yang, S. Liu, Y. Liu, X. Fan, and W. Ye. (2015). Growth differentiation factor 11 is a protective factor for osteoblastogenesis by targeting PPARgamma. *Gene*, 557: 209-14.

Zhang, Y., Y. Xie, E. D. Berglund, K. C. Coate, T. T. He, T. Katafuchi, G. Xiao, M. J. Potthoff, W. Wei, Y. Wan, R. T. Yu, et al. (2012). The starvation hormone, fibroblast growth factor-21, extends lifespan in mice. *Elife*, 1: e00065.

Zhao, Y., J. L. Ren, M. Y. Wang, S. T. Zhang, Y. Liu, M. Li, Y. B. Cao, H. Y. Zu, X. C. Chen, C. I. Wu, E. Nevo, et al. (2013). Codon 104 variation of p53 gene provides adaptive apoptotic responses to extreme environments in mammals of the Tibet plateau. *Proc Natl Acad Sci U S A*, 110: 20639-44.

Zhu, Y., T. Tchkonia, T. Pirtskhalava, A. C. Gower, H. Ding, N. Giorgadze, A. K. Palmer, Y. Ikeno, G. B. Hubbard, M. Lenburg, S. P. O'Hara, et al. (2015). The Achilles' heel of senescent cells: from transcriptome to senolytic drugs. *Aging Cell*, 14: 644-58.

Zimmerman, L. M., L. A. Vogel, and R. M. Bowden. (2010). Understanding the vertebrate immune system: insights from the reptilian perspective. *J Exp Biol*, 213: 661-71.

Zimmers, T. A., Y. Jiang, M. Wang, T. W. Liang, J. E. Rupert, E. D. Au, F. E. Marino, M. E. Couch, and L. G. Koniaris. (2017). Exogenous GDF11 induces cardiac and skeletal muscle dysfunction and wasting. *Basic Res Cardiol*, 112: 48.

Supplementary Information

I.- Manual characterization and comparative analysis of the genome of two long-lived giant tortoises: extended data

Supplementary Table S1. Highlighted variants and truncations found during manual analysis of *C. abingdonii*'s genome.

Gene	Variant	Affected site/Predicted effect	Present in (besides *C. abingdonii*)
ADORA2B	C72D; A150G; T153P; N163Q	Transmembrane receptor 7	G.aga
AGTR1	C355T	Lipidation residue	G.aga; A.gig
AICDA	D96N; L104M	RNF126 interaction region	G.aga (L104M)
ALDH2	Q366M	NAD binding site	Galapagos tortoises
ALDH2	M487T	Homotetrameric interface	Galapagos tortoises; A.gig; Continental outgroups
ALKBH3	E248D	Region of alpha-ketoglutarate binding	
ANKRD17	Multiple	Whole protein	G.aga
ANXA1	N153C; E158D; T169V; C324F	Annexin domain	G.aga (N153C; E158D; T169V; C324F)
APEX1	K31A	TOMM20 binding	A.car; G.gal; P.sin; C.pic; G.aga; A.gig
APLF	S116N	Diminishes phosphorylation by ATM	A.car; G.gal; P.sin; C.pic; G.aga; A.gig
ARRB2	L244S	TRAF6 interaction domain	
ATM	R250Q	Variants related to ataxia-telangiectasia	Galapagos tortoises; A.gig; Continental outgroups
ATM	Y316H	Variants related to ataxia-telangiectasia	Galapagos tortoises
ATM	V2873I	Catalytic loop	Galapagos tortoises; Fishes
BCL2L1	D61A	No cleavage by caspase-1 nor caspase-3	G.gal; P.sin; C.pic; G.aga; A.gig
BIN2	N49D	Dimer interface	C.pic; G.aga; A.gig
BRCA1	S308N	Phosphoserine	P.sin; G.aga; A.gig
BRCA2	S491V; S755V; S2095Q; T3387P	Phosphoserine/Phosphothreonine	A.car; P.sin; C.pic; G.aga; A.gig
C1QA	K100R	Hydroxylysine	
C1QBP	D177N	C1Q globular heads binding domain	
C6	N167K	Calcium binding site	A.gig
C6	L673M	Receptor-ligand interactions	P.sin; C.pic; G.aga; A.gig
C7	N600R	Receptor-ligand interactions	G.gal; P.sin; C.pic; G.aga; A.gig
C8A	N437S	Loss of glycosylation site	C.pic; G.aga
C8B	W554S	Loss of glycosylation site	C.pic
CAMP4	Q34Lfs*9	Frameshift leading to premature stop codon	A.gig
CANT1	D169N	Activity reduced by 96%	A.car (D169E); G.gal (D169E); P.sin (D169E); C.pic (D169E); G.aga (D169E); A.gig (D169E)
CARD11	S466G	Phosphoserine	C.pic; G.aga; A.gig
CARD14	Q711*	Premature stop codon	
CAV1	K5Q	Acetyllysine	G.aga, A.gig
CDH1	Y754H	CBLL1 interaction site	G.gal (Y754N); C.pic; A.gig
CDK6	S222N	Active site and substrate binding	A.car; G.gal; P.sin; C.pic; G.aga; A.gig
CDKN1B	Y89F	Reduced CDK4 binding and increases inhibition of CDK4	A.car; P.sin; C.pic; G.aga; A.gig
CHGA	S300N	Phosphoserine	A.car; G.aga
CHUK	D154E; I159T; I160V; H306Y	Serine-threonine kinase domain	M.mus (I159T); P.sin (D154E); C.pic (H306Y); G.aga (H306Y)
CLIP4	Q438*	Premature stop codon	A.gig
CLNK	L333M; E353R	Hydrophobic pocket	
CNDP1	A274Dfs*1; V295Sfs*7	Frameshifts leading to premature stop codons	Galapagos tortoises; A.gig; Continental outgroups
CRYAA	Q50H	Deamidated glutamine	P.sin; C.pic; G.aga; A.gig
DCLRE1B	R498C	TERF2 interaction site	G.aga; Galapagos tortoises; A.gig; Continental outgroups
DDX58	S532del; K814R; G900S	S532del Helicase domain; K814R G900S RIG domain	G.aga (S532del; G900S)

DHX58	D83N	Helicase domain	
DLL1	G417E; V444M	Calcium binding EGF-like domain	C.pic; G.aga (V444M)
DNAJA3	R293H	CARM1 methylation site of activation. Zn binding motif	
DRD2	L170I; R217Q; L236M; V255I	G-coupled receptors domain	A.car (L236M); G.gal (L170I; L236M); P.sin (L236M); C.pic (L236M); G.aga (L170I; V255I)
EBI3	E213N	Cytokine binding motif	G.aga
EIF2AK3	S1022N	Binding site	C.pic; G.aga; A.gig
EPHB6	A321T	GCC domain	
	R677L	Fibronectin type 3 domain	
	L959F	SAM domain tyrosine kinase receptor	
EPRS	V1302I; R1415K; T1429N	Prolyl-anticodon binding domain	G.aga (R1415K; T1429N)
	K844R	tRNA binding WHEP-TRS domain	G.aga
ERN1	K837R	Ligand binding site	P.sin; C.pic; A.gig
EXO1	S610G	Phosphoserine in MSH2 interaction domain	G.aga; A.gig
F10	E91K	Involved in Factor 10 deficiency	G.aga (E91D); A.gig
F11	E315K	Involved in Factor 11 deficiency	G.aga; A.gig
F7	S113D; F64L	Involved in Factor 7 deficiency	G.aga; A.gig
FADD	E37A; V39I	DED-FADD domain	
FAS	D93H; G112D; N124D	TNFRSF domain	C.pic (G112D; N124D); G.aga (D93H; G112D)
	A301F	DD death domain	G.aga
FGA	R123I	Cleavage site by plasmin	
FGF19	S116A	Receptor-interaction site	A.gig
FOXJ1L	F158Y	DNA binding domain	G.aga
GSK3A	R272Q	Activation loop	C.pic; G.aga; Galapagos tortoises; A.gig; Continental outgroups
HMGB1	S107A	DNA binding site	C.pic; G.aga; A.gig
HSPA5	T643E	Phosphothreonine	C.pic; G.aga; A.gig
HSPD1	K125R	Lys acetylation site	P.sin; C.pic; G.aga; A.gig
	K369R	Lys acetylation site	C.pic; G.aga; A.gig
IGF1R	N724D	IGF1/2 binding site	G.aga; Galapagos tortoises; A.gig; Continental outgroups
IGF2R	N1757_Y1758del	N1757 is a glycosylation site	G.aga, Galapagos tortoises; A.gig; Continental outgroups
IRAK4	V37I	IRAK4-IRAK2 interaction site	
ITGA1	R990*	Premature stop codon	
JAK2	L579V	ATP binding site	G.aga; A.gig
LY75	Q471R; K785R	Ligand binding surface	P.sin; C.pic; G.aga; A.gig
MAP3K8	E279D	Activation loop	P.sin; C.pic; G.aga; A.gig
MAP4K2	G159A; R169K	Activation loop	P.sin; C.pic; G.aga; A.gig
MARCH8	S253A	Phosphoserine	A.gig
MB	K97T	Heme interaction site	
MDM2L	E430*; P451*; N478*	Premature stop codons	G.aga; A.gig
	S235*	Premature stop codon	
MEP1A	W317Lfs*3; N529Tfs*6	Frameshifts leading to premature stop codons	Galapagos tortoises
MIF	N111C	Locked trimer	G.aga; Galapagos tortoises; A.gig; Continental outgroups
MSH2	V102I	Variant related to HNPCC1	C.pic; G.aga; A.gig
MSH6	S137P	Phosphoserine	A.gig
MYO5AB	E114K	ATP binding site	P.sin; C.pic; G.aga; A.gig
NEIL2	K154R	Acetylation site	A.gig
NF2L	S13G	Phosphoserine	P.sin; C.pic; G.aga; A.gig
	D268E	Peptide binding site	P.sin; C.pic; G.aga; A.gig
	K289Q; K291Q	PIP2 binding site	P.sin; C.pic; G.aga; A.gig
NFKBID	Y66Q; A94T; P98A; L154Q; Q194H; A217D; A218G	Interaction sites	P.sin; C.pic; G.aga; A.gig
NFKBIZ	L553F; L631F	Interaction sites	C.pic; G.aga; A.gig
NLN	W50*	Premature stop codon	G.aga (R45*, evolutive convergence); Galapagos tortoises
	L532Ffs*1	Frameshift leading to premature stop codons	Galapagos tortoises; Continental outgroups

NOTCH1	A2022G	Hydroxylated by HIFAN	A.gig
NTRK1	L333del	Receptor binding site	G.gal; P.sin; C.pic; G.aga; A.gig
NUTM1	A672*	Premature stop codon	
PDE4DIP	H1598R	Associated with risk of ischemia	C.pic; G.aga; A.gig
PIK3R1	I287V	Putative GTPase interaction site (RAS)	C.pic; G.aga; A.gig
PKN3	L623V; T639M; F641Y; C757S	Active sites	G.gal; P.sin; C.pic; G.aga
	Multiple	Rho binding domain	G.gal; P.sin; C.pic; G.aga
PLAG1	P346S	Repression domain	
PLG	R134L	Fibrin-binding site	G.aga; A.gig
	R136K	Fibrin-binding site	P.sin; G.aga; A.gig
PPP2R1A	T78A	Polypeptide binding site	C.pic; G.aga; A.gig
PRDM1	G74S	Irritable bowel syndrome-diarrhea	C.pic; G.aga; A.gig
PRDM1L	D69E	Autoimmune diseases	A.car; G.aga; A.gig
PRF1G	Q386*	Premature stop codon	Galapagos tortoises
PRF1I	W483*	Premature stop codon	C.dun
PRF1K	S388*; H398*; T450*; T452*; T453*; C511*	Premature stop codons	
PRG4	A1246V	Metal binding site (ion binding site)	P.sin; C.pic; G.aga; A.gig
PRKACA	V105I	Active site	G.aga; A.gig
PRKCH	V374I	Increases cerebral infarction risk in human	M.mus; C.pic; G.aga
PRKCZ	A155G; R160K	Putative DAG/PE binding sites	G.gal (R160K); P.sin (A155G; R160K); C.pic (A155G; R160K); G.aga
PRKDC	S2612T	Phosphoserine in catalytic subunit	C.pic; G.aga; A.gig
PRSS12	R691*	Premature stop codon	
PSEN1	R352E	Pathological significance	G.aga; Galapagos tortoises; A.gig; Continental outgroups
PSIP1	A153S	Nuclear localization signal	P.sin; C.pic; G.aga; A.gig
PSMD10	E54D; A72S; K116R	Oligomer interface	A.car (E54D); C.pic (K116R)
PTGS1	F209L	Heme-binding site	A.gig
	L534F	Substrate binding site	P.sin; C.pic; G.aga; A.gig
PTGS2	I331V	Substrate binding site	C.pic; G.aga; A.gig
PTK2B	R309K	Putative peptide binding site	A.car; G.gal; P.sin; C.pic; G.aga
	D578E	Activation loop	A.car; G.gal; P.sin; C.pic; G.aga
PTPRC	V1125S	Active site	G.aga
PTX3	N275S	Intermolecular salt bridges	M.mus; G.gal; P.sin; C.pic; G.aga
PVRL1	V89I; R110Q; F126Y; M143L	Ligand binding site	C.pic (V89I; R110Q; M143L); G.aga (V89I; R110Q; M143L)
RAB17	L48M; K58Q; V59L	GEF interaction sites	A.car (K58Q); G.gal (K58Q); P.sin (K58Q; L48M; V59L); C.pic (K58Q; V59L); G.aga (K58Q; V59L)
	G28T; S29A; K45R	GTP/Mg^{2+} binding sites	A.car (K45R); G.gal (G28T); P.sin (G28T; S29A; K45R); C.pic (G28T; S29A; K45R); G.aga (G28T; S29A; K45R)
	L35I; L37F; D43V; T101A; V125L	Rab subfamily motif	P.sin (L37F); C.pic (L35I; L37F; T101A; V125L); G.aga (T101A; V125L); A.gig (D43V)
RAD51B	S194T	ATP binding site	P.sin; C.pic; G.aga; A.gig
RAD51D	S197L	ATP binding site	P.sin; C.pic; G.aga; A.gig
RB1	K720R	Binding site 2 (LxCxE peptide; DNA; CDK2)	A.car; G.gal; P.sin; C.pic; G.aga; A.gig
REL	I230S	Ankyrin protein binding site	G.gal; P.sin; C.pic; G.aga
RELA	R253K	Ankyrin protein binding site	A.car; P.sin; C.pic; G.aga
RELB	R231K; I308M	Ankyrin protein binding site; DNA binding site	A.car; G.gal; P.sin; C.pic; G.aga
RGCC	T111A	Loss phosphorylation site. Less CDK1 stimulation	M.mus; P.sin; C.pic; G.aga
RGS1	N97V; D194E; I195A	Homodimer interface	P.sin (I195A); C.pic; G.aga; A.gig (N97V; D194E; I195A)
RHOH	N62S	GAP/GEF interaction site	A.car; G.gal; P.sin; C.pic; G.aga; A.gig
	L71I	GTP/Mg^{2+} binding site GAP/GEF/GDIa/Effector interaction site	G.gal; P.sin; C.pic; G.aga; A.gig
RIPK1	S25A; I43V	Active sites	A.car (S25A); G.gal (S25A; I43V); P.sin (S25A; I43V);

			C.pic (S25A; I43V); G.aga (S25A; I43V); A.gig (S25A; I43V)
RNF168	R57W	May loose ability to ubiquitinate H2A	C.pic; G.aga; A.gig
RNASE1	C68*	Premature stop codon	
ROS1	P182S	Cytokine receptor motif (FN type 3 domain)	P.sin; C.pic; G.aga; A.gig
	E274P	Cytokine receptor motif (FN type 3 domain)	A.car; G.gal; P.sin; C.pic; G.aga; A.gig
	S641Y	Interdomain contacts (FN type 3 domain)	P.sin (S641F); C.pic; G.aga; A.gig
SDHCL	R50H	Iron-sulfur protein interface	G.aga; A.gig
	R72H	Iron-sulfur protein interface and proximal heme binding site	G.aga (R72G); A.gig
	L78T	Proximal heme binding site	G.aga (L78M in SDHC and SDHCL); A.gig (L78M); C.abi (L78M in SDHC)
SERPING1	E472D	Reactive centre loop	C.pic; G.aga; A.gig
SETBP1	TQ1462-1463FS	DNA binding	A.car; G.gal; P.sin; C.pic; G.aga; A.gig
SIRT6	T294L; S330A	Phosphothreonine; Phosphoserine	P.sin; C.pic; G.aga; A.gig
SNAP23	M169L; Q183R	Heterotetramer interface	C.pic; G.aga; A.gig
SOX21	I171Pfs*64	Premature stop codon	A.gig
TAS1R1	T436*	Premature stop codon	G.aga (W297*); A.gig
TERF2	S161T	DCLRE1B interaction site	A.car; G.gal; P.sin; C.pic; G.aga (S161E); A.gig
	M164T		P.sin (M164K); C.pic (M164K); G.aga (M164I)
	N176G		A.car (N176H); G.gal; P.sin; C.pic; G.aga (N176V); A.gig
	M180L		A.car (M180K); G.gal; P.sin; C.pic; G.aga (M180I); A.gig
TICAM2	S16N; C117S	Phosphorylation site; dimerization site	G.gal (S16N); P.sin (S16N; C117S); C.pic (S16N; C117S); G.aga (S16N; C117S)
TIRAP	S180K	S180L protects against pneumococcal disease, malaria, bacteraemia and tuberculosis	G.gal; P.sin; C.pic; G.aga
TLR10	D508*; S512*; E530*; D540*; V542*; L567*; M572*; I602*; L610*; R620*	Premature stop codons	A.gig
TMEM173	V147I	(V147L) vascular disease in human	A.car; P.sin; C.pic; G.aga
TP53	R72P	Human polymorphism	A.car; G.gal; C.pic; G.aga; A.gig
	S106E	Adaptation to hypoxia	P.sin; C.pic; G.aga; Galapagos tortoises; A.gig; Continental outgroups; M.oec; B.bar; L.for
	R290C	DNA-binding domain. Li-Fraumeni mutation	G.aga; A.gig
TP53BP1	T543I	Thr phosphorylation site	G.aga; A.gig
TRAIP	R18K	TRAF interacting protein	G.aga; A.gig
TRIM24	S862R	Histone H3 binding site	P.sin; C.pic; G.aga; A.gig
TSHR	K621R	K621 is important for G alpha subunit activation	Galapagos tortoises; A.gig; Continental outgroups
WHSC1L1	K245L	Sumoylation site	A.car; G.gal; P.sin; C.pic; G.aga; A.gig
XPNPEP1	D16*	Premature stop codon	Galapagos tortoises; A.gig; Continental outgroups
XRCC5	K568N	Sumoylation site	P.sin; C.pic; G.aga; Galapagos tortoises; A.gig; Continental outgroups
XRCC6	K556R	Sumoylation site	Galapagos tortoises; A.gig; Continental outgroups
	N275S; R403C	DNA binding site	A.gig
ZBTB16	A469T	DNA binding site	A.gig

Supplementary Table S2. Gene variants validated by Sanger sequencing and supported by aligned RNA-Seq reads.

Gene	Observation	Validations	
		Sanger sequencing	**RNA-Seq**
ALDH2	Variant p.Q366M	Galapagos tortoises	Confirmed
	Variant p.M487T	Galapagos tortoises; A.gig; Continental outgroups	Confirmed
APOBEC1	7 copies	C.abi; A.gig	All copies confirmed in C.abi and A.gig
ATM	Variant p.R250Q	Galapagos tortoises; A.gig; Continental outgroups	Confirmed
	Variant p.Y316H	Galapagos tortoises	Confirmed
	Variant p.V2873I	Galapagos tortoises	Confirmed
CDH1	Variant p.Y754H	Galapagos tortoises; A.gig; Continental outgroups	Confirmed
CHIA	Triplication	Galapagos tortoises; A.gig; Continental outgroups. One of these copies is specific of Galapagos tortoises	No reads aligned
CMA1L	Duplication + pseud.	Galapagos tortoises; A.gig; Continental outgroups. Only one copy validated by Sanger sequencing	No reads aligned
CNDP1	A274Dfs*1	Galapagos tortoises; A.gig; Continental outgroups	No reads aligned
	V295Sfs*7	Galapagos tortoises; A.gig; Continental outgroups	No reads aligned
CTSGL	8 copies + 1 pseud.	Galapagos tortoises; A.gig; Continental outgroups. Two copies were not validated by Sanger sequencing	No reads aligned
DCLRE1B	Variant p.R498C	Galapagos tortoises; A.gig; Continental outgroups	No reads aligned
EEF1A1	Duplication + 1 pseud.	Galapagos tortoises; A.gig; Continental outgroups. The pseudogene was not confirmed	Non-specific reads
GAPDH	Duplication + retrogene	Galapagos tortoises; A.gig; Continental outgroups. The retrogene was not confirmed	One copy confirmed
GSK3A	Variant p.R272Q	Galapagos tortoises; A.gig; Continental outgroups	Confirmed
GZMB	5 copies + 1 pseud.	Galapagos tortoises; A.gig; Continental outgroups	No reads aligned
GZMH	Duplication + 3 pseud.	Galapagos tortoises; A.gig; Continental outgroups	No reads aligned
IGF1R	Variant p.N724D	Galapagos tortoises; A.gig; Continental outgroups	Reads only in A.gig granuloma
IGF2R	N1757_Y1758del	Galapagos tortoises; A.gig; Continental outgroups	Confirmed
LRAS	New gene	Galapagos tortoises; A.gig; Continental outgroups	Confirmed
MEP1A	W317Lfs*3	Galapagos tortoises	No reads aligned
	N529Tfs*6	Galapagos tortoises	No reads aligned
MIF	Variant p.N111C	Galapagos tortoises; A.gig; Continental outgroups	Confirmed
MYCN	Duplication	Galapagos tortoises; A.gig; Continental outgroups	Only one copy with reads in A.gig granuloma
NEIL1	Duplication	Galapagos tortoises; A.gig; Continental outgroups	Confirmed
NF2	Duplication	Galapagos tortoises; A.gig; Continental outgroups	Confirmed
NLN	Stop codon W50*	Galapagos tortoises	Confirmed
	L532Ffs*1	Galapagos tortoises; Continental outgroup	No reads aligned
P2RY8	Duplication	Galapagos tortoises; A.gig; Continental outgroups	Only one copy confirmed in C.abi. Both copies confirmed in A.gig
PML	Duplication	Galapagos tortoises; A.gig; Continental outgroups	Confirmed
PRF1	9 copies + 3 pseud.	C.abi; 1 pseud. present in Galapagos tortoises but absent in A. gig and Continental outgroups; another pseud. is unique to C.abi; last pseudogene is not present in A.gig but it is not validated in other turtles	Few reads
PRSS12	Stop codon R691*	C.abi	No reads aligned
PSEN1	Variant p.R352E	Galapagos tortoises; A.gig; Continental outgroups	Confirmed
	Duplication	Galapagos tortoises; A.gig; Continental outgroups	Confirmed

RMI2	Duplication	C.abi; A.gig	Only one copy confirmed in C.abi. Both copies confirmed in A.gig
SMAD4	Duplication	Galapagos tortoises; A.gig; Continental outgroups	Confirmed
TLR13	Duplication	C.abi; A.gig	No reads aligned
TLR2	Duplication + 2 pseud.	C.abi; A.gig	No reads aligned
TLR5	Duplication	C.abi; A.gig	No reads aligned
TLR8	Duplication	C.abi; A.gig	No reads aligned
TP53	Variant p.S106E	Galapagos tortoises; A.gig; Continental outgroups	Confirmed
TSHR	Variant p.K621R	Galapagos tortoises; A.gig; Continental outgroups	No reads aligned
USP12	Duplication	Galapagos tortoises; A.gig; Continental outgroups	Confirmed
XPNPEP1	Stop codon D16*	Galapagos tortoises; A.gig; Continental outgroups	Confirmed
XRCC5	Variant p.K568N	Galapagos tortoises; A.gig; Continental outgroups	Confirmed
XRCC6	Variant p.K556R	Galapagos tortoises; A.gig; Continental outgroups	Confirmed

Supplementary Table S3. Primer sequences used for validation of gene alterations identified in *C. abingdonii*'s genome.

Gene	Target	Forward	Reverse	Tm (ºC)	Product size
ALDH2	Variant p.Q366M	AACGCCTTCCTAACTCCATGT	CTCTGTCTGCAGCAGGATTG	60	214
	Variant p.M487T	TGCTCTGGAGCAACAAACTG	GAGGGCCAACTTCCTTCTTC	60	256
APOBEC1	Copy A	GTTGCCATAGAACTGGAACGA	CCCACAGGGACTCCAGGACA	62	124
	Copy B			64	124
	Copy C	GGATCTGTAGTGCTGGCGGTG	ACCAGGTGATGGAGCAGTG	64	101
	Copy D	GTTGCCATAGCACTCGAACAG	ACCAGGTGATGGAGCAGTG	62	101
	Copy E	GTTGCCATAACTCCCTCACAG	CCCACAGGGACTCCAGGACA	60	124
	Copy F	GTTGCCATAACTCCCTCACAG	CCCACAGGGACTCCAGGACA	61	124
	Copy G	GTTGCCATAACTCCCTCACAG	ACCAGGTGATGGAGCAGTG	60	101
ATM	Variant p.V2873I	TCGGAAAAGACAACTGAAAGC	GGTGAATGTGTAAGGCATAATCA	59	244
	Variant p.Y316H	CAATATTGCGTGATCCTGAAGA	TTCTCTGCTCATCTGCGAAC	60	228
	Variant p.R250Q	GAACACGAACCTGCAGTTGA	CAGACAGGAGAACGCCTCTG	60	209
CDH1	Variant p.Y754H	AGCAACAGCTTCAGCACTCC	TCCTGGTGCTACAGCCAGAT	60	207
CHIA	Copy A	TCCCCTTTTTCCTCCCTAGA	GAGGAGCTGGTTTCCTCCTT	60	207
	Copy B	CCAACTGGGGCCAATATAGA	GCCCCTAAGAAGCAAGACAA	60	218
	Copy C	GCCCCGATCTTCTCCTTCTA	TTGATGCCAGCATAGAGTGC	60	215
CMA1	Copy A	GGGCAGTACCTTTAGCAGCA	TGGAGCCAGCTTACCATACA	60	207
	Copy B	CCGCCATATTTTCCCCTTGG	CCTGTAGCAGTGTGAGGTCA	63	206
CNDP1	Frameshift in r. 274	ACACAAGCCAACTGAACCAC	TCAGGGAAGTTTTGGAGGCA	59	150
CTSG	Copy A	GTCAGTGGGGGTGGTACCTT	CTGTCCAATGGGCACTAACA	60	201
	Copy B	TTGCTTTTTCAGCGAGATCA	TAGTGCATGAGTGCGAGGTC	60	200
	Copy C	GCTCTGGGCTTTTACAGCAA	TTCAGCAGCATGAGGTCACT	62	203
	Copy D	GGCTCACTCCAAACCCTACA	CAGTAAGCCGCAACTGACC	60	203
	Copy E	GCCCCTACATGGCATATCTC	GATGGATGCTGCACTGCTAA	60	223
	Copy F	GTTGTGGAGACTCCCCTTTG	CACGAAGTTCTTCGACACCA	60	217
DCLRE1B	Variant p.R498C	AGAGCCCATCCTCTCTCCTG	TCTGCCTGCAGACTGAGAAA	60	207
EEF1A1	Copy A	GCAGCCTCCTTCTCGAACTT	GGTGTCTCTCCCGTAGGTGT	60	203
	Copy B	TGTGACGCTGGCTTGTTACT	CCCGCACTTGTAGATGAGGT	58	204
GAPDH	Copy A	GTGCTGCTTTACTGGAGCTG	AGGGGCCAATCACCACTCAT	60	272
	Copy B	ACTGGTGCTGCTAAGGCTGT	CAACCAGGTCCTCGGTGTAT	60	214
GHR	Variant p.P177L	ACAACCTGATCCTCCTGTCG	TCATACCTCCCTCCATTTCG	60	184
	Variant p.E191K				
GSK3A	Variant p.R272Q	TGAGATGGTTGACCCCACAC	GGTGGGAGCTCACCTATGTT	60	264
GZMB	Copy A	CCCCCTTCTTCACCTTCTTC	GTAGGCACATGGCATCACAG	60	217
	Copy B	CACTTTTGGGGTGGAATGAA	GCAGCTGGTTCCCAGACTAA	62	201
	Copy C	GACCAGTCACATCACCAGGA	GCGTCAGGTGCTGTACAAAT	62	222
	Copy D	CATTGCAGTGAGTGGCTGTC	CCAGACTGGTCCAAGGAGAT	58	200
GZMH	Copy A	CAGGAACCCTCCACAGTGTC	GGTTGAGGATGAGGGTAGGG	58	200
	Copy B	CTGCAGGTATCGCCCCTAT	CACAGCCCCTGGTTTTACTC	58	224
IGF1R	Variant p.N724D	ACAGAAGAAGCCACCGAACC	ATTACCGCTAGTCCCCACCT	60	215
IGF1R	Variant p.R204H	AGGAAGAGGCACACACAAAAA	GACTTGTGTCCAGGGACGAT	60	162
IGF2R	NY1757-1758del	CCAAGTAGCTGCATCTTCCA	CAAACTTGTTCCTCTTTTACAATGG	60	233
LRAS	New gene	CTTTTGTCATGCCAGGGAGT	TACACACCAAAAGGGGCTCA	60	203
MEP1A	Frameshift in r. 274	GGCATGAACCAAGTGACCTT	TGGACCAGTGTGCTTTTGAG	59	200
	Frameshift in r. 295	TGTCTGTCGTGAAGCTCCTG	CCTGAGGGCTATGGTTATGG	59	213
MIF	Variant p.N111C	AGATGTGCAGGTCCAGGAAT	GGAAAATGTGAAACCACATCC	59	277
MYCN	Copy A	CAGCCCAACCAAGGAATTAG	GGAGACAGAGGAGGGGTAGG	60	200
	Copy B	GGGAAGCAGAGTCTGGACTG	CTTGCAGGTCTTGGGAGAAG	60	208
NEIL1	Copy A	GGTCAGCTTGATCTCCTTGC	CTTCATTTGGGCAGGTGTCT	60	200
	Copy B				

| Gene	Variant/Copy	Forward Primer	Reverse Primer	Temp	Size
NF2	Copy A	GACTTGCTGGCTGAAAAAGC	ATCTGGAAAGTGGAGCATGG	58	245
	Copy B	AAGAAGAGGCCAAACTGCTG	CACCAGACCCTCAAGCAAAT	56	191
NLN	Stop codon W51*	GAGCCTGCACAGTGTTCTCA	CTGGTGGTCCAAGGCTTTTA	59	228
	FS in residue 532 (E533*, K550*)	GAAGAGCATCTGCAACATGG	TGGAGGGTTTTTGGTTGTGT	59	202
P2RY8	Copy A	AGACCTCACACTGGCTTGCT	GGGATACACCACTCCCAAGA	58	181
	Copy B	CCCTTTGGACAGGTTCTGTG	TTCATGAGTGGGAAGTGCAG	60	212
PML	Copy A	GGTGCTCTGAGTGTGAGGAA	TGGGATTGGAACAGAAGAGG	58	194
	Copy B	CTGCTGCCTCTGTTGGATTT	ACGAAGGAGAACTGGCACTG	60	212
PRF1	Copy A	TGCTAGGATGCCACAGAGTG	CGGTATGCAGCTGAGTCGTA	68	200
	Copy B	GGTCTTCTTTGGGAGAAGGG	CGTGGTTCAGGTAGCAATCC	64	227
	Copy C	AGCAGCAATGAGCAGCTTG	CAGCACGTCAGTCGTGATCT	68	216
	Copy D	CCAAGGTTAACGTCCAGGTG	CCTTCCCCAGACCTAGCTG	70	201
	Copy E	ACGACGAGATCAAGGACTGC	ATCATTCCCCGAGAACAGC	62	204
	Copy F	GTCTGGGGCCTTAGCATG	GGGTGCCATAGTTGCTGATT	61	222
	Copy G	GTGGAGGTGAAGCCCAGC	GGCACCCAACACAACCTCTA	64	225
	Copy H (pseudogene)	AGACAGGCGGTGAAGGAGTA	GTGTCTCCCCACAGGTTTGT	62	212
	Copy I	CAGTTTGTTCAGGTGCAAGG	GTCTGCCTGCCTCACGTAGT	70	202
	Copy J (pseudogene)	ATGATAACGACCCCATCTGG	CTCCAGCGTGTAGTAAAACTGC	64	213
	Copy K	CACACTCCAAACTGGCTGAA	AGACATCCCGGTGTGTCATC	64	211
	Copy L (pseudogene)	GCTGACGAGGTCAAGGACTG	CCTCAGAGAACAGCAGGTCG	68	205
PRSS12	Stop codon R691*	CTTCTGGTCCCTGCAATCTC	TGTGTGATGTGAGCCCTGAT	59	201
PSEN1	Variant p.R352E	TTTCAGCCCGTCCTATGTGT	ATGCTGACATGGATGATGGA	59	258
PTPN11	Copy A	TCTGGAAAAGAAGCGGAAAA	CATGACATGGGTCACTTTCG	56	183
	Copy B	CCCCACATTTTCGTTGTAGG	CAAGAGTGCATGCCTGAAAA	58	219
RMI2	Copy A	GCTCCATGTGCTCCTGTGTA	GATGCAGGGCACGGTACT	60	225
	Copy B	TTTCTGGCATCTGCAAAAATAA	CAAACCCACCTGGAGTCCT	62	214
SMAD4	Copy A	TTCAGGTGGCTGGTCGTAAA	CAGGTGACACTACTCGCTCA	60	174
	Copy B	TCAAGTACGACAGCGTCTGC	AGAGGGCTTGACATGAAAGG	58	238
STC1	Exon 1	CTCGGCTCTAAAGCCCTCTT	TTTGCTGAAGCCGAAGAAAG	60	211
	Exon 2	CAAGCATTTGAGTGCCACAG	TGTCCTATGCCTGTCTTCCA	60	248
	Exon 3	TTTCACATAAGGAAACATCCACA	ATGCAGTTGCACATTAAGATGA	60	208
	Exon 4	CACCCATTCTCTCTCCCCTA	TTTGCTCTAGCTTGGGATCAA	60	368
STC2	Exon 1	AACCCACCAAGGTCTCCAGT	AGACCAGCGTCTTCAAGCAT	60	235
	Exon 2	CCCTCACCCCCATTTATGA	AGTTGGGCATGTGGAAGAGA	60	351
	Exon 3	CACCCGATGTGCTTAATGG	AATACCAGGCTCCTTGCACA	60	300
	Exon 4	TCCCCTTCTGCTGTTTGATT	TGGAGGAAGTTTTGGTGGAG	60	469
TLR13	Copy A	ACCAGGAGTGGGTGATCAAT	GAAAACTGGCCACCTGGAT	60	213
	Copy B	TGGGGAAGAGCATTGTTGAC	GAGCATCACCTTCCTCATGC	60	227
TLR2	Copy A				
	Copy B (pseudogene)	GCTGATGTCTTGGCTAACTGG	CAAGCCCAGGTCATTTTCAT	60	218
	Copy C	CACTCGCTGTTGACGAAGTT	CTCCTACAGCTGCTCAGACG	60	201
	Copy D (pseudogene)	GCAGGTCCTGAATGAAAATCA	CAGAACAAGTGGGTTGTTGG	60	207
TLR5	Copy A	TGAGATCCAGCCTTTTGAGG	TGGAGAGAAGGCCTTTGAGA	60	200
	Copy B	GTCTTGAGGAATCCATTCTGG	TTTTCCCTGGAAGCTAGCAA	60	200
TLR8	Copy A	TTGACAACCTTGCACAGAGC	GATCCTCCTTCTCAGCCTCA	60	203
	Copy B	GCACCGGCTCCAGTAGAATA	TGTTTGGAGGAAAGGGACTG	60	205
TP53	Variant p.S106E	GACCTGGGCCTGTCTGACT	TACGGTGCAGGTGACAGACT	60	207
TSHR	Variant p.K621R	TTCATGATGGCAGACAAAGC	CGTTGGCTCAAGCCTACATT	60	220
USP12	Copy A	AAAGAAAAATGGATTCCTGAAAG	GACAAACAAAATGGCCGTCTA	60	200
	Copy B	TGCTCTTTCATTCTTCCCAATCT	CGTTGGTTAGTGTTCCCTGG	59	242
		CAGGAGAAACAGAATGGCAAA	AATTAGGGAAAATGGTCCAGTG	59	201
XPNPEP1	Stop codon D16*	GGCTCTGCACTCCTCAATTG	AATAGGACCCTGCCTGCTAC	59	193
		CTTCCCATCTTGTGCACCTG	TCACTGGAAGACGCTAGCTC	57	203

| XRCC5 | Variant p.K568N | GGGAGGTTGGTTTGTTTTGA | AGTCCCCAAGGGAAGGTCTA | 60 | 207 |
| XRCC6 | Variant p.K556R | TAAACCCTGCATGCTTCCTT | AAGTTTTGCAGTGTTTTCCCTA | 60 | 200 |

II.- Functional analysis of the contribution of cell-extrinsic mechanisms to the development of a premature ageing phenotype: extended data
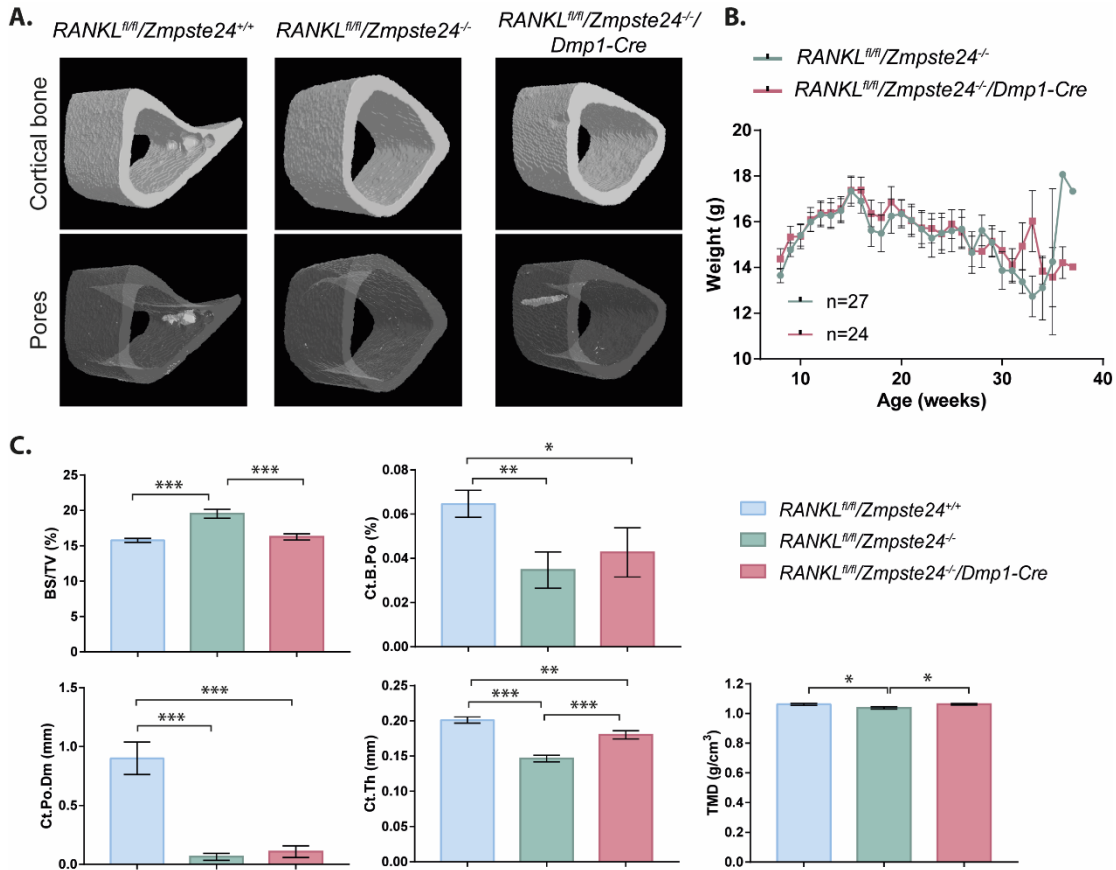

Supplementary Figure S1. Deletion of RANKL in the osteocyte population of *Zmpste24*-deficient mice reduces cortical bone resorption. A. Representative μCT images of proximal tibia from 6-month-old *RANKL^{fl/fl}/Zmpste24^{+/+}*, *RANKL^{fl/fl}/Zmpste24^{-/-}* and *RANKL^{fl/fl}/Zmpste 24^{-/-}/Dmp1-Cre* littermates. **B.** Comparison of body weight between *RANKL^{fl/fl}/Zmpste24^{-/-}/Dmp1-Cre* and *RANKL^{fl/fl}/Zmpste24^{-/-}* control mice over the indicated time period. **C.** Cortical bone parameters in μCT analysis. BS/TV, cortical surface/tissue volume ratio; Ct.B.Po, cortical bone porosity; Ct.Po.Dm, cortical pore diameter; Ct.Th, cortical thickness, TMD, tissue mineral density). *RANKL^{fl/fl}/Zmpste24^{+/+}* (n=14), *RANKL^{fl/fl}/Zmpste24^{-/-}* (n=12), *RANKL^{fl/fl}/Zmpste24^{-/-}/Dmp1-Cre* (n=12). Data shown are mean ± SEM. *$P<0.05$, **$P<0.01$, ***$P<0.001$, unpaired two-tailed Student's t-test with Welch's correction and Mann–Whitney tests were used to determine statistical significance.

III.- Exploring the role of the hepcidin modulator matriptase-2 on the development of HFD-induced obesity in mice: extended data
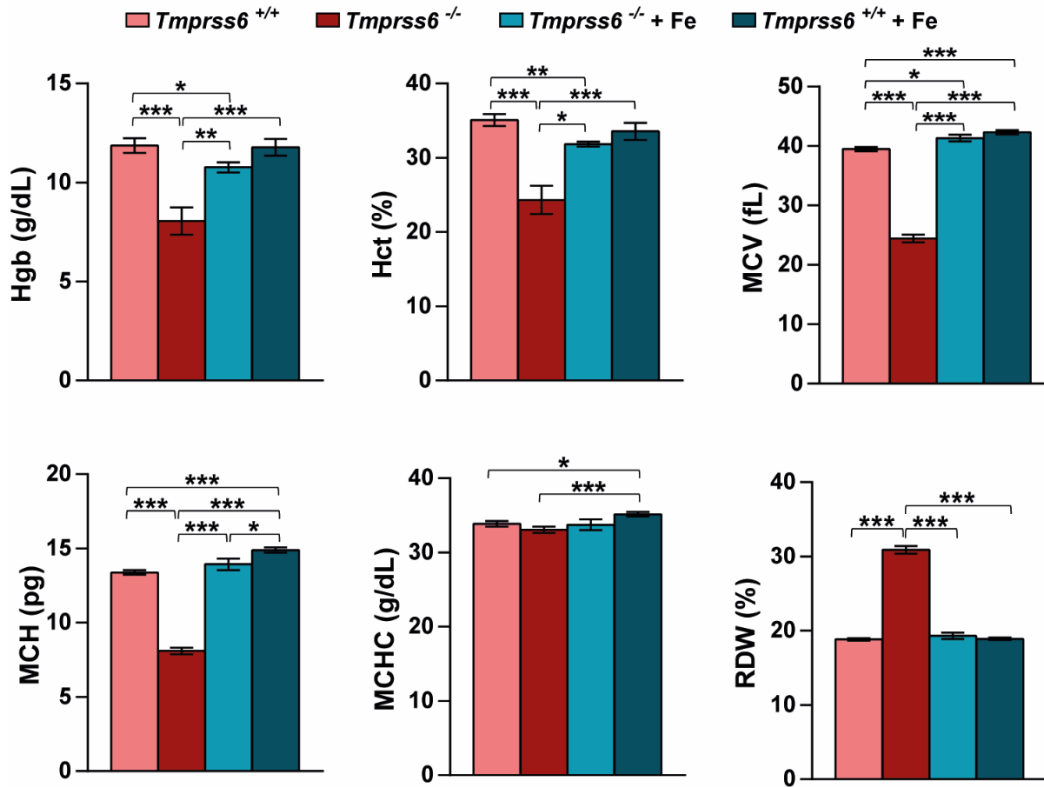

Supplementary Figure S2. Haematologic parameters of HFD-fed *Tmprss6*^+/+^, *Tmprss6*^-/-^ and both iron-treated *Tmprss6*^-/-^ and *Tmprss6*^+/+^ mice. Complete blood counts were measured from whole blood of *Tmprss6*^+/+^ (n=8), *Tmprss6*^-/-^ (n=7), and both iron-treated *Tmprss6*^-/-^ and *Tmprss6*^+/+^ mice (n=6 and n=9 respectively) fed a HFD for 20 weeks upon overnight fasting. Hgb, haemoglobin; Hct, haematocrit; MCV, mean corpuscular volume; MCH, mean corpuscular haemoglobin; MCHC, mean corpuscular haemoglobin concentration; RDW, red cell distribution width. Data shown are mean ± SEM. *P <0.05, **P<0.01, ***P<0.001, two-tailed Student's t-test and Mann-Whitney test.
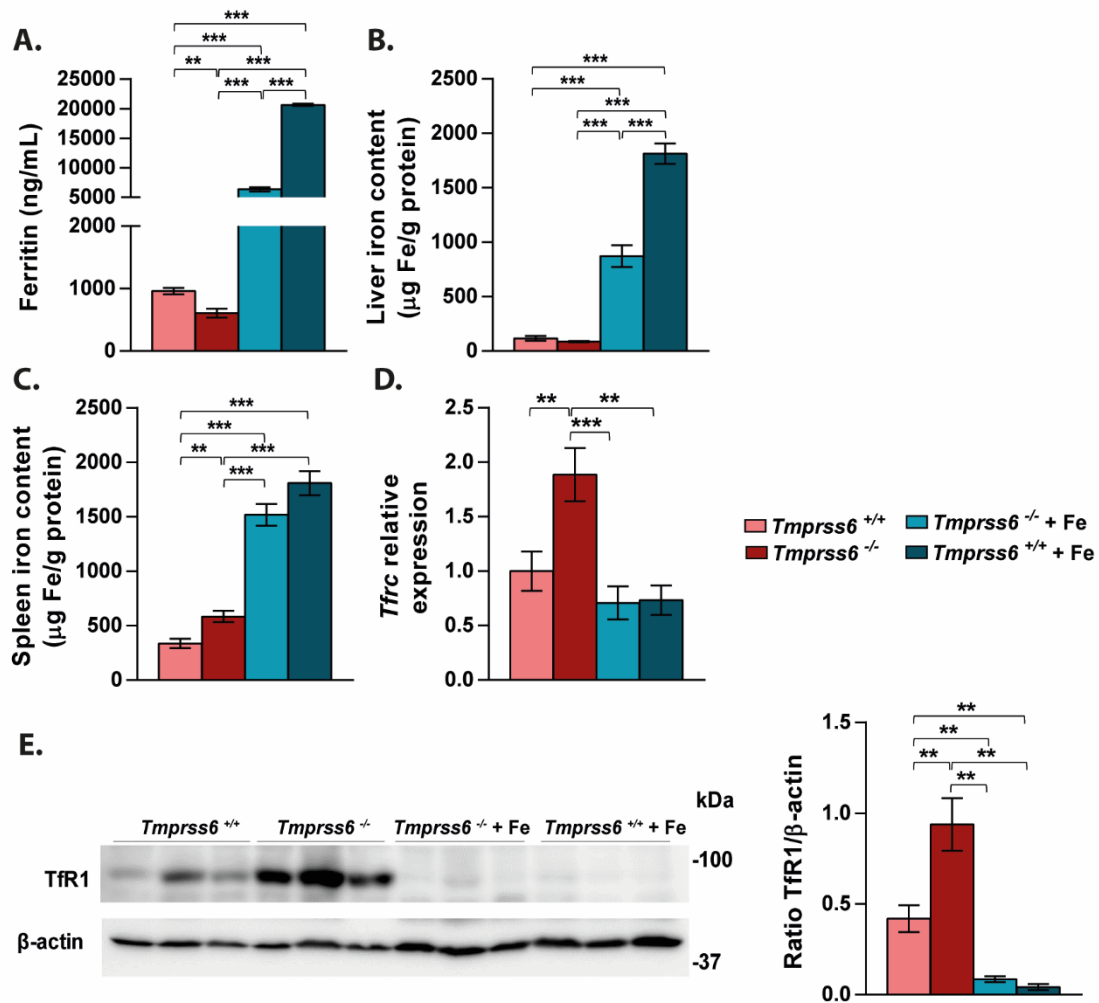
Supplementary Figure S3. Altered iron homeostasis in *Tmprss6⁻/⁻* and both iron-treated *Tmprss6⁻/⁻* and *Tmprss6⁺/⁺* mice. **A.** Fasting plasma concentration of ferritin in HFD-fed *Tmprss6⁺/⁺* (n=8), *Tmprss6⁻/⁻* (n=6), and both iron-treated *Tmprss6⁻/⁻* and *Tmprss6⁺/⁺* mice (n=7 respectively). **B.** Liver iron content relative to total protein in HFD-fed *Tmprss6⁺/⁺* (n=9), *Tmprss6⁻/⁻* (n=8), and both iron-treated *Tmprss6⁻/⁻* and *Tmprss6⁺/⁺* mice (n=9 and n=8 respectively). **C.** Spleen iron content relative to total protein in HFD-fed *Tmprss6⁺/⁺* (n=6), *Tmprss6⁻/⁻* (n=5), and both iron-treated *Tmprss6⁻/⁻* and *Tmprss6⁺/⁺* mice (n=7 and n=8 respectively). **D.** Relative gene expression of *Tfrc* in liver samples from HFD-fed *Tmprss6⁺/⁺* (n=11), *Tmprss6⁻/⁻* (n=9), and both iron-treated *Tmprss6⁻/⁻* and *Tmprss6⁺/⁺* mice (n=10 and n=8 respectively). **E.** Western-blot analysis of TfR1 protein expression in liver samples from HFD-fed *Tmprss6⁺/⁺* (n=6), *Tmprss6⁻/⁻* (n=6), and both iron-treated *Tmprss6⁻/⁻* and *Tmprss6⁺/⁺* mice (n=6 and n=7 respectively). (left) A representative result showing increased TfR1 protein levels in hypoferremic *Tmprss6⁻/⁻* mice compared to wild-types and iron-treated mice. (right) Quantification of TfR1 protein levels relative to loading control β-actin. Data shown are mean ± SEM. *$P < 0.05$, **$P < 0.01$, ***$P < 0.001$, two-tailed Student's t-test and Mann-Whitney test.
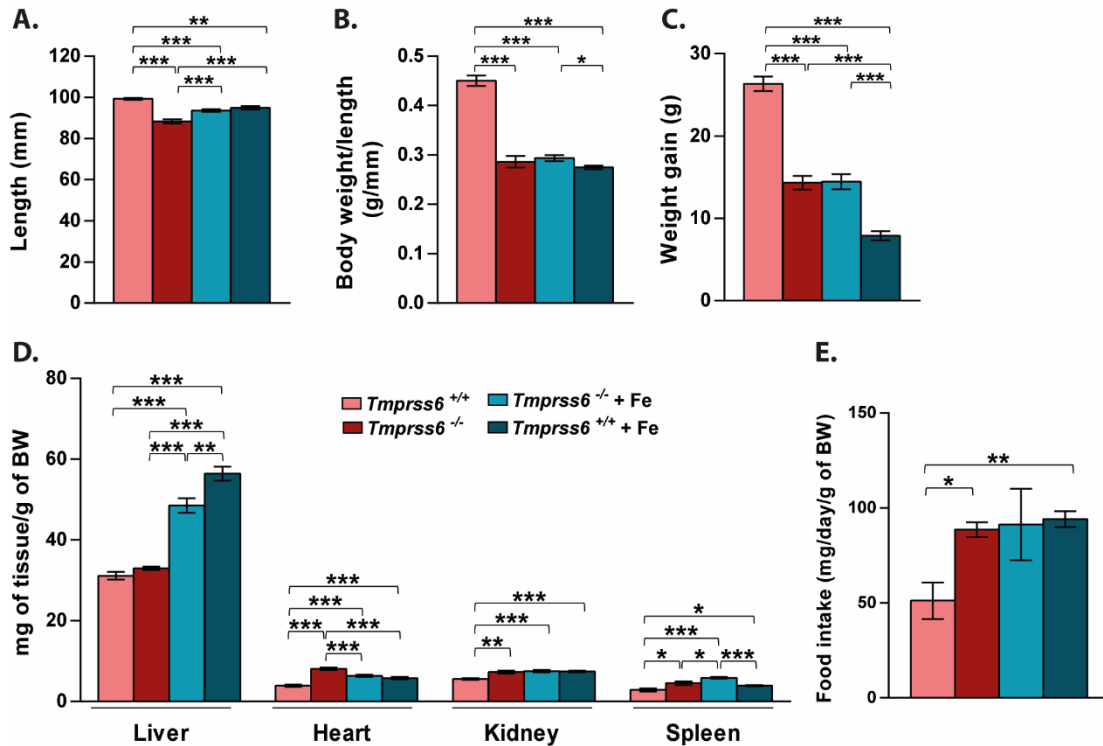
Supplementary Figure S4. Reduced body weight and increased food intake in *Tmprss6-*deficient mice upon HFD feeding. Length (**A**), body weight relative to length (**B**) and weight gain (**C**) of *Tmprss6$^{+/+}$* (n=7), *Tmprss6$^{-/-}$* (n=10), and both iron-treated *Tmprss6$^{-/-}$* and *Tmprss6$^{+/+}$* mice (n=11-13 and n=10 respectively) fed a HFD for 20 weeks. **D.** Organs weight relative to body weight of the same mice. **E.** Food consumption of *Tmprss6$^{+/+}$* (n=5), *Tmprss6$^{-/-}$* (n=5), and both iron-treated *Tmprss6$^{-/-}$* and *Tmprss6$^{+/+}$* mice (n=5 and n=6 respectively) fed a HFD. Data shown are mean ± SEM. *$P<0.05$, **$P<0.01$, ***$P<0.001$, two-tailed Student's t-test and Mann-Whitney test.
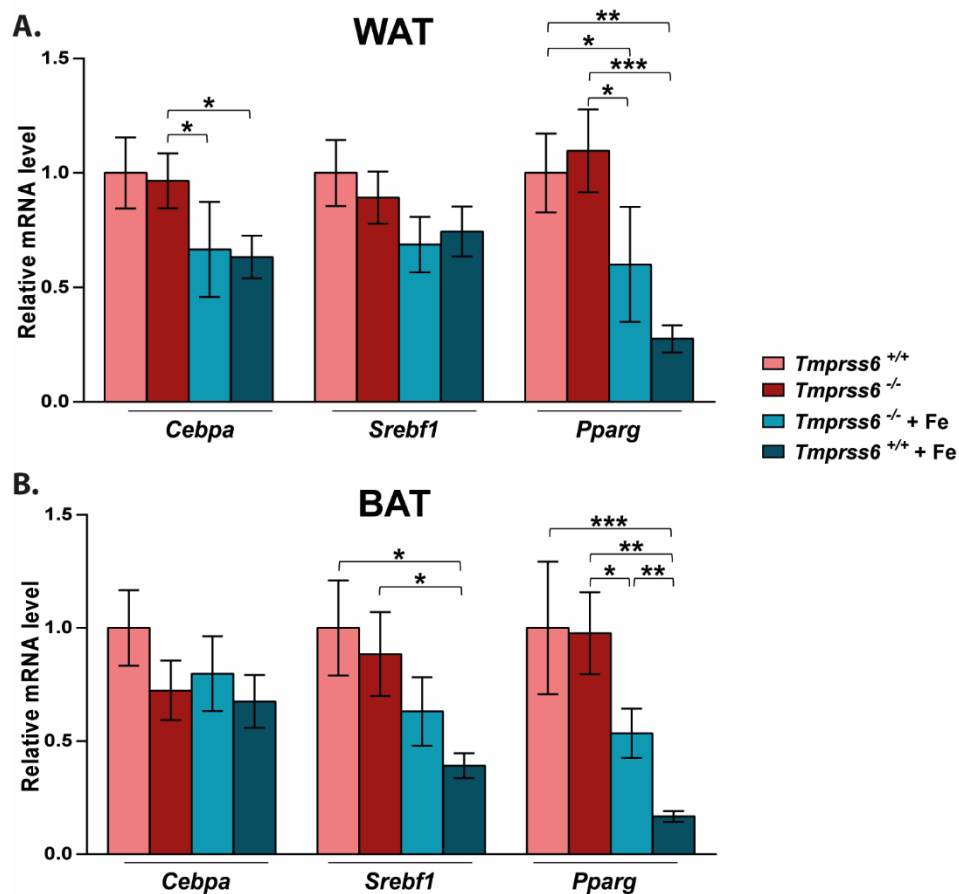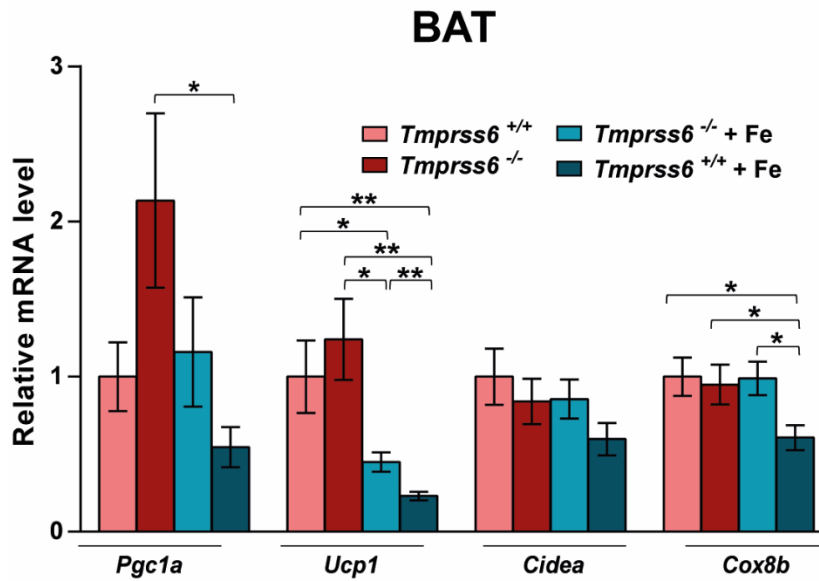
Supplementary Figure S5. Gene expression analysis of adipocyte differentiation markers in *Tmprss6*-deficient mice fed a high-fat diet. Relative expression levels of genes involved in adipocyte differentiation in WAT (**A**) and BAT (**B**) samples from HFD-fed *Tmprss6*^{+/+} (n=11), *Tmprss6*^{-/-} (n=7-9), and both iron-treated *Tmprss6*^{-/-} and *Tmprss6*^{+/+} mice (n=11 and n=8 respectively). Data shown are mean ± SEM. *P <0.05, **P<0.01, two-tailed Student's t-test and Mann-Whitney test.
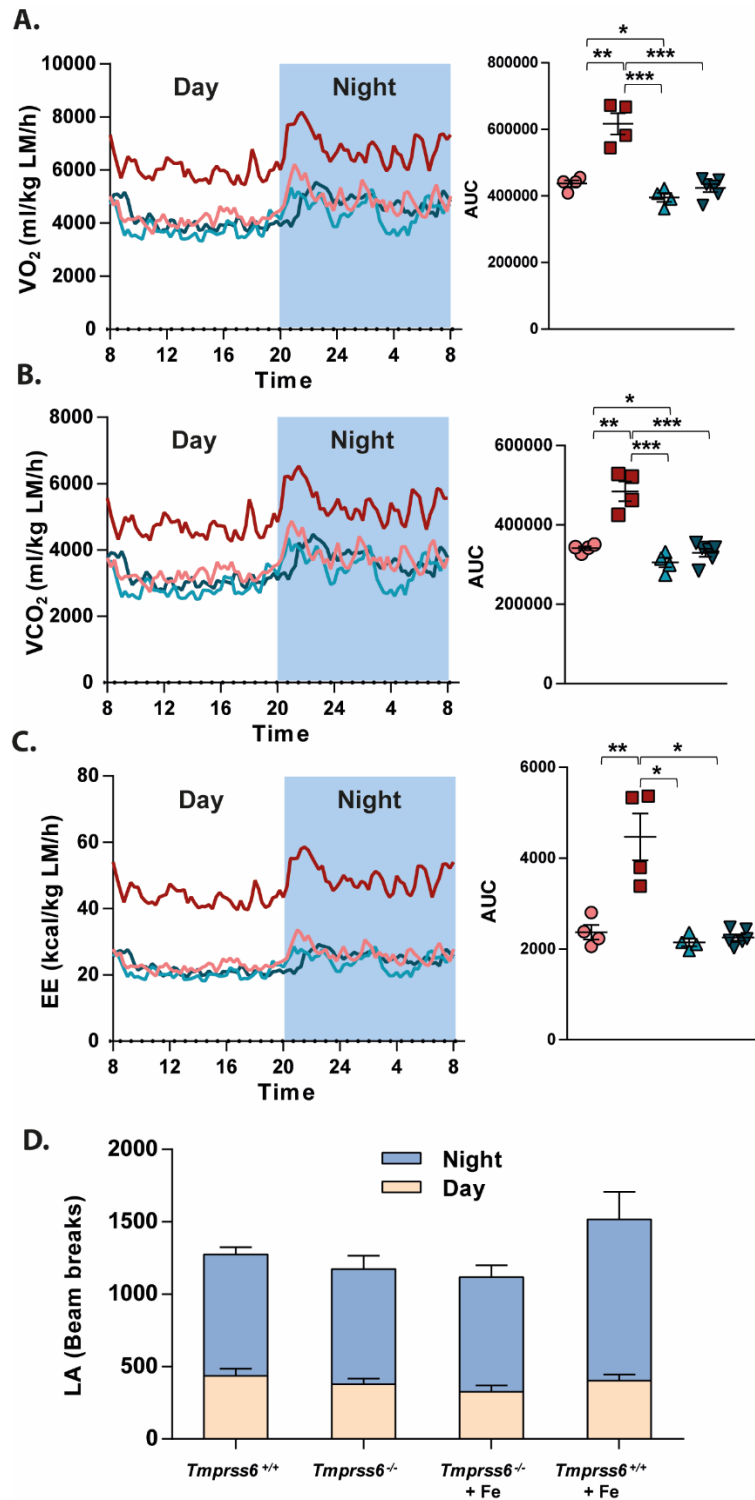
Supplementary Figure S6. Energy expenditure and locomotor activity of HFD-fed *Tmprss6*-deficient mice. Oxygen consumption rate (VO_2) (**A**), carbon dioxide production (VCO_2) (**B**) and energy expenditure (EE) (**C**) in HFD-fed *Tmprss6*^{+/+} (n=4), *Tmprss6*^{-/-} (n=4), and both iron-treated *Tmprss6*^{-/-} and *Tmprss6*^{+/+} mice (n=4 and n=6 respectively). Data are normalized to lean mass. **D.** Total ambulatory activity of HFD-fed *Tmprss6*^{+/+} (n=4), *Tmprss6*^{-/-} (n=5), and both iron-treated *Tmprss6*^{-/-} and *Tmprss6*^{+/+} mice (n=5 and n=6 respectively). Data

were determined by indirect calorimetry during a 24 h period. AUC, area under the curve. Data shown are mean ± SEM. *P <0.05, **P<0.01, ***P<0.001, two-tailed Student's t-test.

Supplementary Figure S7. Gene expression analysis of thermogenic genes in *Tmprss6-*deficient mice fed a high-fat diet. Relative expression levels of thermogenic genes in BAT samples of HFD-fed *Tmprss6$^{+/+}$* (n=11), *Tmprss6$^{-/-}$* (n=8-9), and both iron-treated *Tmprss6$^{-/-}$* and *Tmprss6$^{+/+}$* mice (n=10 and n=8 respectively). Data shown are mean ± SEM. *$P<0.05$, **$P<0.01$, two-tailed Student's t-test.
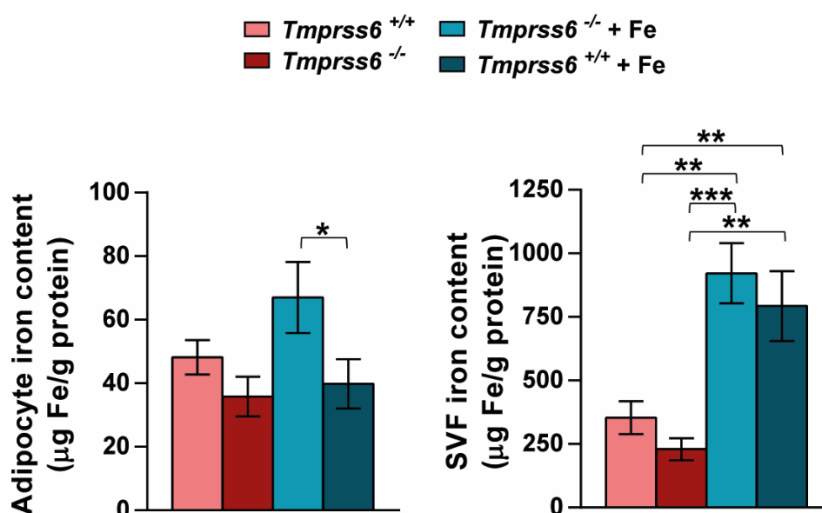
**Supplementary Figure S8. Adipocyte iron content in HFD fed *Tmprss6*-deficient mice.** Adipocytes and the stromal vascular fraction (SVF) were isolated from WAT samples of HFD-fed *Tmprss6*^{+/+} (n=5-6), *Tmprss6*^{-/-} (n=5), and both iron-treated *Tmprss6*^{-/-} and *Tmprss6*^{+/+} mice (n=6 and n=8 respectively) and iron levels were determined relative to total protein. Data shown are mean ± SEM. *$P<0.05$, **$P<0.01$, ***$P<0.001$, two-tailed Student's t-test and Mann-Whitney test.
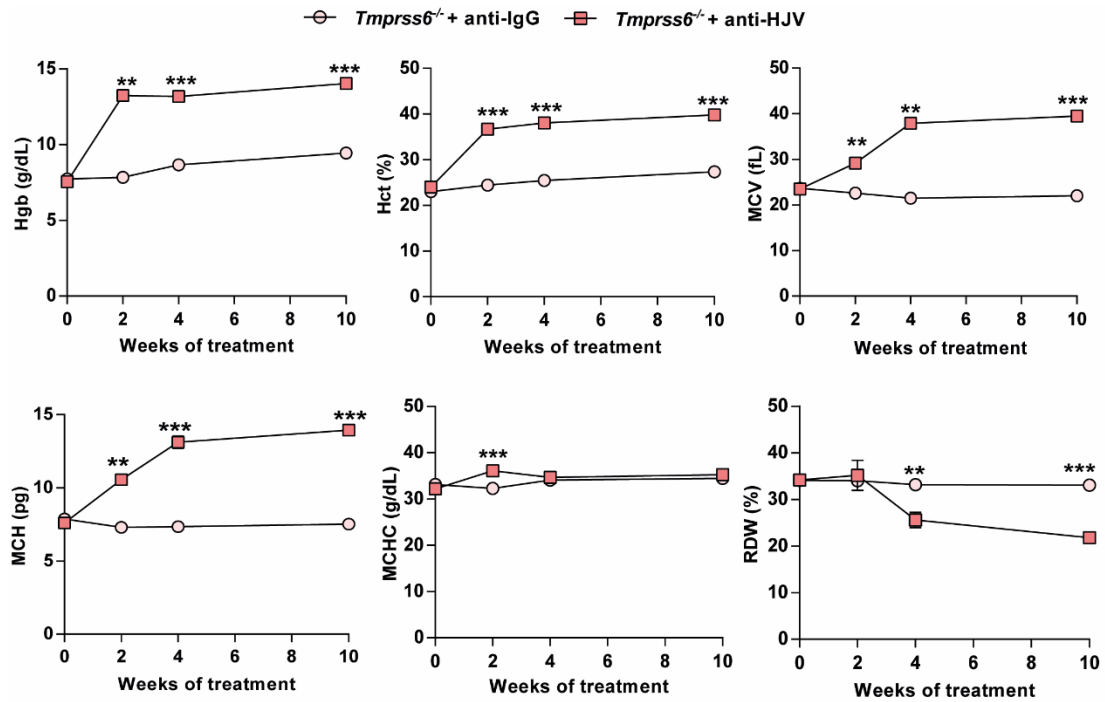
Supplementary Figure S9. Anti-HJV therapy rescues the hematologic parameters of *Tmprss6*-deficient treated mice. Complete blood counts were measured from whole blood of HFD-fed anti-IgG-treated *Tmprss6*^{-/-} (n=3-5) and anti-HJV-treated *Tmprss6*^{-/-} (n=4-8) mice to monitor the efficacy of the treatment over time. Hgb, haemoglobin; Hct, haematocrit; MCV, mean corpuscular volume; MCH, mean corpuscular haemoglobin; MCHC, mean corpuscular haemoglobin concentration; RDW, red cell distribution width. Data shown are mean ± SEM. **$P<0.01$, ***$P<0.001$, two-tailed Student's t-test and Mann-Whitney test.
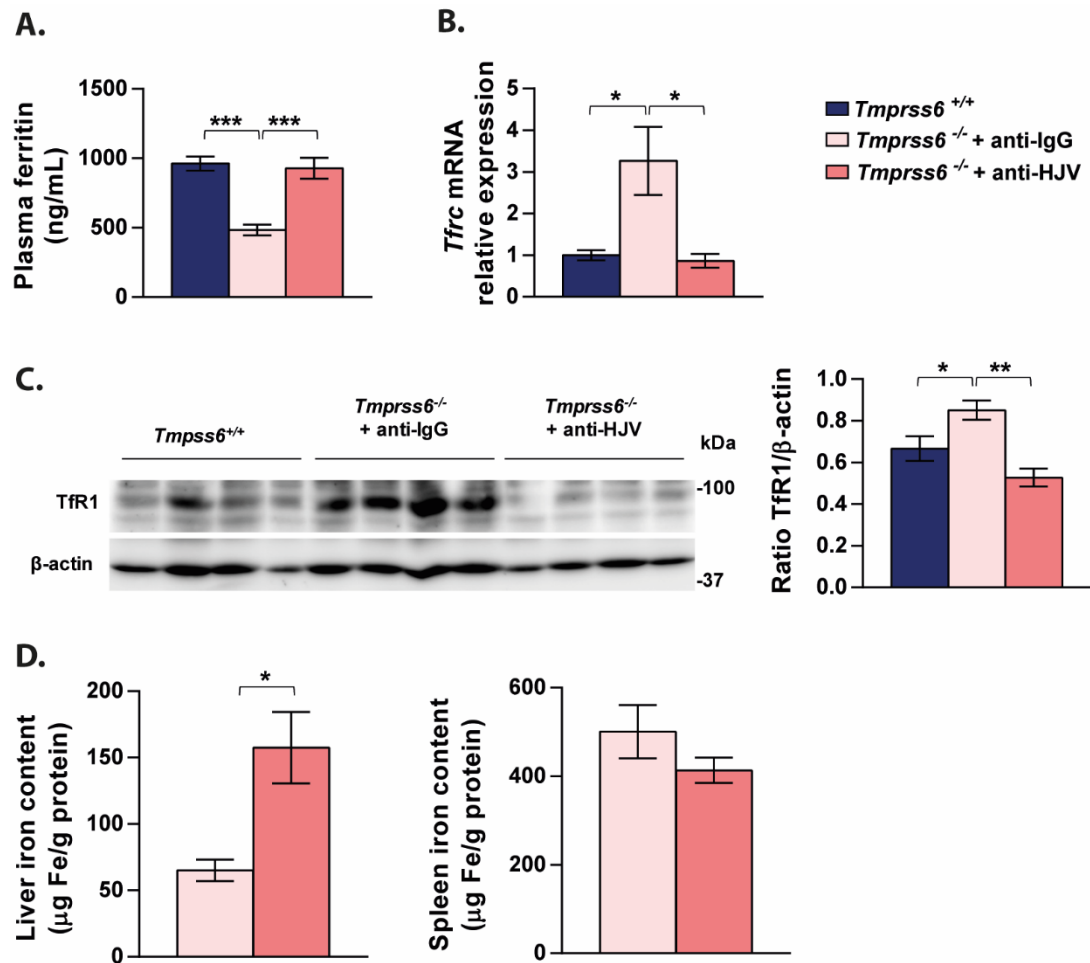
Supplementary Figure S10. Restored iron homeostasis in *Tmprss6*^{-/-} mice upon anti-HJV therapy. A. Fasting plasma concentration of ferritin in HFD-fed *Tmprss6*^{+/+} (n=8), anti-IgG-treated *Tmprss6*^{-/-} (n=5), and anti-HJV-treated *Tmprss6*^{-/-} (n=8) mice. **B.** Relative gene expression of *Tfrc* in liver samples from HFD-fed *Tmprss6*^{+/+} (n=7), anti-IgG-treated *Tmprss6*^{-/-} (n=5), and anti-HJV-treated *Tmprss6*^{-/-} (n=8) mice. **C.** Western-blot analysis of TfR1 protein expression in liver samples from HFD-fed *Tmprss6*^{+/+} (n=4), anti-IgG-treated *Tmprss6*^{-/-} (n=4), and anti-HJV-treated *Tmprss6*^{-/-} (n=5) mice. (left) A representative result showing decreased TfR1 protein levels in *Tmprss6*^{-/-} anti-HJV treated mice compared to *Tmprss6*^{-/-} anti-IgG treated mice. (right) Quantification of TfR1 protein levels relative to loading control β-actin. (**D**) Liver (left) and spleen (right) iron content relative to total protein in HFD-fed anti-IgG-treated *Tmprss6*^{-/-} (n=5), and anti-HJV-treated *Tmprss6*^{-/-} (n=8) mice. Data shown are mean ± SEM. *$P<0.05$, **$P<0.01$, ***$P<0.001$, two-tailed Student's t-test.
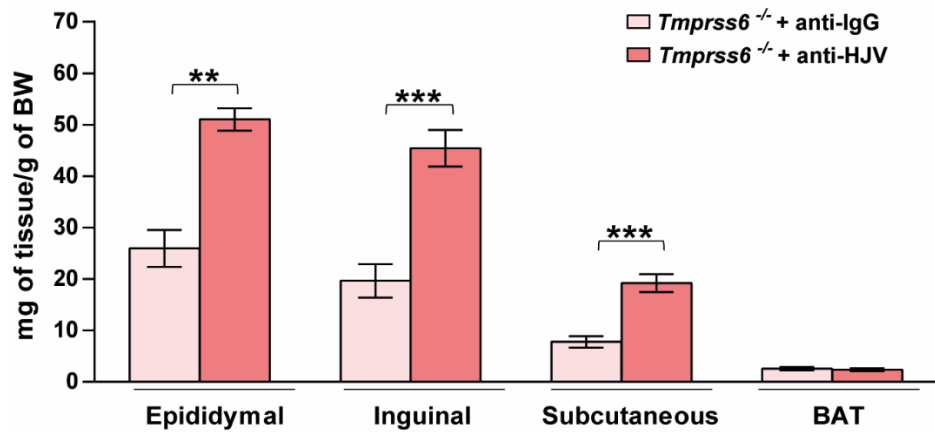
Supplementary Figure S11. *Tmprss6*-/- **mice increase their fat mass upon anti-HJV therapy.** White adipose (epididymal, subcutaneous and inguinal) and brown adipose tissue (BAT) masses were determined relative to body weight in anti-IgG-treated *Tmprss6*-/- (n=5), and anti-HJV-treated *Tmprss6*-/- (n=8) mice fed a HFD for 20 weeks. Data shown are mean ± SEM. **$P<0.01$, ***$P<0.001$, two-tailed Student's t-test.

Supplementary Table S4. Summary of HFD-induced phenotypes in mouse models of iron imbalance and hepcidin up-regulation.

Mouse model	Tmprss6+/+	Tmprss6-/-	Tmprss6-/- + Fe	Tmprss6+/+ + Fe
Iron status	Basal	Hypoferremia	Iron overload	Iron overload
Hepcidin levels	Basal	Up-regulated ↑	Up-regulated ↑↑	Up-regulated ↑↑
Fat mass	~ 40 %	~ 26 %	~ 13 %	~ 15 %
Leptin levels	Basal	Low	Low	Low
Hepatic steatosis	Yes	No	No	No
Glucose tolerance	Low	Increased	Increased	Increased
Insulin sensitivity	Low	Increased	Moderated	Moderated
Energy expenditure	Basal	Increased	Basal	Basal
Fat lipolysis	Basal	Increased	Increased	Increased

Supplementary Table S5. Primer sequences used for real-time quantitative PCR.

Gene	Forward primer (5'-3')	Reverse primer (5'-3')
Acaca	CTGTATGAGAAAGGCTATGTG	AACCTGTCTGAAGAGGTTAG
Actb	CTGAGGAGCACCCTGTGCT	GTTGAAGGTCTCAAACATGATCTG
Adrb3	CCAAGCTACACGATGCCATGT	GAGCTCAGCAGCTCCTTCCT
Cebpa	CAAGAACAGCAACGAGTACCG	GTCACTCGTCAACTCCAGCAC
Cidea	TGACATTCATGGGATTGCAGAC	GGCCAGTTGTGATGACTAAGAC
Cox8b	GCGAAGTTCACAGTGGTTCC	GAACCATGAAGCCAACGACT
Cpt1a	GGGAGGAATACATCTACCTG	GAAGACGAATAGGTTTGAG
Fasn	GATTCAGGGAGTGGATATTG	CATTCAGAATCGTGGCATAG
Fsp27	ATGGACTACGCCATGAAGTCT	CGGTGCTAACACGACAGGG
Fbp1	AAGTACTGATGAGCCTTCTG	GCTCACCATAATGAATTCTCC
G6pc	TTCAAGTGGATTCTGTTTGG	AGATAGCAAGAGTAGAAGTGAC
Gck	TGTACGAAAAGATCATTGGC	TCAGGATGTTAAGGATCTGC
Lipe	CAT GGCTCAACTCCTTCCTG	CTG TGCCCAGTAAGCCCTCA
Pck1	AATATGACAACTGTTGGCTG	AATGCTTTCTCAAAGTCCTC
Pfk1	AAGAGACTGATTTTGAGCAC	CTCAGAAACCCTTGTCTATG
Pgc1a	TCCTCTTCAAGATCCTGTTA	CACATACAAGGGAGAATTGC
Pklr	GTGAAGAAGTTTGATGAGATCC	CAAGAAACCTTCTCTGCTG
Pnpla2	CAACCTTCGCAATCTCTAC	TTCAGTAGGCCATTCCTC
Pparg	TCGCTGATGCACTGCCTATG	GAGAGGTCCACAGAGCTGATT
Rn18s	GTAACCCGTTGAACCCCATT	CCATCCAATCGGTAGTAGCG
Scd1	GTGGGGTAATTATTTGTGACC	TTTTTCCCAGACAGTACAAC
Srebf1	GATGTGCGAACTGGACACAG	CATAGGGGGCGTCAAACAG
Tfrc	CCCATGACGTTGAATTGAACCT	GTAGTCTCCACGAGCGGAATA
Ucp1	CTTTTTCAAAGGGTTTGTGG	CTTATGTGGTACAATCCACTG